The lateral distribution of Cerenkov light in large cosmic ray showers as a measure of longitudinal development

M.A.B Craig

How to cite:

Craig, M.A.B (1984) The lateral distribution of Cerenkov light in large cosmic ray showers as a measure of longitudinal development. Doctoral thesis, Durham University.

The Lateral Distribution of Cerenkov Light in Large Cosmic Ray Showers as a Measure of Longitudinal Development

by

M. A. B. Craig, B.Sc.

A thesis submitted to the University of Durham
in accordance with the regulations for
admittance to the degree of
Doctor of Philosophy

Department of Physics,
University of Durham.

January, 1984.

ACKNOWLEDGEMENTS

I wish to thank Professor B.H. Bransden for the provision of facilities in the Department of Physics, University of Durham. I would also like to express my gratitude to my supervisor, Dr. K.E. Turver, for his advice and encouragement throughout the course of this work.

I thank all my colleagues in the Extensive Air Shower group - Dr. M.P. Chantler, Dr. T.J.L. McComb, Dr. K.J. Orford and Mr. G.M. Walley - for their assistance and many useful discussions.

The U.S. Army Technical and Evaluation Command is thanked for provision of land and support facilities at Dugway Proving Grounds.

The provision of a Research Studentship by the Science and Engineering Research Council is gratefully acknowledged.

ABSTRACT

This thesis reports measurements made on the longitudinal cascade of high energy cosmic ray showers using observations of atmospheric Cerenkov light. The lateral distribution of the Cerenkov light shower has been shown to be one of the measurable ground parameters which is sensitive to cascade development. The interpretation of such measurements together with other depth sensitive parameters in recorded showers has allowed inferences to be made about the mass distribution of the primary particles and about the nature of the high energy interactions which govern the generation of the cascade through the atmosphere.

Measurements of atmospheric Cerenkov light from showers between 10^{15} — 10^{18}eV were made at Dugway Proving Grounds, Utah, U.S.A. between October 1977 and March 1980, using an array of fast photo multipliers to record both the lateral distribution of light density and the time structure of the light pulses. This thesis concerns the detailed analysis and interpretation of the lateral distribution data. These results were subsequently combined with those from pulse timing measurements to present composite results on the gross feature of shower development, the depth of cascade maximum.

Analysis techniques have been developed to determine both the average characteristics of the lateral distribution and the fluctuations in the data which could be attributed to intrinsic fluctuations in cascade development. The results of these analyses were then related, through the results of computer simulations of shower development, to the depth of cascade maximum. A change in the elongation rate and the magnitude of fluctuations between 10^{16} and 10^{17}eV has been observed and this is interpreted as a change in primary mass composition from predominantly heavy particles $\sim 10^{16}$eV to include a greater proportion of light nuclei $\sim 2 \times 10^{17}$eV. The combined measurement of the mean and fluctuations in the depth of maximum has allowed certain interaction models to be rejected. These were those involving scaling in the central region or using an interaction cross section which remains constant with energy.

Results from other observations of cosmic ray showers show further indication of the change in primary mass composition between $\sim 10^{16}$eV and $\sim 2 \times 10^{17}$eV. At higher energies these other results indicate a mass composition changing little with energy.

PREFACE

This thesis describes the analysis and interpretation of the observations of atmospheric Cerenkov light made by the University of Durham Extensive Air Shower Group between September 1977 and March 1980 at Dugway, Utah, U.S.A. The present author was involved in the routine operation of the Dugway Cerenkov Light Array for one observing period in 1979 and played a major role in the analysis of the data collected by the array.

Along with other members of the group she contributed to the preanalysis scrutiny of the shower records. The development of analysis routines to analyse and interpret the measurements of the lateral distribution of Cerenkov light in high energy showers in terms of cascade development was the responsibility of the author. The results obtained from these analysis techniques, described in Chapter 4 are presented in Chapter 5 and represent the major contribution of the author. These techniques were also applied, though not by the author, to the lower energy data from the Dugway array. The calculation of the response of the Dugway array to a known shower flux was also undertaken by the author in order to account for the effects of selection bias in the datasets used for both pulse timing and lateral distribution analysis.

The relationship between the Dugway estimates of the mean and the fluctuations in depth of cascade maximum has already been examined by another member of the EAS group. The comparison between the Dugway results and those from other measurements at higher energy, and the interpretation based on the proportion of iron-like nuclei in the primary flux is the work of the author.

CONTENTS

Chapter 1 Introduction

Chapter 2 Cerenkov Light

Page

Chapter 3 The Dugway Cerenkov Light Detector Array

Chapter 4 Analysis Procedures Used in the Determination of Lateral Distribution

CHAPTER 1

INTRODUCTION

1.1 The Cosmic Radiation

Our knowledge of the extra-terrestrial Universe is based on photons and matter arriving at the top of the atmosphere from space. At energies above 10^6eV this radiation is largely particles and is known as the cosmic radiation. The study of this radiation has lead to advances in the two extremes of physics - what Greisen (1960) terms the "small scale" and "large scale" searches.

In the small scale quest, the study of the nature and interactions of elementary particles, the cosmic radiation provided the only source of high energy particles before the advent of large particle accelerators in the 1950's. The positron was one of many particles first discovered in the cosmic radiation (Anderson (1932)). Though most particle physics experiments now take place under controlled conditions in accelerators, cosmic rays extend to energies more than five orders of magnitude greater than the largest earth-based accelerator. There is therefore, still knowledge about the highest energy interactions available only from cosmic ray experiments.

The "large scale" quest is the study of astrophysics and the first contribution of cosmic ray physics to this field was in probing the galactic magnetic fields. The existence of such energetic particles produced within the galaxy or beyond poses problems about the nature of the sources and accelerating mechanism.

The cosmic radiation was first observed by C.T.R. Wilson (1901) as an ever-present background radiation which produced ionisation in shielded chambers. The pioneering experiments of Hess (1912) making measurements of ionisation high in the atmosphere with balloon-borne detectors established that an extraterrestrial radiation was continually incident on the upper atmosphere. This started the search to understand the phenomenon in order to use it as a tool in the study of astrophysics.

Current interest in the primary cosmic ray flux has settled into three main areas. The primary energy spectrum, the number of particles incident at different energies, is probably the best measured of these but considerable uncertainty remains about the intensity of particles above 10^{19}eV. The primary mass composition can be well measured at lower energies (up to $\sim 10^{14}$eV) but is not understood at higher energies where the greater interest lies. It is the aim of the present work to elucidate the primary mass composition $\sim 10^{16} - 10^{17}$eV. The third area of interest is the search for any anisotropy in the arrival direction of the primary radiation which might offer some indication of the source of the radiation. Each of these studies attempts to discern any change in behaviour with increasing energy which might be associated with changes in the origin or propagation of the particles. One of the most discussed questions is whether the source of cosmic rays is within the galaxy or extragalactic.

While astrophysical interest in cosmic rays is concerned with the primary flux of particles, knowledge about these particles at energies greater than 10^{15}eV is gained from the detection of secondary particles in extensive air showers (EAS). These showers are produced by the interaction of the primary particle with air nuclei forming cascades of energetic particles through the atmosphere. It is from the secondary particles that the early discoveries of high energy physics were made. It is necessary to understand the physics of the high energy interactions which produce these secondary particles in order to infer the nature of the primary particle. This remains one of the problems of cosmic ray physics, which the current work investigates.

In this chapter it is intended to explain these phenomena and to outline the aims of the present work.

1.2 The Primary Energy Spectrum

The primary energy spectrum is probably the best measured of the characteristics of the cosmic radiation. Figure 1.1 shows the integral flux of primary particles between 10^{11}eV and 10^{20}eV. A variety of measurement techniques has been used to obtain data over 9 decades of primary energy. At low energies satellites above the atmosphere and balloon borne detectors can determine the flux of primary particles directly from calorimeters and emulsion chambers. Measurements at energies greater than 10^{14}eV are made by the indirect method of detecting extensive air showers.

Figure 1.1 The flux of all primary cosmic rays at the top of the atmosphere shown as an integral spectrum. Experimental uncertainties are represented by cross hatching. (From Gaisser and Yodh (1980)).

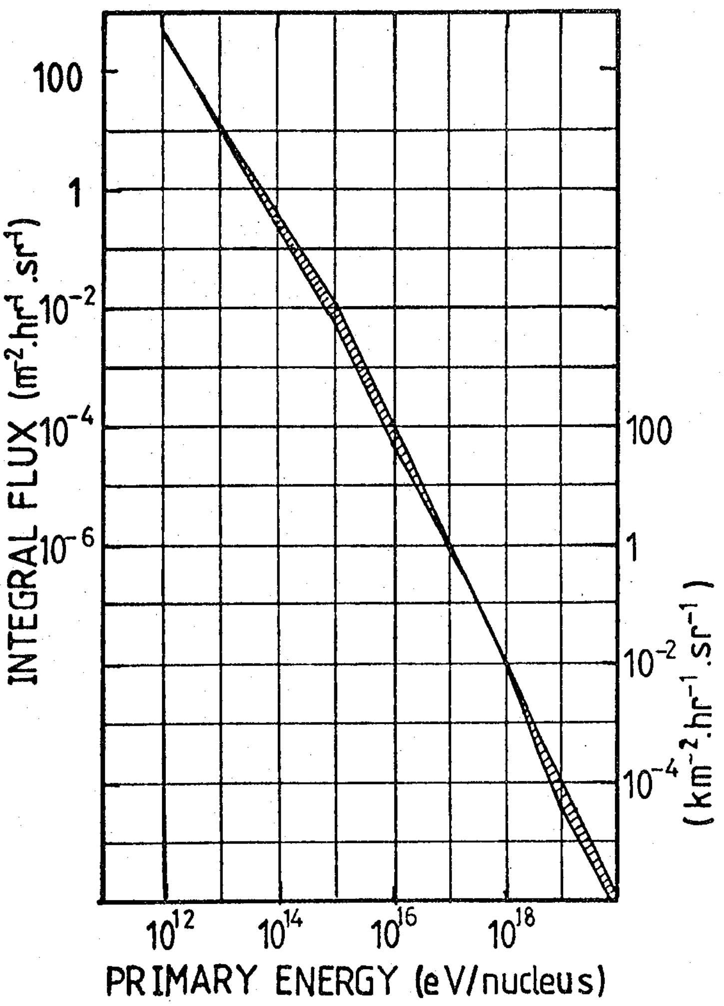
100
1
10^{-2}
10^{-4}
10^{-6}
INTEGRAL FLUX ($m^{-2}.hr^{-1}.sr^{-1}$)
100
1
10^{-2}
10^{-4}
($km^{-2}.hr^{-1}.sr^{-1}$)
10^{12}
10^{14}
10^{16}
10^{18}
PRIMARY ENERGY (eV/nucleus)

The striking feature of the primary energy spectrum is the rapid fall in intensity with increasing energy but also of note is how little structure is observed in this large spread of primary energy. The rapid decline in the flux at higher energies poses considerable difficulties in detecting showers and this explains why recourse must be made to indirect methods.

The significant features of the spectrum are the "knee" at $\sim 10^{15}$eV where the spectrum steepens from an exponent of -1.6 to a value of -2.2. There is also a possible "ankle" at $> 10^{18}$eV where the spectrum flattens once more. This however is less definitely determined than the "knee".

The principal theory used to explain the steepening of the spectrum above $\sim 10^{15}$eV invokes the mechanism of galactic confinement (Peters (1961)). This predicts that the galactic magnetic field fails to confine particles within the galaxy above a certain energy (rigidity cut-off being dependent on the nature of the cosmic ray particle) and the progressive leakage is reflected in the primary energy spectrum. An alternative suggestion is that pulsars provide the dominant source of cosmic rays between 10^{14}eV and 10^{16}eV (Karakula et al. (1974)) and the upper energy limit explains the steepening of the spectrum.

The flattening of the spectrum above 10^{18}eV is more difficult to account for. The most usual theory proposed is that a source of extragalactic particles, possibly protons, is contributing at these energies. However, after the discovery of the 2.7°K black body radiation, it was quickly pointed out by Greisen (1966) and Zatsepin and Kuzmin (1966) that the cross-section for photo-pion production between the black body photons and protons rises rapidly at particle energies above 10^{19}eV and therefore there should be a cut-off of particles at $\sim 5 \times 10^{19}$eV. Whilst there remains some uncertainty about whether the "ankle" is a true effect models have been suggested of enhanced cosmic ray production in galactic clusters (Giler et al. (1980)) or of heavy nuclei produced within the galaxy and confined by extensive magnetic fields (Hillas and Ouldridge (1975), Hillas (1981)) which can be made to fit a flattened energy spectrum.

1.3 The Primary Mass Composition

The determination of the primary mass composition of cosmic rays is a more difficult problem than the primary energy spectrum. Direct measurements are only reliable up to $\sim 4 \times 10^{12}$eV. Figure 1.2 shows a summary of results for different types of nuclei (Wolfendale (1974)). It may be noted that the low energy measurements have been reasonably established for some time while at extensive air shower energies only slight evidence of primary mass composition is available. The most important feature of the results in Figure 1.2 is that the spectrum of heavy nuclei is flatter than that of other components. If this is continued above 10^{12}eV heavy primaries will form a

Figure 1.2 Primary spectrum of protons and nuclei below 10^{12}eV/nucleon (from Wolfendale (1974)). Nuclei are grouped as follows:

L - $3 \leqslant Z \leqslant 5$

M - $6 \leqslant Z \leqslant 9$

H - $10 \leqslant Z$

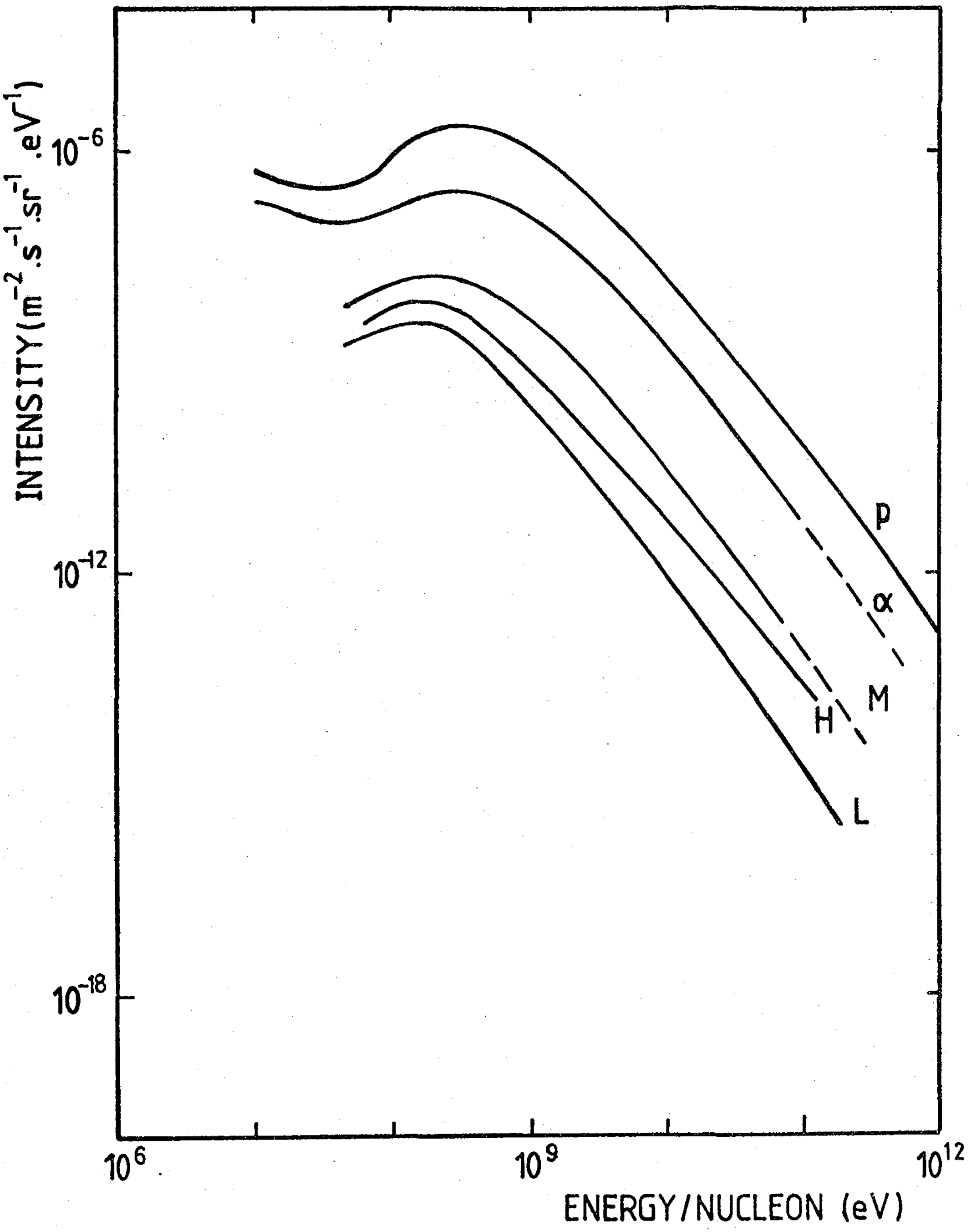
INTENSITY $(m^{-2}.s^{-1}.sr^{-1}.eV^{-1})$
10^{-6}
10^{-12}
10^{-18}
10^{6}
10^{9}
10^{12}
ENERGY/NUCLEON (eV)
p
α
M
H
L

significant proportion of the cosmic ray flux.

Between ~ 4×10^{12} and 10^{15}eV where extensive air showers become the only way of making measurements, experiments to distinguish primaries of different masses become confused. Increased numbers of measurements from satellite-borne detectors may clarify the issue in the future.

At extensive air shower energies (> 10^{14}eV) the work of Goodman et al. (1979) on the detection of delayed hadrons in the shower core has had some success in determining that an increased proportion of heavy nuclei, possibly ~ 60% iron-like nuclei, are present in the cosmic ray flux below 10^{15}eV. The current experiment is one of a number attempting to infer information about the primary mass composition from the structure of air showers.

Theories of the origin of cosmic rays are closely linked to a determination of the primary mass composition at the top of the atmosphere. The model of leakage of cosmic rays from the galaxy due to a rigidity cut-off used to explain the "knee" in the energy spectrum predicts that the percentage of light nuclei decreases progressively with increasing energy. Models which invoke an extragalactic source of protons at high energies would also be resolved by the determination of the primary mass composition. Understanding of both the origin and propagation of cosmic rays demands a knowledge of the primary mass composition which must then be linked back to the primordial composition at the source.

1.4 Arrival Directions

The search for some angular anisotropy has been conducted in order to gain information about the source of cosmic rays. At energies below 10^{12}eV the arrival directions of primary particles are dominated by magnetic fields within the solar system and therefore, no evidence of sources can be gained. As the particle energies increase the deflection by galactic magnetic fields is reduced and any anisotropy in arrival directions would become more pronounced.

Contrary to the earlier belief that the cosmic ray flux was highly isotropic recent evidence suggests that on an anisotropy exists at $\sim 10^{14}$eV and that its effect increases with increasing energy. Kiraly et al. (1979) give a review of anisotropy data. Subsequent to that review, Coy et al. (1981a) have reported a significant anisotropy at $\sim 10^{17}$eV.

A survey has been undertaken by Krasilnikov (1979) of the arrival directions of the 58 events at energies $>$ 5×10^{19}eV where the effects of galactic magnetic fields on the particle trajectories are small and therefore more direct evidence of the particle source is given. These have shown a consistent tendency to arrive from higher galactic latitudes and this suggests that an extragalactic source may be significant at these energies. However, a galactic source could be acceptable if the primary flux were predominantly heavy nuclei. Between 10^{19} - 10^{20}eV Lloyd-Evans et al. (1979) have observed a correlation between primary energy and galactic latitude which would be consistent with an increasing proportion of extra galactic protons in the primary flux in this energy range. Interpretation of these results must, however, depend on a determination of the nature of the primary flux from which the Larmor radius in the galactic magnetic field is calculated. Two point sources have recently been observed at low air shower energies associated with Cygnus X-3 (Samorski and Stamm (1983)) and the Crab pulsar (Dzikowski et al. (1981), Boone et al. (1983)).

1.5 Extensive Air Showers

The sharply falling primary energy spectrum means that beyond $\sim 10^{15}$eV measurements of cosmic rays using satellite or balloon-borne detectors demands resources of both money and patience beyond reasonable limits. Only by enhancing the effect of each particle can measurements be made at higher energies. The phenomenon of extensive air showers is thus both the solution to making measurements above 10^{15}eV and the source of considerable problems of analysis. The atmosphere itself acts as an absorber and detector of particles by generating a shower of particles for each primary and spreading the effect over an area of up to a few square kilometers. However, in the process of making measurements possible it degrades the information available from the measurements. Only by observing the development of the shower through the atmosphere is it possible to make inferences about the energy and nature of the primary particle and only by understanding the high energy physics of the interactions creating the shower can the showers be interpreted.

1.5.1 Production

An extensive air shower is built up by a series of collisions between high energy particles and air nuclei. The primary particle has a mean free path of approximately 80 g cm^{-2} and is incident on an atmosphere with a vertical depth to sea level of ~ 1000 g cm^{-2}. The first collision between the primary particle and an air nucleus results in the production principally of protons, neutrons and pions. Other hadronic particles are also produced but their effects on shower development are not appreciable. The leading particle itself and the produced hadrons continue through the atmosphere to further collisions and a hadronic cascade is built up. This component of the air shower extends typically over a few metres around the direction of the incoming primary particle. This does not significantly increase the probability of detecting high energy cosmic rays.

The detectable or extensive components of the air shower are produced principally by the charged and neutral pions resulting from collisions in the hadronic core. The π°s decay rapidly as

$$\pi^{\circ} \longrightarrow 2\gamma$$

and the production of particle-antiparticle pairs, dominantly $e^{+}e^{-}$ results from these high energy photons. The process of bremsstrahlung results in the production of more high energy photons which feed the electron-photon cascade.

This shower builds up until bremsstrahlung no longer produces photons of sufficient energy to produce an electron-positron pair. Beyond this the principal loss of energy is through Compton scattering and ionisation and electrons are gradually lost from the shower. Coulomb scattering of the electrons causes the shower to spread laterally from the shower core and this enhances the probability of detecting the cosmic ray event. The development of the electron-photon cascade is one of the most studied of the features of extensive air showers since it is sensitive to the primary particle and the depth of the first interaction.

The second main component is produced by the decay charged pions from the shower core. The predominant decay channels are

$$\pi^- \longrightarrow \mu^- + \nu_\mu$$
$$\pi^+ \longrightarrow \mu^+ + \bar{\nu}_\mu$$

and for slow pions this process also dominates over a further collision of the pion with an air nuclei. Whilst the neutrino can be discounted from measurements of extensive air showers the muons are a major source of information about the primary particle. The interaction cross section for muons is smaller than for electrons, thus more muons penetrate through the atmosphere to ground level. The build up of the muon component is slower than the electron shower but the decay is equally less rapid. Therefore not only measurements of the muon component alone but also the relationship between the observed muon and electron signals provide information about the primary particle. Like the electron shower this component extends over a wide area when observed at ground level (~1km at 10^{18}eV).

The hadronic core and the electron-photon and muons components (the "soft" and "hard" components) are the main constituents of the air shower. Secondary emissions from these particles also take place and Cerenkov radiation, which the present experiment detects, is probably the most important of these.

1.5.2 Measurement Techniques

Measurement of extensive air showers usually involves sampling the density of particles across the shower front. In order to cover a large area of the shower (the current experiment uses a collecting area of radius 400 m to investigate at ~ 10^{17}eV) an array of small detectors operating in coincidence is deployed on the ground. The detectors may be sensitive to any of the components of the shower - the array at Volcano Ranch used plastic scintillators to detect the electron component whereas the Haverah Park array uses deep water tanks to record a mixture of the electron and muon components. The distribution of detectors is chosen appropriate to the energy of the showers to be studied. An array with a large collecting area will have a good data collection rate for higher energy showers but the spacing between the detectors determines a minimum energy below which the particles in the air shower cannot trigger more than one detector. Only at lower energies (below ~ 10^{15}eV) is the hadron core investigated since its limited lateral spread does not overcome the problems of data collection caused by the steepness of the primary energy spectrum.

Secondary emission from the air shower may also be a source of measurements of the cascade and the present work is concerned with the most widely used of these - Cerenkov light produced by relativistic electrons in the shower. The production of Cerenkov light in cosmic ray showers is described in Chapter 2. Measurements have also been made of radio emission from the shower. A novel technique is being implemented by the "Fly's Eye" experiment (Bergeson et al. (1977)) which detects the scintillation light produced by de-excitation of the air nuclei along the path of the air shower. The value of this technique is that it does not demand that the core of the shower lands within the array boundary and therefore the detector has a much greater collecting area than a conventional array. This should prove an effective way of detecting high energy showers ($\sim 10^{19}$eV).

1.5.3 Fluctuations

An extensive air shower is the result of a stochastic process in the distance travelled by particles between interactions. The effect is to produce showers which, on average, behave consistently but which, in individual cases, fluctuate from the average behaviour. It has long been realised that the magnitude of these fluctuations could be as important in detecting the nature of the initiating particle as the average characteristics.

The most significant factor in determining fluctuations in shower development is the depth at which the early interactions take place. The gross measure of shower development, used in the present work, is the depth at which the electron shower maximises, t_{max}, and this reflects these early interactions.

The fact that the mean depth of maximum and the size of fluctuations changes with the mass of the primary particle can be seen by considering a simple superposition model of the development of showers initiated by heavy nuclei. This assumes that the nucleus fragments at the first interaction and each nucleon initiates its own sub-shower thus producing an earlier shower development and averaging out the effects of individual fluctuations. (While the superposition model has been shown to be an oversimplification of the breakup of the primary particle (Dixon and Turver (1974)) the result is similar with a more realistic model.) A flux consisting of heavy primaries would therefore exhibit smaller fluctuations in t_{max} than a predominantly protonic flux.

The distribution of t_{max} from which a given shower is sampled is characteristic of the mass of the initiating particle. Thus the fluctuation in t_{max} obtained from a mixed primary mass composition is a combination of the distribution characteristic of each of the components in the primary flux. The fluctuations are therefore enhanced by the spread in mean depth of maximum as well as the intrinsic fluctuation due to the stochastic nature of shower development.

The most recent extensive air shower observations have concentrated on identifying parameters available from ground based measurements which reflect the depth of cascade maximum and which can be determined with sufficient accuracy to show the distribution due to shower development. The measurements described in the present work determine both the average value of $\overline{t_{max}}$ and fluctuation Δt_{max} which reflect the primary mass composition.

1.6 The Scope of the Present Work

The present work reports measurements made by the Cerenkov Light Detector Array located at Dugway Proving Grounds, Utah. The particular area of study described in the present work is the analysis of the lateral distribution of the Cerenkov light component of high energy cosmic rays ($\sim 10^{17}$eV) and its interpretation as a measure of the longitudinal development of the shower. The specific measurement made is of the depth at which the showers maximised and this is related to the primary mass composition.

In Chapter 2 the background to the study of Cerenkov light is presented together with an outline of the method and results of computer simulations of the development of the air shower and the associated Cerenkov light signal. These simulations are used to interpret the data collected by the Dugway array.

Chapter 3 contains a description of the operation of the Dugway Cerenkov Light Detector Array. The calibration procedures are also outlined and a general summary of the data collected by the array is presented.

The main analysis procedures developed to provide a coherent and reliable dataset from which to deduce depth of maximum measurements are reported in Chapter 4. Emphasis is placed on the accurate interrelation of the detector gains and on accounting for experimental uncertainty in reconstructing the lateral distribution shape. The justification for the choice of parameter sensitive to depth of maximum and primary energy estimator is presented together with the method used to determine their values. Finally the effects of selection bias and sampling errors in the determination of the depth-sensitive parameter are investigated.

In Chapter 5 the results of the analysis of data presented in Chapter 4 are presented and interpreted as measurements of depth of maximum. The mean depth of maximum, $\overline{t_{max}}$ and fluctuation, Δt_{max}, are calculated for the energy range accessible to the largest configuration of the Dugway array ($\sim 10^{17}$eV). Other depth of maximum measures are investigated to show the consistency in interpretation which the computer simulation results provide.

All the depth of maximum determinations from the Dugway array are collected in Chapter 6 and comparison with the results of computer simulations allow certain conclusions about the hadronic interactions and the primary mass composition to be drawn on the basis of the simultaneous determination of mean depth of maximum and fluctuations in depth of maximum.

Chapter 7 concludes by comparing other current measurements of $\overline{t_{max}}$ and Δt_{max} with the results from the Dugway Cerenkov Light Detector Array. This shows the measurement of depth of maximum over 10^{15} - 10^{19}eV and the consequences of these results as an indication of primary mass composition are discussed.

CHAPTER 2

CERENKOV LIGHT

2.1 Introduction

The detection and measurement of the Cerenkov radiation associated with high energy particles has been widely used over the past thirty years, both in accelerator experiments and in observations of cosmic ray showers, to investigate the interactions between these particles. The information available from such measurements is dependent on the production mechanism of Cerenkov radiation and the detection system used. In this chapter a brief description of the Cerenkov light phenomenon is given with a discussion of how a Cerenkov light signal builds up in association with an extensive air shower. Early measurements of fast light pulses from the night sky confirmed the gross features of the Cerenkov light shower and led to theoretical consideration of how the detailed structure of the light signal would reflect the growth and decay of the particle shower - in particular how light density measurements made on the ground could determine characteristics of the particle which produced the shower. Interpretation of air shower data is usually based on rigorous computer simulations of shower production and for this reason calculations of the Cerenkov light in large showers were carried out. Such simulations allow assessment of the sensitivity to the initiating particle and the model for particle interaction and therefore the model and mass dependences of the shower characteristics can be found. In this experiment a simulation study specifically tailored to the location and construction of the Dugway Cerenkov Light Detector Array was undertaken. (It also produced results of much wider applicability allowing other air shower experiments to be interpreted through a consistent set of calculations). The aim of the study was initially to identify the measurable parameters which would give the greatest mass dependence with insensitivity to interaction model and subsequently to provide the framework for interpretation of the results obtained from the experiment. Since the experiment depends so heavily on this simulation, a description of the calculation is given in this chapter and its predictions displayed.

The chapter finally gives a summary of recent Cerenkov light experiments which have been designed to detect sensitivity to the details of air shower development. This allows a comparison between the type of information available from the present experiment and that from other observers. In Chapter 7 the results of the present experiment will be related to these other observations.

2.2 Essential Features of Cerenkov Light

The phenomenon of Cerenkov light was first noticed by Mallet (1926) as the bluish light produced by the products of radioactive decay passing through dense dielectrics. Independently, Cerenkov (1934) started a series of experiments establishing the light as a phenomenon quite different from fluorescence, also associated with radioactive decay. The observed radiation was seen to be produced by fast electrons moving through the medium, the intensity being dependent on the path length and the light being emitted only in the same sense as the motion of the particles, indeed in a cone about the path of the radiating particle.

A theoretical explanation of these effects was given by Frank and Tamm (1937) who described the radiation satisfactorily in the arguments of classical physics and the latter part of Cerenkov's work was devoted to confirming the predictions of this theory. A complete quantum description was presented by, among others, Ginzberg (1940). The following gives a qualitative description of the phenomenon and is drawn from the reviews by Jelley (1958) and Boley (1964).

Cerenkov radiation is essentially a shock wave produced by a charged particle moving through a dielectric at a velocity greater than the phase velocity of light in that medium. The charged particle produces transient local polarisation of the atoms of the medium. For a slow moving particle this polarisation is symmetric and hence no resultant field is produced. However, at velocities comparable with that of light, the polarisation is assymmetric in front of and behind the particle and this results in a radiated pulse. Constructive interference occurs only if the velocity of the particle is greater than the phase velocity of light in the medium. Cerenkov radiation is then observed. Figure 2.1 shows the Huygens construction of the generated light pulse and demonstrates the coherence condition.

Figure 2.1 The Huygen's construction for the production of Cerenkov light from a particle with velocity v in in a medium with refractive index n.

$v < c/n$

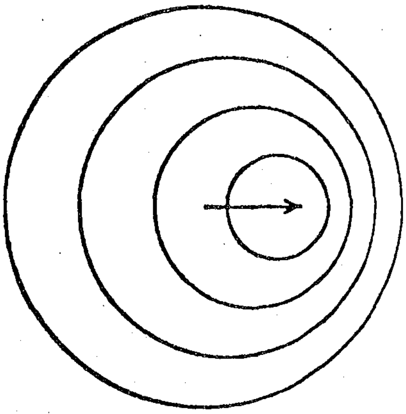

$v = c/n$

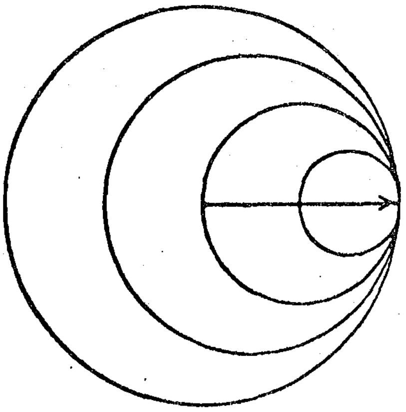

$v > c/n$

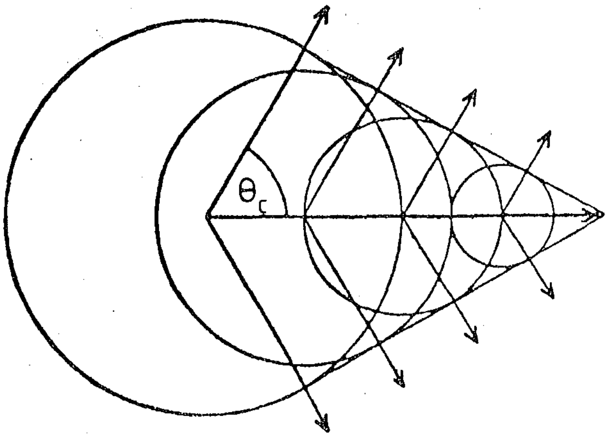

The essential features of Cerenkov radiation are:-

(1) the energy threshold - the velocity requirement demands that $\beta n > 1$ (where as usual n is the refractive index and β is the particle velocity divided by the velocity of light in vacuo),

(2) the direction of emission - Cerenkov light is emitted in a cone about the direction of motion of the radiating particle determined by the coherence condition

$$\cos\vartheta = {}^{1}/_{\beta n} \qquad (2.1)$$

which gives a maximum angle of emission

$$\cos\vartheta_{max} = {}^{1}/_{n} \qquad (2.2)$$

and the light is polarised with the E vector perpendicular to the surface of the cone,

(3) the wavelength distribution - Frank and Tamm give the expression for energy loss per unit path length for a particle of charge e moving at a velocity β through a medium of refractive index n as

$$\frac{dE}{dh} = 4\pi^2 e^2 \int (1 - \frac{1}{\beta^2 n^2}) \frac{d\lambda}{\lambda^3} \qquad (2.3)$$

This shows that the spectral distribution falls away as ${}^{1}/_{\lambda^2}$ leading to predominantly blue light being produced.

2.3 Cerenkov Light in Cosmic Ray Showers

It was Blackett (1948) who first suggested that the single particle flux of cosmic rays could fulfil the conditions for the production of Cerenkov light in the atmosphere and that this would contribute about 10^{-4} of the total sky brightness. The refractive index of air at sea level is 1.00029 which means that electrons of energy 21 MeV attain the threshold for production of Cerenkov radiation. The bulk of the electrons in an extensive air shower at sea level have energies above this threshold. The much greater energy thresholds of 4.3×10^3 MeV for muons and 39×10^3 MeV for protons show that the Cerenkov light signal in large showers is essentially a product of the electron cascade alone.

The experiments of Galbraith and Jelley (1953) showed that Cerenkov light was indeed observed in association with extensive air showers. Having made observations on Cerenkov radiation in air at STP in the laboratory they realised that in an extensive air shower the high concentration of energetic particles traversing the atmosphere in a very short time interval would give rise to a fast, intense pulse of light which would stand out clearly against the background sky noise. They confirmed this by making observations of the night sky using a light detector consisting of a photomultiplier at the focus of a parabolic mirror operated in conjunction with an array of particle detectors. As predicted they detected fast light pulses in coincidence with triggers from the particle detectors (Galbraith and Jelley (1953)). Their subsequent investigations at the Pic du Midi Observatory under ideal atmospheric conditions demonstrated that the directionality, wavelength distribution and the polarisation were consistent with Cerenkov light and not with the alternative proposition that the light was produced by ionisation or ionic recombination.

Measurements of light pulses below known cloud bases sought to establish the height of origin of the light (Galbraith and Jelley (1955), Nesterova and Chudakov (1955) and White et al. (1961)). The last group claimed that most of the light originated below 2 km in conflict with the other results and with the then available theoretical ideas. However, these measurements were made within 50m of the shower core and present shower simulations predict that at small core distances most of the observed light does indeed originate low in the atmosphere.

These and related experiments up to 1955 established the characteristics of atmospheric Cerenkov light. Experimental and theoretical work moved on to consider what the optimum measurable parameters of the light shower were and how these might reveal the longitudinal cascade of the air shower or act as a worthwhile estimator of the energy of the initiating particle. The particular interest in the Cerenkov light component rests on the ability of the Cerenkov photons to penetrate from their height of origin to the observation level. Because of the low refractive index of air, the maximum angle of emission of the photons is 1.3° and so the light accurately follows the path of the radiating electron. While the photon then penetrates through the atmosphere to observation level carrying this angular information from its height of origin, the radiating electron will probably undergo many interactions with particles in the atmosphere. Hence the ground based measurements of Cerenkov light flux give a record of the whole cascade while electron measurements sample only the local status of the air shower.

Observations of Cerenkov light carry the further advantage that the number of photons is large (see Figure 2.2) and, even given the reduction due to the detection efficiency of the photomultiplier, a Cerenkov light experiment is freed from the problems of counting statistics. Balanced against these advantages is the disadvantage that Cerenkov light detectors must operate under clear moonless night skies whereas an array of particle detectors is continuously operable. Hence the quality of Cerenkov radiation measurements with a high information content is set against the reduced number of observations obtained from an array with a duty cycle of only about 5%.

2.4 Sensitivity to Electron Cascade Development

Having established the ability to measure the Cerenkov light component of cosmic ray showers, experiments were developed to extract information about the development of the shower and hence about the primary particle (see e.g. Kreiger and Bradt (1968)). Shower development is dependent on the rate of energy deposition in the atmosphere (which changes with primary energy, E_p, and the depths at which interactions take place, predominantly the early interactions). The production of the cascade is a statistical process and both the average characteristics and the fluctuations in these characteristics from shower to shower carry information about the development of the shower cascade

Figure 2.2 The lateral distribution at sea level of pions (π), muons (μ), electrons (e), gamma rays (γ) and Cerenkov light photons (C) for a 10^{15}eV shower. (From the simulations of Protheroe (1977)).

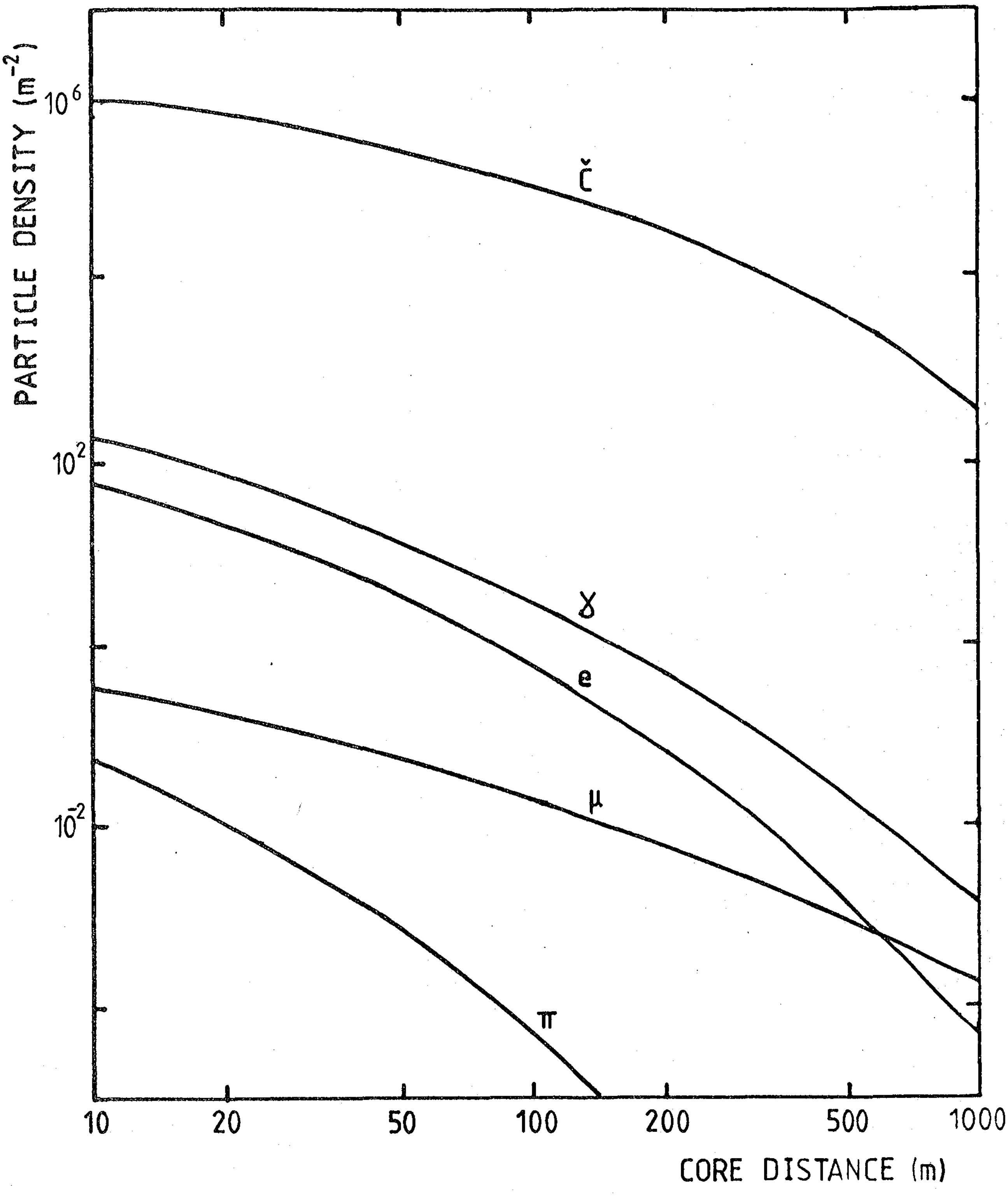
PARTICLE DENSITY (m^{-2})
10^6
10^2
10^{-2}
Č
γ
e
μ
π
10
20
50
100
200
500
1000
CORE DISTANCE (m)

and hence about the primary particle. A gross measure of shower development (though rarely directly attainable) is the depth at which the electron cascade maximises (t_{max}) and it is this which the present experiment seeks to measure and interpret as an indication of primary mass composition.

The measurement $\frac{\partial t_{max}}{\partial E_p}$, the dependence of the mean depth of maximum on the primary energy, E_p, has been termed the Elongation Rate (Linsley, 1977). For a fixed primary energy, fluctuations of any of the observable depth sensitive parameters about their mean value at that energy depend on the statistical spread in the early interactions. The shower initiated by a nuclear primary can be thought of in a simplified picture as the superposition of many nucleon-initiated showers averaging out individual fluctuations in constituent showers. The showers due to a flux of heavy nuclei would therefore be expected to show smaller deviations from average than those caused by a proton flux. It is usual to consider the characteristics of proton-initiated showers compared to those of a heavy nucleus e.g. iron. Clearly any successful mass estimator should be capable of separating primaries of smaller mass differences. These three measurements - the absolute depth of maximum, the Elongation Rate and fluctuations in depth of maximum - provide the evidence against which distributions of primary mass and interaction models may be tested.

Cerenkov light may realistically be thought of as a penetrating component with the signal observed at the ground originating at all depths in the atmosphere and not simply reflecting the local particle density. Thus the Cerenkov light component might be expected to provide a particularly fruitful source of development sensitive measurements. One such effect would be in the lateral spread of light density from the shower core. Photons produced high in the atmosphere from electrons of given angular spread will intersect the ground at a greater distance from the shower core and hence a high developing shower should have a greater lateral spread and consequently flatter lateral distribution than a deep developing one. This simple argument suggests that a measurement of lateral distribution shape in a shower would reflect the depth of shower maximum. The predictions of rigorous shower simulations clearly showing the validity of this are given in Section 2.5 and allow a quantitative interpretation of the measurements.

The experiments of Chudakov et al. (1965) and of Kreiger and Bradt (1969) both investigated the energy dependence of the lateral distribution. In both cases the Cerenkov detectors operated in conjunction with a particle array which provided the basic shower parameters - the position of the core, the size of the shower and in the latter experiment, its arrival direction. Chudakov selected only vertical showers, within 3-4° of the zenith, but obtained average lateral distributions at two altitudes, 3860 m and sea level, thus investigating the effect of moving the observation level away from the depth of shower maximum. If these data were fitted to a size independent structure function they showed fluctuations beyond those attributable to detector uncertainties and this was interpreted as demonstrating statistical spread in the depths of shower development.

Kreiger and Bradt made their observations at Mt. Chacaltya at an altitude of 5200 m, near shower maximum. For instrumental reasons they also chose showers in a narrow zenith angle band (< 30°), and hence did not observe changes in structure function shape due to the change in atmospheric depth which ensues from development through an inclined atmosphere. They used the shower measurements from the BASJE particle array to obtain the mean shower parameters. In addition to obtaining the mean lateral distribution shapes over different energy intervals, they attempted a shower-by-shower analysis by calculating a variable which they termed the "track length integral" (essentially the coefficient, k, of the structure function $k\ f(N,r)$) which was interpreted using simulations to test for shower fluctuations. These experiments were not measuring the depth of maximum directly as in the present experiment but clearly demonstrated changes in the observed shower due to changes in the height above the observation level at which the shower maximised.

Boley (1961) was the first to suggest a further Cerenkov light measurement which was available in a shower - the time structure of the light pulse. This should reflect the growth and decay of the electron shower, if the height at which the light is produced is related to the time at which the light arrives at the ground. His original observations, carried out at the Kitt Peak Observatory (at 2070 m) measured the radius of curvature of the shower front and its mean width, essentially the full width at half maximum of the light pulse.

At the Yakutsk array, Efimov et al. (1973) made measurements of the dependence of pulse shape, e.g. FWHM, on the radial distance from the shower core. This work was stimulated by a geometrical argument that the time interval between stages in the development of the light pulse at a fixed distance from the shower axis relates to the path difference between different stages in cascade development and is therefore a function of the depth of maximum.

This idea was carried further by Orford and Turver (1976) who based their argument on the results of rigorous simulations of the time of arrival of light from electron sub-showers initiated at different depths in the atmosphere. They showed that, beyond 200 m from the core, the light arrived in the same sequence as it had been produced. Thus each pulse contained a record of the shower development - percentage levels in the rise and fall of the pulse corresponding to percentage levels in the development of the cascade. Measurements of the relative time of these percentage levels in pulses at different core distances within a single shower would therefore, allow a geometrical reconstruction of an image of the growth and decay of the shower. This was observed at Haverah Park (described by Hammond et al.(1978)) on a small sample of large showers

(> 10^{17}eV). (A discussion of the Haverah Park Cerenkov Light experiment is given in 2.6 since this was the precursor of the present work and its results provided the design specifications of the Dugway Cerenkov Light Detector Array).

The measurements of lateral distribution and pulse shape present independent determinations of shower development using one shower component. If accurate measurements of these quantities, lateral distribution, pulse shape and depths in the shower image, are available within individual showers then these depth of maximum sensitive parameters should correlate. Analysis of individual showers allows the deviation of each parameters from its mean value, after accounting for systematic changes due to energy and zenith angle, to be calculated and these residual fluctuations to be interpreted as fluctuations in depth of shower maximum. The observation of a correlation between residual fluctuations in different parameters in the same shower provides the ultimate test of this interpretation.

2.5 Computer Simulations

In order to make inferences about the primary particle from extensive air shower measurements it is necessary to make model calculations based on assumptions about the behaviour of the nuclear interactions which generate the cascade. Extensive air showers involve the interactions of particles at energies far beyond those for which the present generation of accelerators provides experimental data (5×10^{13} eV) and hence all shower calculations must involve extrapolation of some assumed relationship between the interaction parameters and the particle energy. The particle mass and the high energy physics are both variables in the calculations and so unambiguous interpretation of data using such calculations may be difficult. However certain combinations of mass and interaction model will be excluded by the accumulation of data on the average behaviour of showers.

Early calculations (Jelley and Galbraith (1953), Gol'danskii and Zhdanov, (1954)) oversimplified the problem, either ignoring the effects of Coulomb scattering in the electron shower or treating it rather simply and in consequence their predicted lateral distributions were widely at variance with observations. Transferring calculations to computers allowed far more complexity to be introduced into the problem, with the modelling of shower development through the atmosphere using Monte Carlo techniques becoming possible. Increasing sophistication gave more realistic results and the latest calculations include atmospheric attentuation of the light, geomagnetic deflection of the electron cascade and produce predictions of the observed shower parameters, both the lateral distribution of the light flux and the shape of the light pulse at different observation depths.

The present experiment is based, both in design and interpretation on the simulations of Protheroe and Turver (1979), extended by McComb and Turver (1981, 1982a). A full description of the method is given in Protheroe (1977) but an outline is given here.

2.5.1 The Hadron Physics

The Cerenkov light shower is produced by relativistic electrons in the air shower and therefore the form of the electron shower dictates the Cerenkov light and is itself dictated by the hadronic showers. The electron shower is fed principally by the decay of neutral pions ($\pi^{\circ} \rightarrow 2\gamma$) which are produced in the interactions between nucleons or pions and air nuclei ($p\,{}^{Z}N_{A}$ and $\pi^{\pm}\,{}^{Z}N_{A}$ collisions). The starting point for simulations of an air shower is hence the production of the hadronic core.

The hadron cascade is described by the equations

$$\frac{dN_{E_o}(E,y)}{dy} = -\frac{N_{E_o}(E,y)}{\lambda_N(E)} + \int_E^{\infty} \frac{F_{NN}(E,E')}{E} \frac{N_{E_o}(E',y)}{\lambda_N(E')} dE' \qquad (2.4)$$

for the nucleon component and

$$\frac{d\Pi_{E_o}(E,y)}{dy} = -\Pi_{E_o}(E,y)\left[\frac{1}{\lambda_{\pi}(E)} + \frac{\varepsilon_{\pi}}{Ey\cos\theta}\right] + \int_E^{\infty} \frac{F_{N\pi^c}(E,E')}{E} \frac{N_{E_o}(E,'y)}{\lambda_N(E')} dE'$$
$$+ \int_E^{\infty} \frac{F_{\pi^c\pi^c}(E,E')}{E} \frac{\Pi_{E_o}(E',y)}{\lambda_{\pi}(E')} dE' \qquad (2.5)$$

for the pion component where $N_{E_o}(E,y)\,dE$ and $\Pi_{E_o}(E,y)dE$ gives the number of nucleons and charged pions at energy between E and E + dE and the atmospheric depth y produced by a primary nucleon of energy E_o. $\lambda_{\pi}(E)$ and $\lambda_N(E)$ are the interaction lengths in air of pions and nucleons related to the inelastic cross-section

$$\text{e.g.} \qquad \sigma_{p\text{-}air} = \frac{2.41 \times 10^4 (\text{mb g cm}^{-2})}{\lambda_{p\text{-}air}\ (\text{g cm}^{-2})} \qquad (2.6)$$

The calculation of the electron cascade in large showers is simplified by treating kaons as pions and strange baryons as nucleons while ignoring completely nucleon-antinucleon pair production. The values of λ_N and λ_π and the production cross-sections F_{NN}, $F_{N\pi}$ and $F_{\pi\pi}$ are obtained by extrapolation from values derived in accelerator experiments using appropriate models. (See Gaisser et al., 1978).

The scaling hypothesis (Feynman, 1969) provides such an extrapolation, that

$$\lim_{E_o \to \infty} F_{ab}(E,E_o) \longrightarrow F_{ab}(E/E_o)$$

(for the interaction a + air nucleus ⟶ b + anything) and this has provided the standard model for the present simulations. Consequences of the scaling model are a mean multiplicity of produced pions which rises as log s (where s is the square of the centre of momentum energy) and an inelastic cross-section which remain constant.

On the other hand, accelerator data can be explained satisfactorily by developments of the Landau hydrodynamical model (Landau, 1953) which gives a multiplicity dependence rising faster than log s due to enhanced pion production in the central region. An adaptation of this giving most pion production is the enhanced model producing a multiplicity $E^{\frac{1}{3}}$ and both the Landau and the enhanced Landau models have been considered. In addition accelerator data indicates that the inelastic cross-section rises slowly with energy while the scaling model indicates a constant cross-section. Energy dependence has therefore been introduced allowing the inelastic cross-section to rise as log S or $\log^2 S$, a reasonable and a more extreme extrapolation of accelerator data. Table 2.1 summarises the models employed.

A further problem is how to treat a primary particle

Table 2.1

Summary of the models of high energy interactions used in the simulations of McComb and Turver (1981, 1982a).

		Central Region Multiplicity		
		scaling	$E^{\frac{1}{4}}$	$E^{\frac{1}{3}}$
Interaction Cross-Section	constant	x	x	x
	rising as log s	x	x	x
	rising as $\log^2$ s	x	x	x

other than a proton. The most commonly used model is the superposition model where the cascade due to a nucleus of mass A and energy E is assumed to produce a shower equivalent to A showers due to nucleons of energy E/A. Dixon and Turver (1974) showed that while this was satisfactory for producing average behaviour it underestimated fluctuations in cascade development and a fragmentation process has been used which allows the progressive break-up of the nucleus based on the data of Freier and Waddington (1975).

For each model, primaries of two atomic mass number have been used (A = 1 and A = 56) and the showers have been simulated at four zenith angles (0°, 35°, 45° and 60°) and 4 primary energies (10^{15}, 10^{16}, 10^{17} and 10^{18}eV). The pion production spectrum was calculated in one dimension using a Monte Carlo technique for the high energy pions and then below a certain threshold (10^{-3} of the primary nucleus energy) a numerical solution was used. The produced pions were stored according to type (charged or neutral), production depth and energy and this store formed the basis of calculations of all other shower components. The average cascades for given input parameters (mass, model, angle and energy) were built up by averaging over 50 showers.

2.5.2 The Electron Cascade

The electron-photon cascade develops by way of the processes of bremsstrahlung and pair production which dominate over collision processes at high energy. Analytic solutions for the propogation are possible using certain simplifying assumptions, usually the approximations stated by Rossi and Greisen (1941) - the so-called Approximation A where only the radiation processes are considered, or Approximation B where a simple allowance is also made for ionisation losses. Calculations of Cerenkov light production demanded more detail of the individual electron track then such analytic solutions provide. However the high energy part of the shower (energy > 75 GeV) may be adequately treated using the approximations and was calculated using a step-by-step method under Approximation A in which both simplifications are valid at these high energies.

A databank was established containing the detail of showers initiated by γ rays and electrons injected with different energies at various atmospheric depths. In this case the cascade development was followed through a representation of a real atmosphere using a full three dimensional Monte Carlo treatment which included accurate treatment of the low energy collision processes. Deflection of the electrons by the geomagnetic field was also considered. These results for each injection height and energy were averaged over a number of simulations to avoid biases due to extreme fluctuations within the databank.

The results of the high energy calculation were combined with the contents of the databank to build up the full electron shower in extensive air showers of energy 10^{15} - 10^{18}eV.

2.5.3 Cerenkov Light in the Air Shower

The Cerenkov light component in large EAS was calculated simultaneously with the electron photon shower. The details of the Cerenkov photon distribution at a range of observation levels were included in the databank of γ ray and electron initiated showers. To derive the Cerenkov light the electron tracks were split into short straight segments and the resultant Cerenkov photons were assumed to emanate from the centre of each short segment. The photons were followed down to observation level where their lateral distribution was recorded. In addition, the time of production was also stored so that the distribution of the time of arrival at observation level could be calculated, i.e. the shape of the Cerenkov light pulse, at all locations in the shower.

The observed Cerenkov signal is dependent on the atmosphere in which it is produced, both in the generation and in the penetration of the photons. The effects of Rayleigh scattering, aerosol scattering and ozone absorption were included using the model atmosphere of Elterman (1968). The representation of the atmosphere used was appropriate to the location of the Dugway array at the season when data were recorded (U.S. standard atmosphere, 40°N, winter warm).

In order to facilitate interpretation of the experimental data from the Dugway array, the time and wavelength response of the detector system (the RCA 4522 photomultiplier and associated electronics) was convoluted with the calculated signal. This represents an important stage, since the alternative - deconvolution of the measured pulses - is not unique.

2.5.4 Results

One of the aims of the computer simulations was to demonstrate the sensitivity of measurable ground parameters to the atomic mass number of the particle initiating the shower. In Figure 2.3 typical calculated lateral distributions are shown. The different shapes of the distribution arise from the range of depths of shower maximum appropriate to the different energies of the initiating particle. In this case a standard scaling model was used with an iron nucleus injected into the atmosphere at four different zenith angles at energies 10^{15} to 10^{18}eV and observed at 862 gcm^{-2} (the depth of the Dugway array). Similar results are available from the six models specified in Table 2.1 and two primary particles (A = 1 and A = 56). The lateral distribution was based on calculations of the density at 20 core distances between 0 and 1000 m, averaged over 50 showers. After careful consideration the parameter chosen to quantify the steepness of the lateral distribution was the ratio between the light density at two core distances. (The parameter is called hereafter $R(r_1,r_2)$ where r_1 and r_2 are the distances of the measurements). The selection of suitable distances is a balance between sensitivity - the further spaced the chosen distances obviously the more sensitive - and the available measurements which depend on the extent of the shower and the size and geometry of the array. Choosing $R(r_1,r_2)$ as the sensitive parameter bypasses the problem of finding a function to represent perfectly the lateral distribution and then using the

Figure 2.3 The lateral distribution of Cerenkov light at three primary energies and a range of zenith angles observed at an atmospheric depth of 862 g cm^{-2}. The calculation used a scaling model to describe the hadronic interactions for an iron nucleus initiated shower.

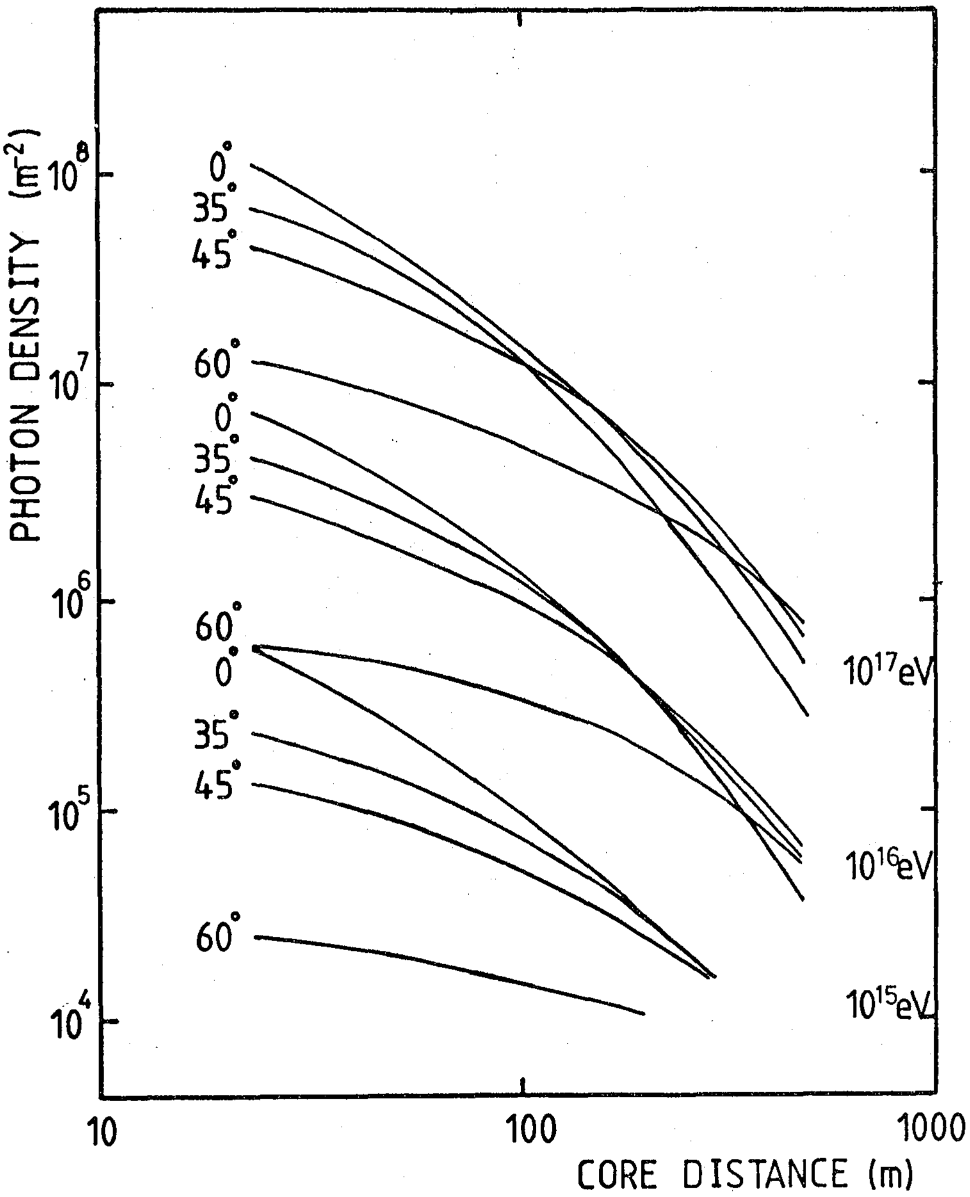
PHOTON DENSITY (m^{-2})
10^8
10^7
10^6
10^5
10^4
10
100
1000
CORE DISTANCE (m)
0°
35°
45°
60°
0°
35°
45°
60°
0°
35°
45°
60°
10^{17}eV
10^{16}eV
10^{15}eV

steepness parameter of the function. The present simulations suggest that no single function would be appropriate at all zenith angles. McComb and Turver (1981) have fitted a function of the form $\Phi(r) = A(r + r_0)^{-\eta}$, (where A and η are adjustable and r_0 is chosen empirically at 50 m), to densities between 50 m and 350 m and have demonstrated the dependence of η on depth of shower maximum. Where it is possible to reproduce the core distance range considered exactly, as in a simulation study, the fact that the shape measure is dependent on the core distance range sampled does not influence the significance of the η and depth of maximum relationship. Experimental data collected from a real array of detectors however cannot reproduce core distance distributions from shower to shower and therefore it has been appropriate to chose the above parameter $R(r_1, r_2)$ where the emphasis is on measuring two spot densities independent of the detector distribution.

Displayed in Figure 2.4 is the ratio between the density at 100 m and that at 250 m as a function of depth of maximum. (This is the ratio chosen in the present study for the highest energy showers). The figure includes predicted $R(r_1, r_2)$ ratio for a selection of combinations of mass, interaction model and energy, hence producing showers with a wide range of depths of maximum.

The essential feature shown in this figure is that there is a near unique relationship between the ground parameter, $R(r_1, r_2)$ and the depth of maximum independent of the mass or interaction model chosen. McComb and Turver (1981) suggest that the Cerenkov light lateral distribution

Figure 2.4 The ratio of the light signal at 100 m and at 250 m, R(100m, 250m), at an atmospheric depth of 862 g cm^{-2} plotted against depth of cascade maximum. The calculations are for average showers with proton and iron primaries using a range of interaction models and the dependence at different zenith angles is shown.

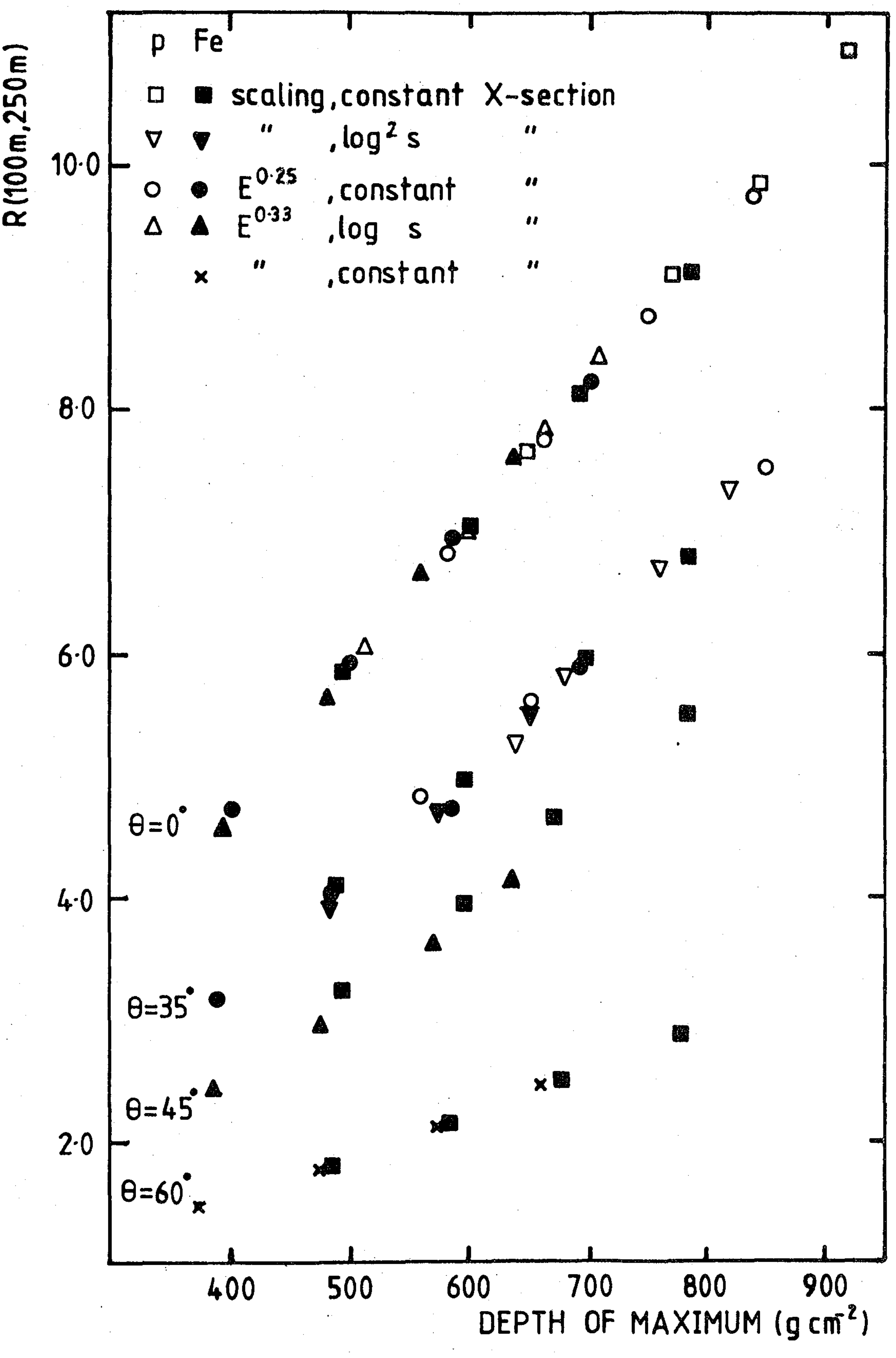

p Fe
□ ■ scaling, constant X-section
▽ ▼ " , log² s "
○ ● E^0·25 , constant "
△ ▲ E^0·33 , log s "
× " , constant "
θ=0°
θ=35°
θ=45°
θ=60°
R(100m,250m)
10·0
8·0
6·0
4·0
2·0
400
500
600
700
800
900
DEPTH OF MAXIMUM (g cm⁻²)

measures the integral of the electron cascade and that the detailed structure, dependent on differences in high energy physics, is lost. Thus the absolute position of maximum development dominates the structure of the shower at observation level. This extremely useful result provides the method of estimating the depth of maximum from measurements of R(100m,250m). (This is also true of other appropriate choices of r_1 and r_2.)

Figure 2.5 shows the relationship between the full width at half maximum of the Cerenkov light pulse at various core distances and the depth of maximum. The full width at half maximum at fixed distance shows the same near model-independent relationship with depth of shower maximum. Other pulse shape parameters are similarly related and are discussed in detail by Chantler (1982).

In Figure 2.6 the zenith angle dependence of R(100m, 250m) at fixed depth of maximum is shown. Interpretation of extensive air showers usually assumes a relationship of the form

$$P = a_o + a_1 \sec\theta + a_2 \log_{10} E_p \qquad (2.7)$$

where P is the measured ground parameter, θ is the zenith angle of the shower and E_p is the energy of the primary particle (see, for example, Craig et al. (1979)). This makes the assumption that changes in the difference between depth of maximum and observation level due to primary energy and zenith angle (where the atmospheric thickness increases as $\sec\theta$) are equivalent and, if this assumption is valid, the elongation rate can be obtained directly. Figure

Figure 2.5 The computed dependence of FWHM for the Cerenkov light pulse recorded by an infinite bandwidth detector system on the depth of cascade maximum at different distances from the shower core and at a range of zenith angles. The relationship is derived from a range of different interaction models with proton and iron primaries. The results are appropriate to an observation level of 862 g cm^{-2}.

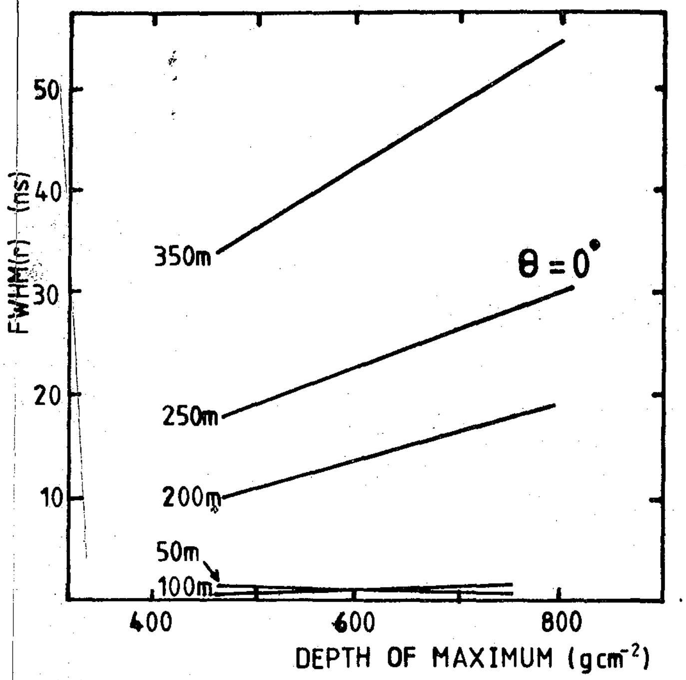
FWHM(r) (ns)
50
40
30
20
10
350m
250m
200m
50m
100m
θ = 0°
400
600
800
DEPTH OF MAXIMUM (gcm^{-2})

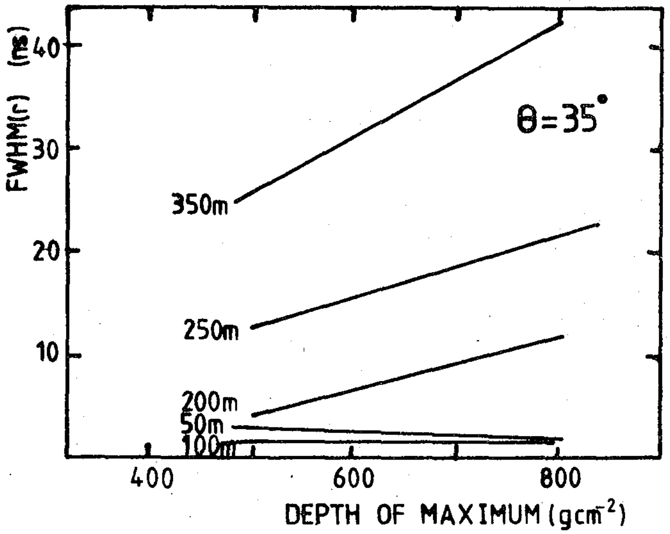
FWHM(r) (ns)
40
30
20
10
350m
250m
200m
50m
100m
θ=35°
400
600
800
DEPTH OF MAXIMUM (gcm^{-2})

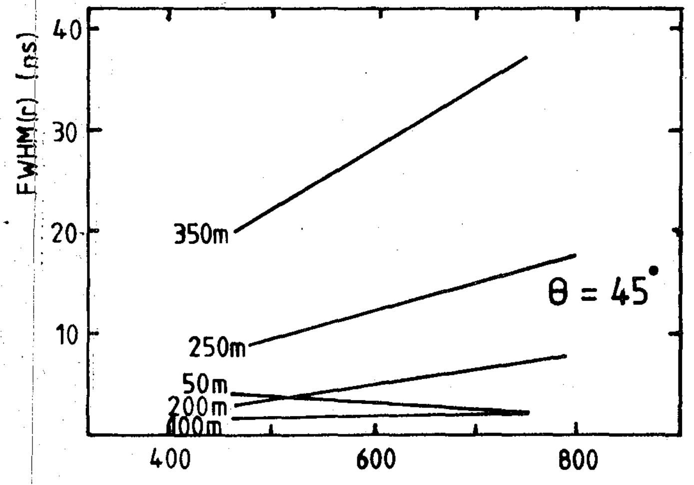
FWHM(r) (ns)
40
30
20
10
350m
250m
50m
200m
100m
θ = 45°
400
600
800
DEPTH OF MAXIMUM (gcm^{-2})

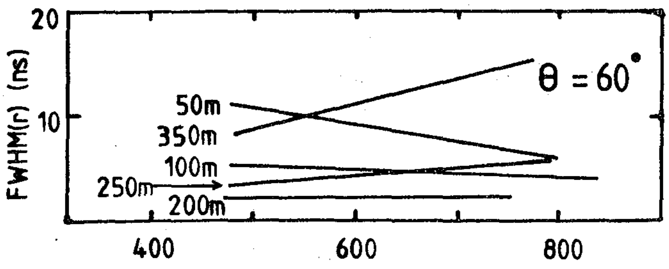
FWHM(r) (ns)
20
10
50m
350m
100m
250m
200m
θ = 60°
400
600
800
DEPTH OF MAXIMUM (gcm^{-2})

Figure 2.6 The calculated zenith angle dependence of the ratio R(100m,250m) for a range of depths of cascade maximum at an observation level of 862 g cm^{-2}. The relationship is virtually independent of the interaction model or the primary particle used.

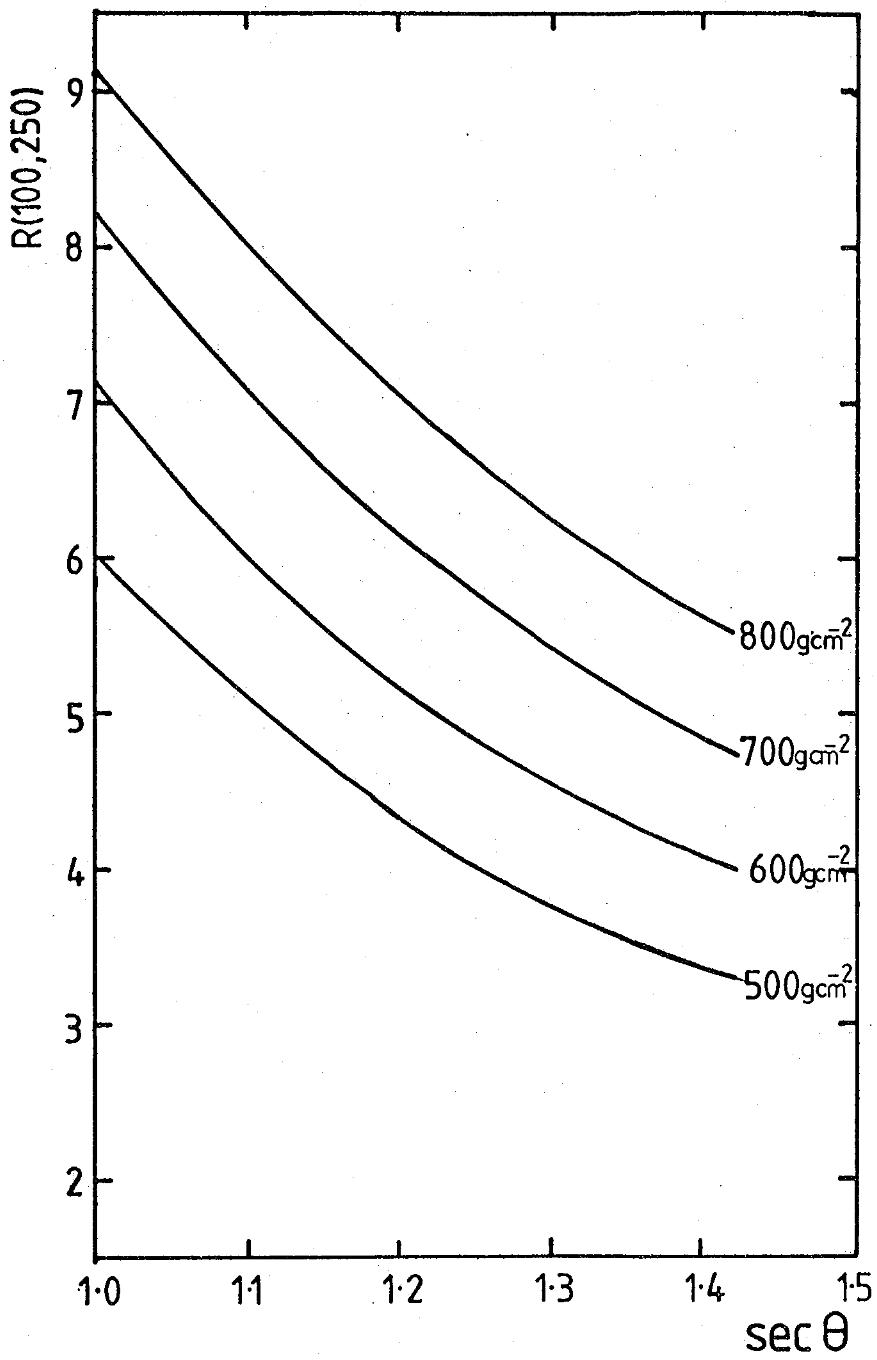
R(100,250)
9
8
7
6
5
4
3
2
1·0
1·1
1·2
1·3
1·4
1·5
sec θ
800gcm⁻²
700gcm⁻²
600gcm⁻²
500gcm⁻²

2.6 shows clearly that this does not hold for the parameter $R(r_1, r_2)$ which does not change linearly with $\sec\theta$. The interpretation therefore demands greater sophistication than the approach specified in equation 2.7. Details of the method used in this experiment are given in Chapter 4.

There is however, a caveat to the use of these simulations in the interpretation of fluctuations. The showers are the result of averaging over many cascades thus removing the effects of individual fluctuations and the assumption must be made that real fluctuating showers show the same depth dependence in the ground parameter. However the fact that the ground parameter is virtually independent of the differences in cascade development due to differences in the high energy physics used gives confidence that statistical fluctuations in the depths of interaction will similarly display the universal relationship between the depth of cascade maximum and the lateral distribution of Cerenkov light density.

This simulation study has clearly shown the power of Cerenkov light measurements as a method of determining the depth of maximum of the electron cascade, independent of the extrapolation of known high energy physics data used.

The earlier results of this series of simulations, described in detail by Protheroe (1977), in which vertical showers only were considered, have already been used in the interpretation of the predecessor of the present experiment, the Haverah Park Cerenkov Light Experiment (see

Protheroe and Turver (1979). It is apposite therefore, to outline the achievements and limitations of that experiment as a prelude to the description of the Dugway Cerenkov Light Detector Array.

2.6 The Haverah Park Cerenkov Light Experiment

Between 1975 and 1977 a Cerenkov light detector array was operated near sea level in conjunction with the Haverah Park particle detector array (see Hammond et al. (1978)). In only 60 hours of good weather operation, information was recorded from showers between 2.10^{17}eV and 2.10^{18}eV. The Cerenkov light shower records were amenable to analysis of the lateral distribution of the light density and pulse shape and to the synchronised timing of the pulse arrival.

Eight five inch photomultipliers, the same type as used in the present work, were spread over an array covering 1 km^2, measuring the Cerenkov light signal in the range 150 - 600 m from the shower core. The time response of this system was measured as 19 ns FWHM pulse from a 2 ns FWHM input pulse. (This should be compared with the 6 ns FWHM response to the same input pulse achieved in the present experiment by transferring from an analogue to a digital data collection system). The core position, energy and arrival direction of each shower were obtained from the University of Leeds analysis of the particle detector array data.

The lateral distribution of the photon density was fitted to a simple power law structure function, ($f(r) \alpha$ $r^{-\eta}$, where r is the distance from the shower core), the exponent η being the parameter examined for depth dependence. The energy and zenith angle dependence of this parameter were observed in the data. Figure 2.7 shows the energy dependence of near vertical showers compared with the work of Diminstein et al. (1972). Interpretation of the energy dependence was undertaken by Protheroe and Turver (1979) producing values of depth of maximum of 680 gcm^{-2} and 800 gcm^{-2} for 2.10^{17}eV and 2.10^{18}eV primary energy showers respectively. The various pulse shape measurements obtained from oscilloscope records of the pulse - the rise time, top time, fall time and full width at half maximum - were seen to show the expected zenith angle dependence and the energy dependence was interpreted as above. A subset of thirty showers gave results from the reconstruction of the direct image of the shower development through the atmosphere. Figures 2.8 and 2.9 show some results of this pulse shape and imaging analysis. Combining the results of all measurements gave depths of 681 ± 20 gcm^{-2} and 766 ± 31 gcm^{-2} for the shower maximum in showers of energies 2.10^{17} and 2.10^{18}eV.

Simulations had suggested that the Cerenkov light signal at 200 m from the core (termed Φ_{200}) should be related to the primary energy for showers detected at sea level and that the parameter is relatively insensitive to the detail of shower development. (This will be further discussed in relation to the primary energy estimator for the present experiment in Section 4.5). Observations made in conjunction with the Haverah Park particle array

Figure 2.7 The lateral distribution of near vertical showers measured by the Haverah Park Cerenkov Light detector Array (Hammond et al. (1978)) (o, Δ) compared with earlier measurements of Diminstein et al. (1972) (▼, ▲). The two sets of measurements are separated by a decade in primary energy.

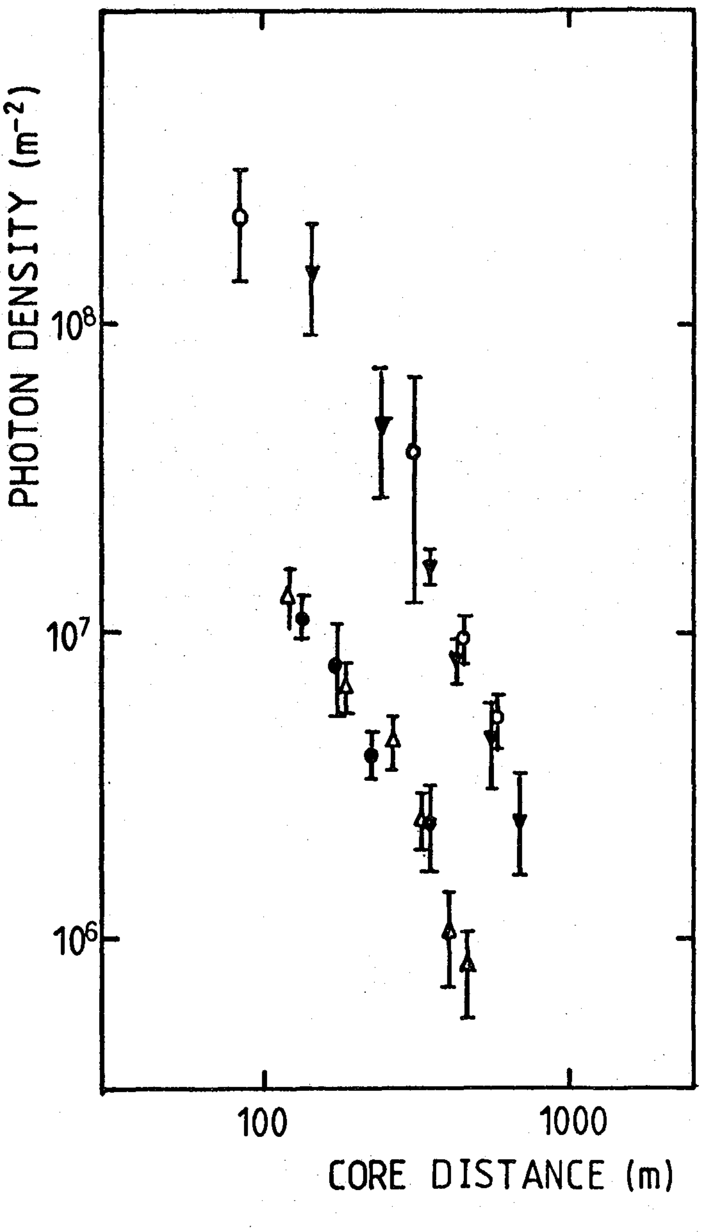
PHOTON DENSITY (m^{-2})
10^8
10^7
10^6
100
1000
CORE DISTANCE (m)

Figure 3.3 The nominal pulse shape sampling times used for the inner and outer ring detectors. The dotted curves represented typical Cerenkov light pulses.

allowed comparison to be made with the well-established primary energy measure ρ_{500} (the deep water Cerenkov tank response at 500 m from the shower core) used for this array and also thought to be development independent. Testing the Cerenkov light signal at different distances against showers ranked in ρ_{500} showed that Φ_{200} correlated strongly with primary energy (see Wellby, 1977). This result was particularly useful since it gave confidence in constructing a Cerenkov detector array operating without a related particle array to supply the primary energy measurement. In addition this provided an inter calibration of the energy measurement of the Haverah Park particle array and the primary energy estimation of the present experiment.

The present work has drawn heavily on the achievements of the Haverah Park Cerenkov Light Experiment. Improved time resolution was seen to be necessary to measure the depth of maximum in individual shower to better than 100 gcm^{-2}, the sensitivity of that experiment (Wellby, 1977). The second limitation was the small data sample caused by the limited periods of clear sky at this site. This was overcome by transferring the work to the clear skies of Northern Utah giving a high data collection rate and therefore good measurement statistics. This suggested the possibility of observing correlations between the different depth sensitive parameters in individual showers.

Even under adverse conditions, the Haverah Park Cerenkov Light Experiment successfully demonstrated the sensitivity to depth of shower maximum of the different Cerenkov light ground parameters and provided measurements of the absolute depth of cascade maximum.

2.7 Other Cerenkov Light Measurements

A number of other Cerenkov light arrays are presently or have recently been operating throughout the world and it is appropriate to mention briefly their construction and the type of measurements they may achieve. This will put the Dugway Cerenkov Light Experiment in context and allow comparison to be made between the results.

2.7.1 The Yakutsk Array

The longest established of the present generation of Cerenkov light experiments is the array operated in conjunction with a scintillator array at sea level at Yakutsk in Siberia USSR (Egorov et al. (1971)). Since 1971 measurements of the lateral distribution of Cerenkov light have been available and in 1973 pulse shape measurements began. The array was designed to measure showers of energy greater than 2.10^{16}eV and to sample the light at distances between 150 m and 700 m from the shower core. Measurements of shower size, core position and arrival direction are available from the associated particle array.

The present form (Kalmykov et al. (1977)) consists of thirteen detectors of the total light density for lateral distribution analysis and five detectors of pulse shape located up to 500 m from the array centre. All photomultipliers view the night sky directly. The time response of the pulse shape measurement system is poorer than that of the Haverah Park and Dugway arrays i.e. 23 ns FWHM for an input pulse of 2ns at the 250 m and 500 m detectors. The typical core distances are however, greater than at Dugway and hence the expected pulse widths are larger and the degrading effects of the system are less important. The intercalibration of the detector gains is achieved by using the signal from single relativistic muons passing through a block of plexiglass.

Data obtained from this array has been compared with that collected by the Haverah Park Cerenkov Light Array and consistency was observed between the two data sets.

2.7.2 University of Adelaide Array

Showers in the energy range 10^{15} to 10^{16}eV are measured by the University of Adelaide at the Buckland Park Air Shower Array (Thornton et al. (1979)). This lower energy region is that investigated in the latter stages of the Dugway experiments. (Original results from this array reported a very high elongation rate (Thornton et al. (1979)) over an energy range then only measured by the University of Adelaide array; the portability of the Dugway detectors allowed one consistent technique to make development sensitive measurements from 10^{15} to above 10^{17} eV and there to overlap the work of the other Cerenkov light detector arrays).

Measurements made before autumn 1979 used nine photomultipliers between 20 m and 300 m from the centre of the scintillator detector array to produce measurements of the lateral distribution of the Cerenkov light shower. One fast response detector (5.3 ns FWHM) was used to make pulse shape measurements. Between 1979 and 1980 two further pulse shape detectors were added allowing direct interpolation of pulse shape at a given distance rather than the model - dependent extrapolation previously necessary.

Lateral distribution measurements span typically 50 to 200 m and the depth sensitive parameter used is the variable b in the expression

$$\Phi(r) = D \exp\left(\frac{-br}{10^4}\right) \quad \text{(Kuhlman \& Clay (1981))}$$

(where Φ is the light density, r is the core distance and D is the normalising constant).

Discussion of these results in relation to those from Dugway will be given in Chapter 7.

2.7.3 Other Measurements

The lowest energy measurements of the Cerenkov light signal are contained in the work of Tornabene (1979) who made lateral distribution determinations at the energies of 2.10^{13}eV and 10^{15}eV. The two different energy measurements were made using the same 10 detector 200 m square array but in the lower energy case each photomultiplier was at the focus of a 1.5 m diameter parabolic mirror acting as flux collector while the higher energy measurement was made with the photomultiplier viewing the sky directly.

Measurements provided a parameter (chosen on the basis of the Durham simulations)

$$P = 20 \cdot \log_{10} (\Phi(50)/ \Phi(150))$$

(where $\Phi(r)$ is the fitted structure function $A \exp\left(\frac{-r}{B}\right)^C$ with A, B and C are variables), which can be inter-related with the interpretation of the data from the Dugway array.

The change from a wide to a narrow opening angle for the detectors between the two energy measurements does however present problems in the reliable interpretation of the low energy point.

2.8 Conclusion

This chapter has sought to supply the background to the present study. The theory of production of Cerenkov light in extensive air showers has been outlined and the significance of the Cerenkov light component as a measurement of shower development has been argued. The results of rigorous computer simulations of air showers have supplied predictions of the dependence of the ground parameters of the light shower on cascade development, principally the depth of maximum of the electron component and demonstrated that Cerenkov light provides an essentially model independent interpretation. Results from the Haverah Park experiment were seen to show the expected dependence without having the resolution to identify primary mass and interaction model. A brief review of present Cerenkov light experiments was also given to allow the results of the present experiment to be put into a wider context in the discussion of Chapter 7.

CHAPTER 3

THE DUGWAY CERENKOV LIGHT DETECTOR ARRAY

3.1 Introduction

The results presented in this thesis were obtained from the Dugway Cerenkov Light Detector Array. This experiment operated for three winters between July 1977 and March 1980 in the Great Salt Lake Desert at Dugway, Utah U.S.A. The array was designed to detect pulses of Cerenkov light from extensive air showers, recording both the light density and the time structure of the pulse. This allowed the reconstruction of several depth sensitive parameters in the one data set.

In this chapter an outline of the design and operation of the array is given. A more detailed description has been given by Shearer (1981) and Chantler et al. (1979).

3.2 Location and Layout of the Array

The efficient detection of Cerenkov light demands clear, cloudless and moonless, night skies and the absence of man made lights. The location of the array was chosen to maximise the hours of operation of the array and the mountain site in the Great Salt Lake Desert in Utah satisfied the darkness and clearness criteria. The precise location was latitude 40° 12' North, longitude 112° 49' West at an altitude of 1451 m, corresponding to a mean atmospheric depth of 862 g cm^{-2}.

The array consisted of eight detectors each containing a fast response photomultiplier tube viewing the night sky directly. The geometrical arrangement is shown in

Figure 3.1. The original layout was two concentric rings of three detectors with radii of 200 m and 400 m located around a central detector. The positions of the detectors on the inner and outer rings were offset by 60° to produce a triangle based layout. Adjacent to the central detector, detector 1 were the central electronics. After the first winter detector 0 was added at the centroid of the triangle delineated by detectors 2, 5 and 7 breaking the symmetry of the array. The data reported in this work was all collected during the second and third season of operation while the array included all eight detectors. The eight detectors were identical in construction but because the inner and outer ring detectors typically collected measurements at different core distances the recording electronics were adjusted to optimise the measurement accuracy.

One of the features of the Cerenkov light detector was its portability and this allowed changes in array size to be made during the last months of operation which dramatically increased the energy range of the experiment giving a total range of 2.10^{15}eV to greater than 10^{18}eV. (Energy assignment is discussed in Chapter 4). While the original array had the outer detectors at 400 m from the central detector, two additional configurations had the outer ring at 200 m and then 100 m with the inner ring dimension reduced similarly. These alterations also allowed the array to operate with two detectors (2 and 0) side by side for a full night to investigate local measurements fluctuations. The coordinates of the array were determined using an infrared tellurometer to an accuracy

Figure 2.9 The Cerenkov light image obtained from synchronised measurements of the time structure of the Cerenkov light signal for a high (■) and a deep (o) developing shower measured at Haverah Park. (From Orford and Turver (1976)).

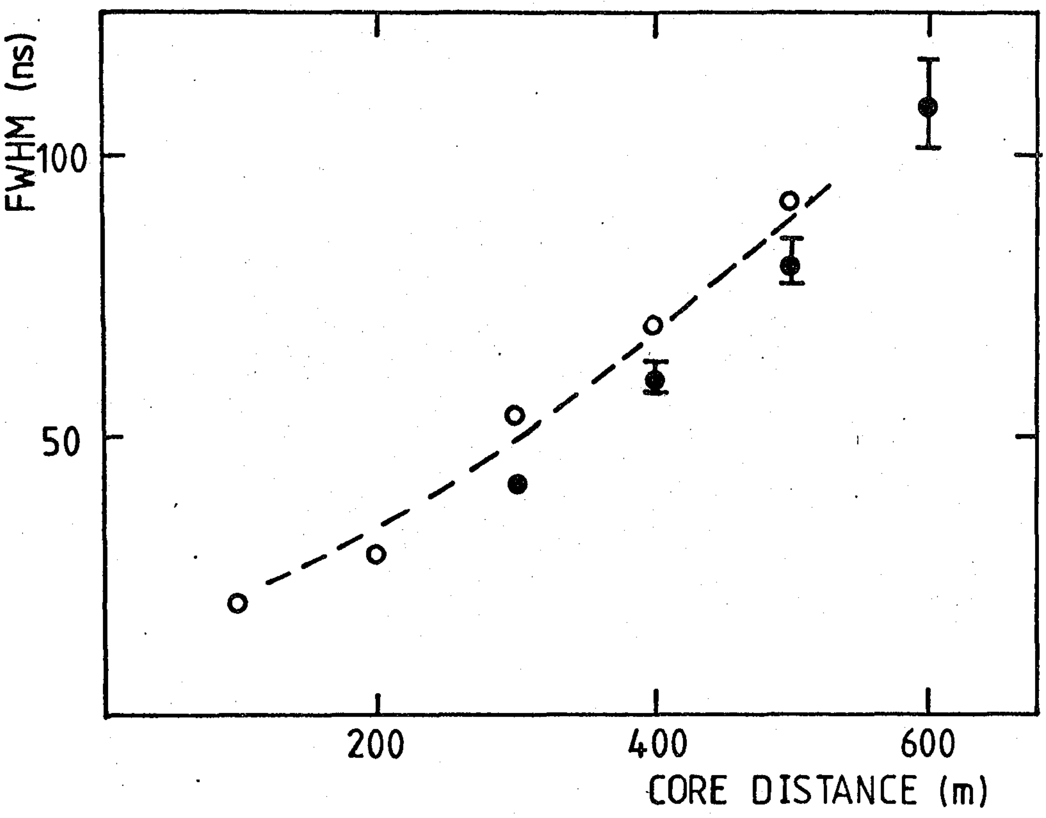
FWHM (ns)
100
50
200
400
600
CORE DISTANCE (m)

Figure 2.8 The average variation of the FWHM of the light pulse with core distance recorded by the Haverah Park Cerenkov Light Detector Array (o) compared with results from the Yakutsk array (Kalmykov et al. (1975)) (●). The dotted line represents simulation predictions for an iron nucleus using a scaling model.

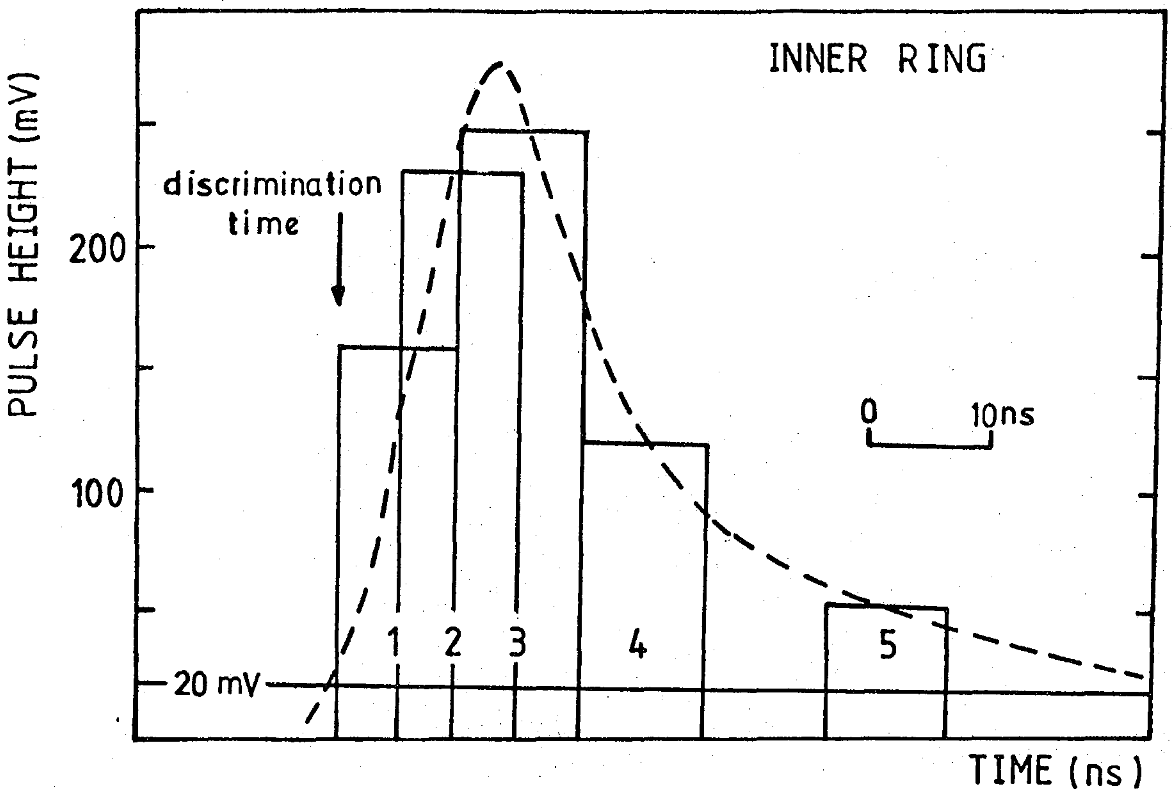
INNER RING
PULSE HEIGHT (mV)
200
100
discrimination time
0
10ns
1
2
3
4
5
20 mV
TIME (ns)

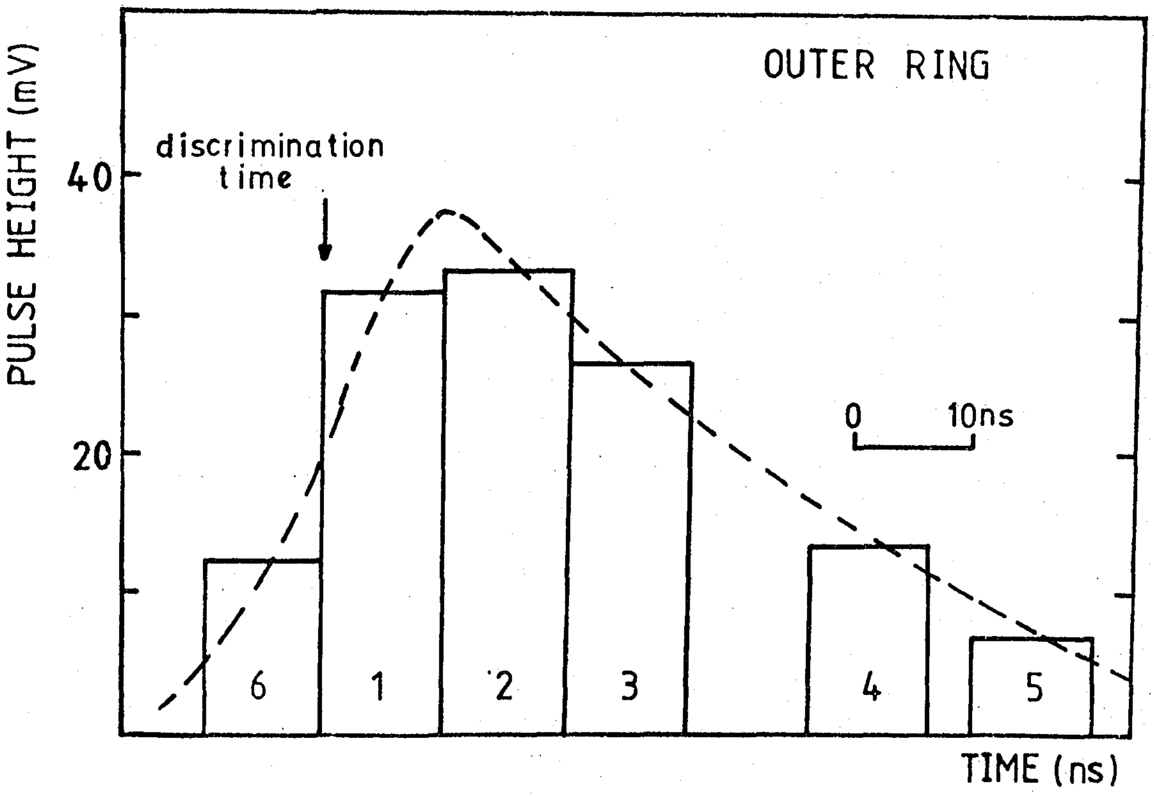
OUTER RING
PULSE HEIGHT (mV)
40
20
discrimination time
0
10ns
6
1
2
3
4
5
TIME (ns)

of better than 5 cm.

The array operated with a high acceptance triggering requirement - coincident pulses on any three of detectors 2, 3, 4, 5, 6 or 7 would cause a shower to be recorded. In practice this meant that triggering was based on triangles of detectors. (Neither detector 0 nor 1 took part in triggering the array at any stage).

In addition to the Cerenkov detectors, 4 1m^2 plastic scintillators were added between 1978-79 to detect the time of arrival and density of particles relative to the Cerenkov light signal. Their positions were shown in Figure 3.1 – accompanying shower particle data were available from October 1979.

3.3 The Shower Record

For each array trigger the following information was required:-

(i) the relative time at which the signal at each detector reached the discrimination level,
(ii) the total light flux in the pulse at each detector,
(iii) measurements of the time structure of each pulse,
(iv) certain environmental information monitoring atmospheric conditions and detector performance,
(v) the absolute time of the coincidence trigger.

A digital recording system was chosen in order to obtain the best time structure information. (This was a development from the Haverah Park Cerenkov Light detectors where each pulse which reached the detector's discrimination level was stored while a coincidence response from the central electronics was awaited. Only after the coincidence signal was generated was the pulse displayed on an oscilloscope and recorded photographically. This delay in recording the signal involved an irreducable degradation of the shape of the pulse and hence a loss of information about the cosmic ray shower development). Each pulse which reached the discrimination level was immediately digitised at the detector and if no coincidence response was received from the central controlling electronics the detector was reset to accept the next signal. The digital record of the time structure was achieved by measuring the light density in five or six 10 ns segments of the pulse at known times relative to the time of discrimination. (The number of segments depended on whether the detector belonged to the inner or the outer ring of the array). This record allowed the pulse shape to be accurately reconstructed in the subsequent analysis.

3.4 The Detector

Each detector consisted of a weatherproof box which housed a photomultiplier, viewing the night sky directly through an ⅛" perspex window, together with its associated electronics. This was connected to the central recording station by a power line and three information cables - one carrying the coincidence signal, one the digital data record and the third monitoring the detector status with certain d.c. signals. While the array was not operating a blind protected the photocathode from the bleaching effects of sunlight and throughout the period of observation it was maintained at a temperature of 20°C against ambient night temperature variations of -10°C to >20°C.

The photomultiplier tube used was a 12cm diameter RCA 4522 with a sensitive area of 122 cm^2 which was surrounded by a Mumetal shield to minimise the effects of geomagnetism and local magnetic anomalies. The signal from the phototube was taken from the 11th dynode allowing the tube to be operated at a low overall gain and hence reduce degradation of the photocathode whilst maintaining the accelerating potential per dynode to minimise transit time jitter. (This design was based on the experience gained from the Haverah Park Cerenkov experiment).

The signal was then amplified by a factor of 100 using 2VV 100 photomultiplier amplifiers (Le Croy Instruments Inc.) Part of the signal was taken from the 1st stage of amplification, after amplification by a factor of 10, and passed directly to the charge to time converter to form the total light density measurements. After the second stage of amplification the signal was separated, part going to the discriminator unit and the remainder to the 8 way fan out to form the basis of pulse shape measurements. The response of the photomultiplier system including the bandwidths of amplifier, fanout and the measuring oscilloscope, to a light pulse of 2ns full width half maximum gave a rise time of 6.2ns and full width half maximum of 5.5ns.

Figure 3.2, from Shearer (1981), shows a schematic diagram of the progress of the signal from the photomultiplier recording.

The discriminator unit, NE 5294 fast discriminator, generated an output which controlled the taking of measurements. A level of 20 mV from the photomultiplier sent a signal to the central coincidence unit, started the time stretcher and initiated the generation of a series of gates to measure segments of the pulse from the fanout. If no coincidence signal was received from the central station within 5 μs the discriminator unit initiated clearance of the signal ready for the next pulse. The propagation time through the discriminator was 20 ns ± 1 ns and this was equalised for all pulse sizes by using a positive feedback system. The E.H.T. of the photomultiplier tubes was adjusted to give an approximately equal triggering rate of less than 10 counts s^{-1}.

From the fanout, 6 parallel outputs went to the charge to time converter unit which sampled the photomultiplier pulse in 10 ns segments. The position of these segments was determined by gated pulses which were generated by the delay shaper module on a signal from the discriminator. (The operation of the QTC is described by Waddoup and Stubbs (1977)). The adjustment of the position of the gates relative to the time of discrimination was effected using trimming cables and Figure 3.3 shows the sampling positions used. The changes in array size in the final season of operation meant a change in the core distance range over which pulses would be measured by a given detector. Hence the positions of the sampling segments were altered to cover the new typical pulse width.

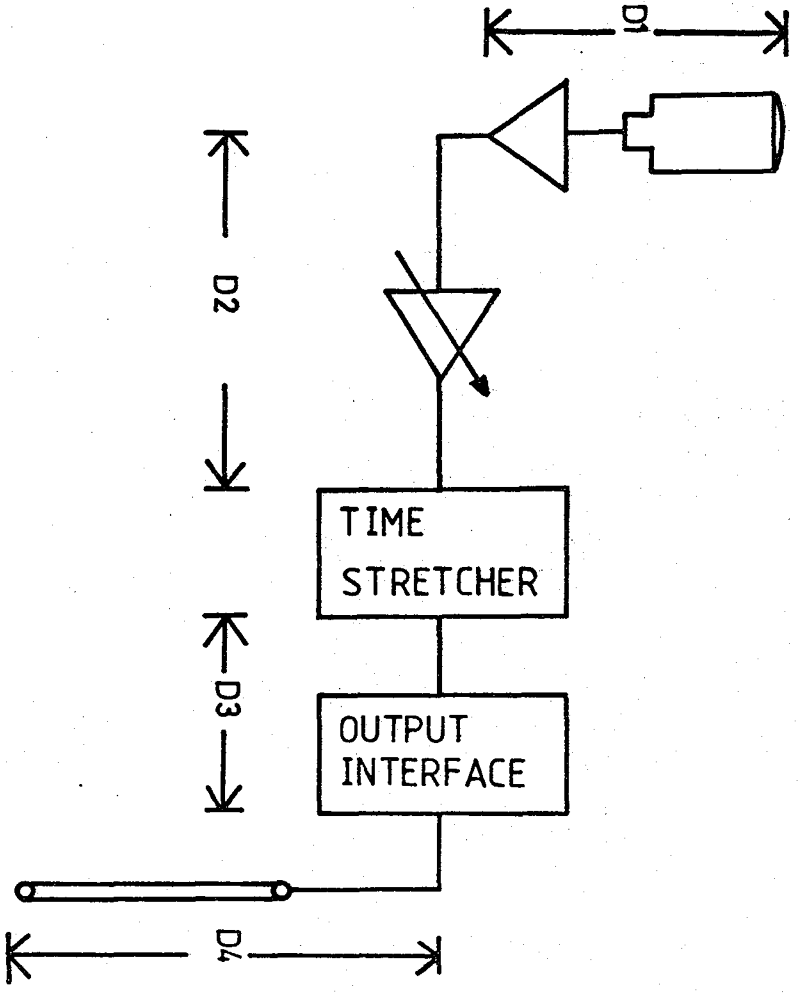
D1
D2
TIME
STRETCHER
D3
OUTPUT
INTERFACE
D4

Figure 3.2 A schematic representation of the progress of the signal through the recording system showing the time delays which were taken into account in synchronising the response from each detector.

D1 - photomultiplier and amplifier delay

D2 - discriminator delay

D3 - output interface delay

D4 - trigger cable delay

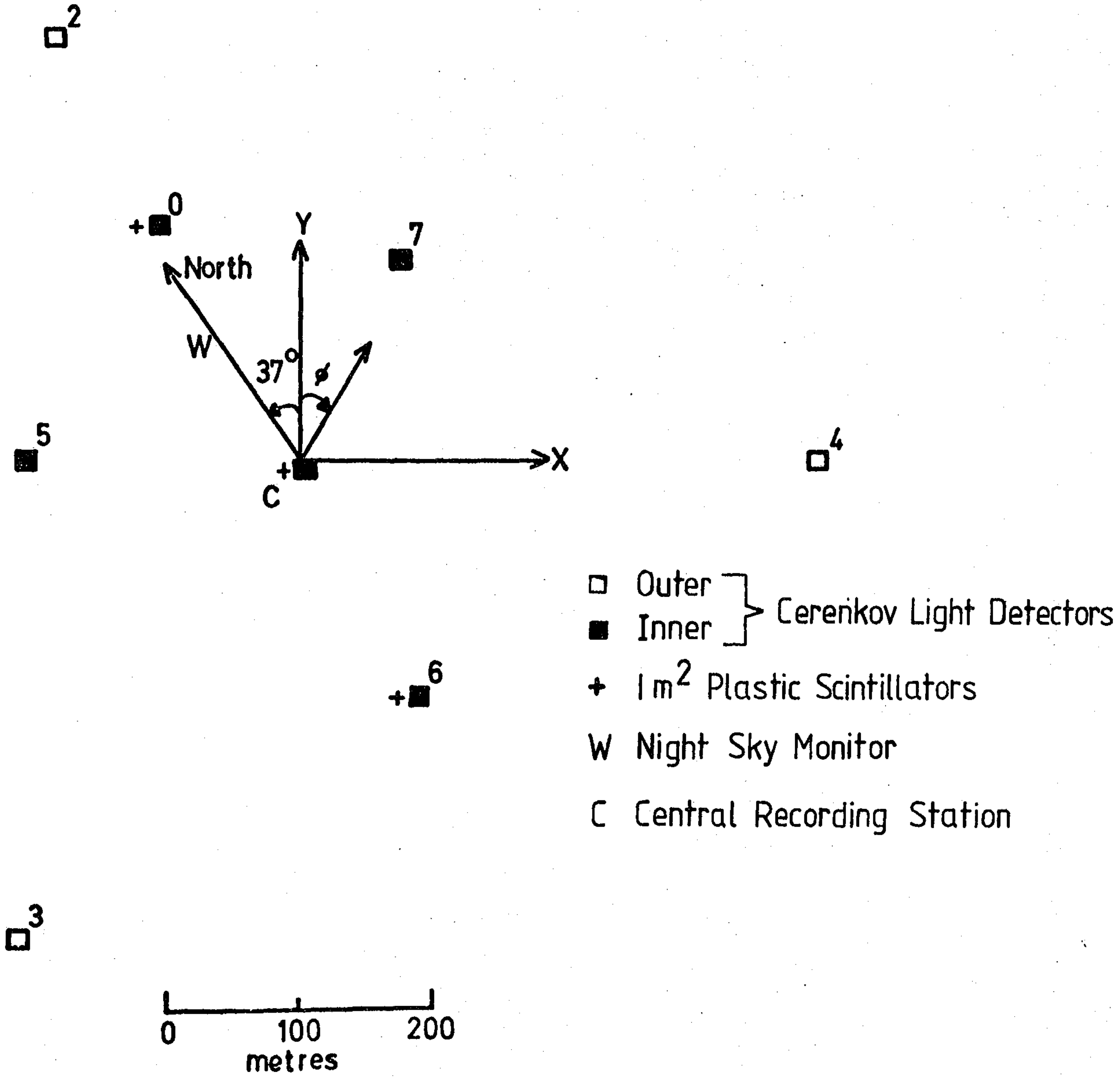
2
0
North
Y
7
W
37°
ø
5
X
4
C
6
3
Outer
Inner
Cerenkov Light Detectors
+ 1 m² Plastic Scintillators
W Night Sky Monitor
C Central Recording Station
0
100
200
metres

Figure 3.1 The layout of the Dugway Cerenkov Light Detector Array in the largest array configuration used to detect showers with energies 10^{17}eV.

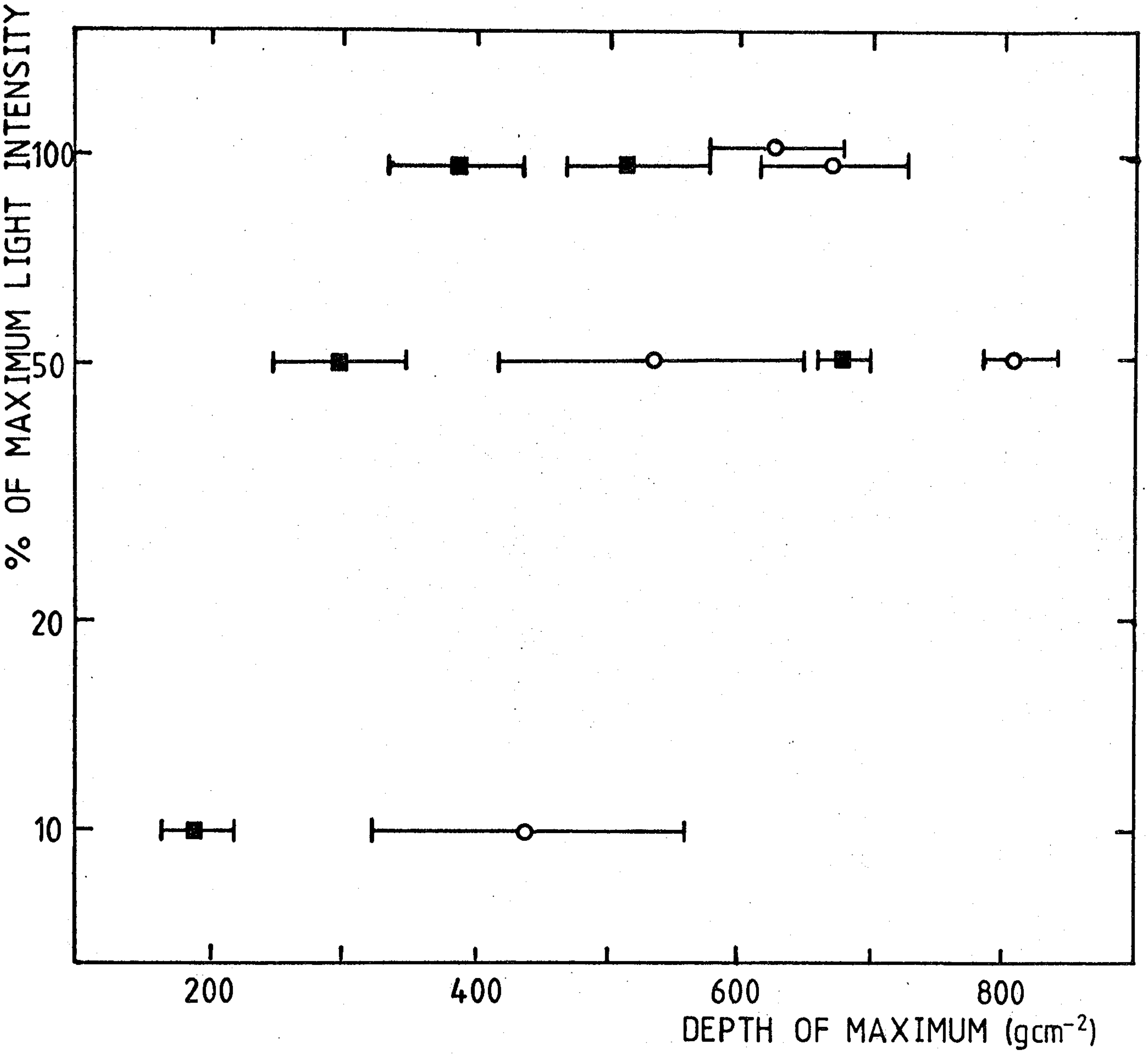
% OF MAXIMUM LIGHT INTENSITY
100
50
20
10
200
400
600
800
DEPTH OF MAXIMUM (gcm^{-2})

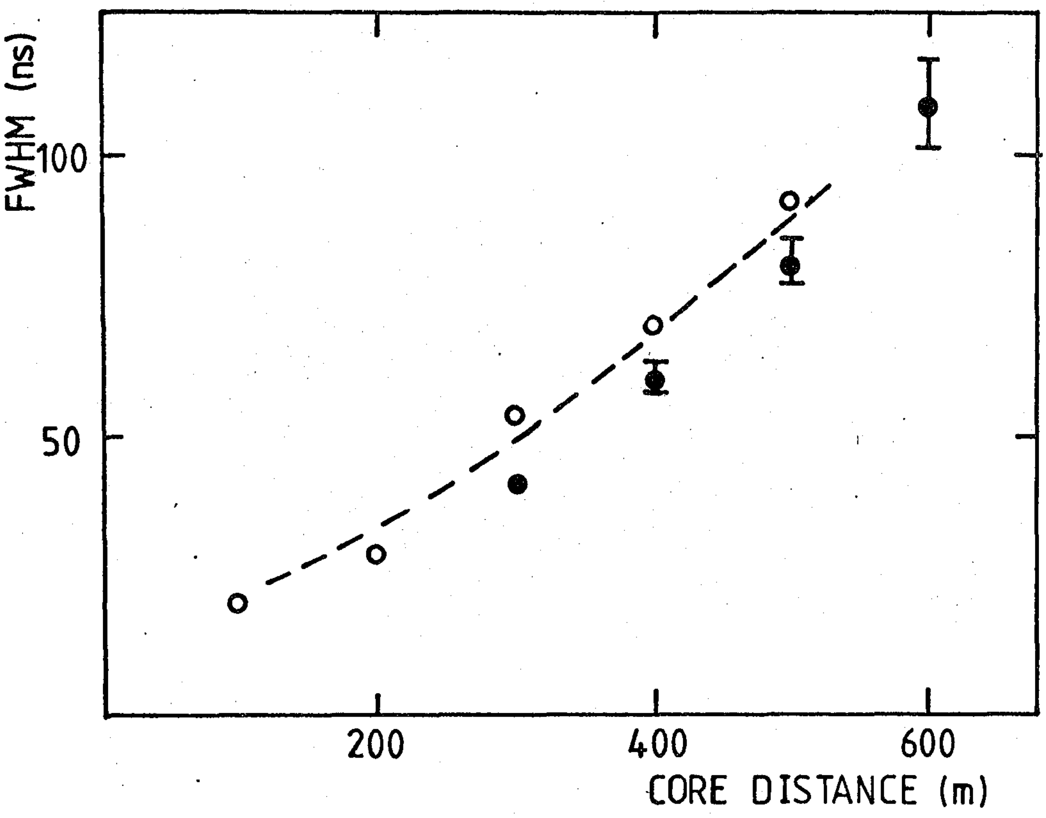
FWHM (ns)
100
50
200
400
600
CORE DISTANCE (m)

Figure 2.8 The average variation of the FWHM of the light pulse with core distance recorded by the Haverah Park Cerenkov Light Detector Array (o) compared with results from the Yakutsk array (Kalmykov et al. (1975)) (●). The dotted line represents simulation predictions for an iron nucleus using a scaling model.

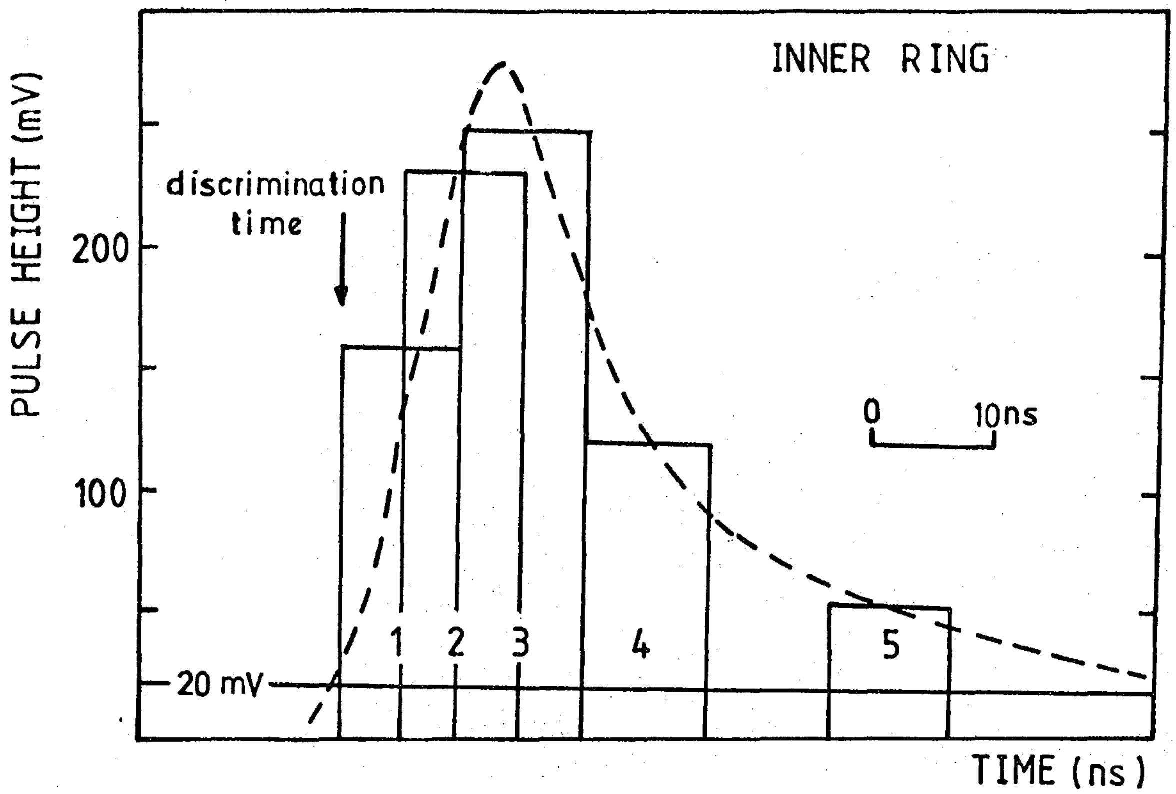
INNER RING
PULSE HEIGHT (mV)
200
100
discrimination time
20 mV
1
2
3
4
5
0
10ns
TIME (ns)

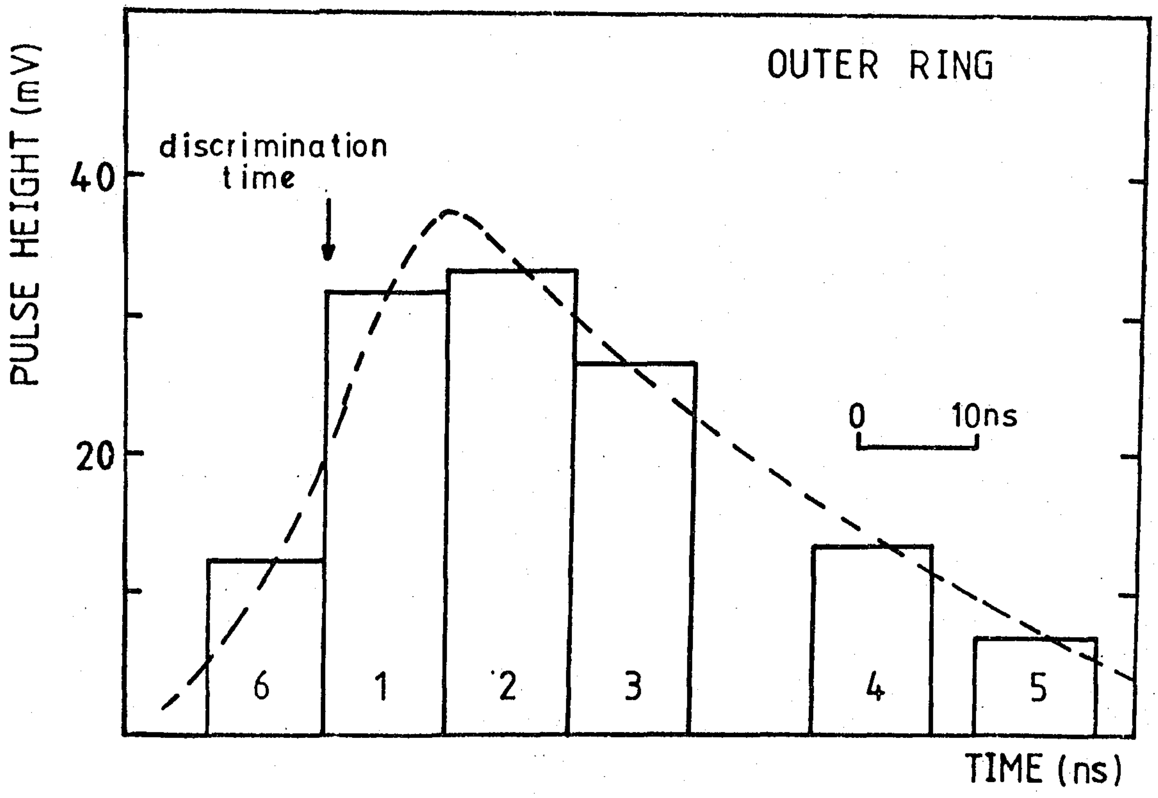
OUTER RING
PULSE HEIGHT (mV)
40
20
discrimination time
6
1
2
3
4
5
0
10ns
TIME (ns)

In addition the pulse from the first stage of amplification went directly to the QTC and was sampled using a gate of width 300 ns hence measuring the total area of the pulse. (This was reduced to 150 ns in the final year of operation giving an improved signal to noise ratio).

The final measurement necessary was the time relative to the coincidence trigger at which each detector responded and this was achieved by using the time stretcher unit (Waddoup and Stubbs, 1976). To obtain a resolution of a few nanoseconds over several microseconds using a 20 MHz crystal controlled clock it was necessary to stretch by a factor of 75 the time interval between the start signal from the discriminator and the stop signal returned from the central electronics.

These measurements - the pulse area, 5 or 6 segments of the pulse and the time - formed the input to the 8 way parallel in , serial out 8 bit scaler described by Waddoup and Stubbs (1977). This scaler was adapted to give a 16 bit word for timing, 6 8 bit words for the integrator and the 5 pulse segments for inner ring detectors or, for the outer ring, 5 8 bit words for integrator and 4 segments leaving 2 slices of 4 bit accuracy.

If no coincidence signal arrived within 5 μs of triggering, the discriminator reset the detector reading for the next pulse. If however a coincidence signal arrived from the central electronics the time stretcher was stopped, the discriminator inhibited from either resetting or accepting further signals, the digitisation was completed and the buffer loaded. Following the coincidence pulse a series of 65 pulses each of duration 1 ms were sent from the central recording station to clock back the digital data. The detector record was completed by the digitisation of the anode current, the temperature of each tube and that of each electronics pack.

3.5 The Central Recording Station

The operation of the array was controlled by a Tektronix 4051 computer which undertook the start up and close down procedures each night and which received, checked and logged the data throughout the night.

An event was recorded if three detector trigger pulses arrived within a coincidence window of 3.6 μs. This was chosen to include large zenith angle events sweeping across the array. The event trigger pulse was returned to each detector simultaneously about 200 ms after the coincidence occurred and the clock pulses sent to retrieve the data. Since the relative not absolute time of each detector trigger was of importance a jitter of 10 ns on this delay was irrelevant. Added to the eight detector responses in the shower record was the absolute time (the clock was set to the time signal broadcast by the radio station WWV each night with sufficient accuracy to calculate the arrival directions of the showers in galactic coordinates).

The record was held in computer storage while certain validity checks were undertaken and the data was then written to magnetic tape. In all the system was "dead" for about 12 seconds during data recording. While the large array was recording showers at a rate of about 15 hr^{-1} this represented a dead-time of 5%. However for the medium sized array with an event rate of 120 hr^{-1} this dead time became significant. The data rate of the small sized array was effectively determined by the system dead-time.

Events on the tape record were blocked into files of 13 showers and 2 check records. One check record consisted of various housekeeping measurements to allow a subsequent assessment of the array performance and the second was a calibration record. In the final season this consisted of a shower trigger signal sent from the central recording station to clock back the readings for zero signal (the pedestal values) allowing both a check on the status of the detector and giving a measurements of the offsets required to decalibrate the data. This replaced the method of the previous season where green LEDs were simultaneously flashed in the field of view of each detector to generate a coincidence signal. This provided a monitor of the tube gain stability and, by observing the rising edge of the LED pulse, an indication of the temporal response.

3.6 Environmental Monitoring

Since measurements of cosmic ray showers using Cerenkov light employ the atmosphere as a detector continuous monitoring of atmospheric conditions must be undertaken. Observations (especially for fluctuation estimates) can only be made under clear skies and several different measurements of sky clarity were made. A 2 inch photomultiplier tube constantly monitored the background sky brightness and this information was added to each shower record. Throughout the night 3 time lapse cameras, giving good sky coverage, recorded sky conditions over 15 minute intervals. The maximum stellar magnitude visible on these photographs gave a quantitative measure of sky clarity. Sporadic cloud cover was clearly detected using this method. Finally the detected shower count rate itself acted as a check on atmospheric conditions.

Cerenkov light shower parameters are sensitive not only to the total grammage of atmosphere but also to changes in local density. Hence changes in atmospheric temperature and pressure would be expected to produce fluctuations in shower development. These must ultimately be accounted for in fluctuation analysis and so measurements of these quantities formed part of each shower record.

In addition the temperatures of each detector, both the tube and the electronics were recorded to ensure stable operating conditions.

Discussion of the suitability and values of these measurements is given in Andam (1982).

3.7 Calibration Procedures

Calibration procedures were carried out regularly throughout the period of operation. Measurements varied from the calibrations made every thirteen event records (discussed above) to the time response measurement of each PMT made before the establishment of the array.

The high accuracy timing information was required principally to investigate pulse shape dependence on shower development. Lateral distribution measurements demanded accurate intercalibration of detector gains. However both measurements were interdependent in that lateral distribution measurements need the zenith angle information available from fast timing and use the relative positions of the pulse segments to calculate the total light density while the pulse shape analysis procedure uses the core position and energy assignment from the lateral distribution analysis.

Regularly in each month of observations, measurements were made of the time delays through the recording system, the time stretcher and digitising electronics were calibrated and the relative amplitude responses of the photo-multipliers were measured.

3.7.1 Calibration of the Fast Timing Measurements

Absolute measurement of the signal delays in each detector system was not required but accurate relative delays between the detectors were. The PMT transit time was measured by generating two pulses; the first of which avalanche pulsed an LED in the field of view of the PMT (giving a pulse with rising edge faster than 6 ns). The resulting signal taken from the PMT amplifier was recorded on an oscilloscope and compared with the second pulse delayed by a fixed amount (100 ns). Reading accuracy from the oscilloscope photograph gave the main uncertainty of ± 0.5 ns.

Measurement of the remaining delays was combined with the calibration of the time stretcher. Using a crystal controlled 20 MHz oscillator, time intervals of 400 ns - 2.8μs in 400 ns steps could be accurately generated. A pulse from the generator into the discriminator started the time stretcher and a second appropriately delayed was sent along a reference cable to the central electronics to trigger the coincidence unit which, in turn, returned a shower trigger to stop the time stretcher. This procedure gave both the slope of the time stretcher calibration and the offset due to the transit time along the reference cable, back down the trigger cable and through the output buffer minus the delay between discriminator and time stretcher start. The same reference cable was used for all detectors and a check was made by repeatedly recalibrating detector 1 between measurements of the different detectors in case of any change in cable length due to mechanical or thermal lengthening.

Fine adjustments were made to these calibrations using data analysis procedures by Chantler (1982) who calculates a combined timing uncertainty for each detector.

3.7.2 Intercalibration of the Detector Gains

High accuracy measurements of relative gains were difficult to make directly and ultimately fine adjustments had to be made to the measured intercalibration on the basis of a subset of the observed data. However three techniques were used to provide the best measurement estimate of the relative response of the PMT and amplifier for each detector.

(i) At least once per month the signal from the amplifier obtained by illuminating the PMT with constant current driven green and red LED pulses was recorded by photographing the output displayed on an oscilloscope. The signal typically produced from the green pulser was approximately 300 mV high with a width of 300 ns. The accuracy of this measurement was limited by the broad output trace obtained and by the difficulty in positioning the pulser reproducably to illuminate the whole photocathode. The ratio between the response of the red and green LEDs gave a crude estimate of the wavelength response.

(ii) A standard light source- Nuclear Enterprises type NE 130 radioactive pulser-(see Wellby (1977)) was used to measure the relative gains and to provide an absolute photon measurement . The light flux produced by the pulser was 1835 ± 300 photons (Hartman and Weekes, private communication). In addition the fast pulse (~ 2 ns) provided a measurement of the time response of the PMT system to a short pulse approximating to a δ function (described above). This response was the basis of the system response included in simulations of pulse shape information (see Chapter 2).

However, the small size of the pulse obtained during this measurement, approximately 300 mVns, meant that this was less accurate than the green LED as a light source for measurements of relative detector response (provided the calibration was not wavelength dependent). The main advantage of the NE 130 source was that the wavelength output of the radioactive pulser was closer to that of Cerenkov light from cosmic ray showers.

(iii) In the laboratory the wavelength response of each PMT was tested using the signal from a Rofin type monochromator fed along a fibre optic light guide to illuminate the photocathode. Reproducing the field operating conditions it was possible to compare the relative gains of the PMTs at the wavelength of the green LEDs and at 400 nm, a typical Cerenkov light wavelength in EAS. Differences in response were within the 6% measuring error hence justifying the field calibration using a green LED. The response at red wavelengths was very poor and the efficiency varied widely between photo multipliers. This demonstrated clearly that the red LED, despite its high output light flux, was not valuable for intercalibration procedures.

This method also gave a measure of the relative tube gain under more controlled conditions than the Dugway field measurements.

Method (iii) gave results which were in general consistent with method (i). The series of field measurements showed considerable statistical fluctuations due to the difficulty in obtaining reproducable conditions. The accuracy achieved however, using method (iii) was no better than 20% and a method is described in Section 4.4 where a subset of the data is used to make small but significant adjustments to the individual detector gains on the basis of the detector's response to EAS Cerenkov light.

The digitising system was calibrated by injecting a 200 ns wide flat topped pulse of variable height into the input of the amplifier and reading out the integrator and pulse segment values over the full dynamic range of the system. This was carried out at least once each month of operation to check against any changes throughout the season. During season 1979-80 the response to zero input was continuously monitored using calibration events during every night (see Section 3.5) and the pedestal changes in the integrator, observed the previous year were accurately determined without recourse to the method described by Shearer (1980). No other calibration drift was observed.

As a result of these calibration procedures the pulse segments were measured to an accuracy of ± 50 mVns and the integrators to ± 200 m Vns.

3.8 General Characteristics of the Data

Table 3.1 shows the aggregated hours of operation of each array and the total number of showers recorded. Column E shows all showers recorded and column F the data, worthy of close examination, having at least 5 detector responses, a zenith angle of less than 60° and the analysed core located within the array. (Since the core fitting procedure used 4 free parameters it was necessary to use at least 5 detector responses to achieve some redundancy in the shower analysis). The number of detectors responding, zenith angle distribution and energy distribution for the data set in column E is shown in Figures 3.4, 3.5

Table 3.1 Summary of the data collected by the three configurations of the Dugway Cerenkov Light Detector Array

A	B	C	D	E	F
Array Size	Period of Operation	Number of hours of good weather observation	Number of 3 fold detector triggers in good weather	Number of 5 fold or greater detector responses within the array with zenith angle less than 60°	Energy Range (eV)
400 m	October 78–March 79	140	2143	792	1.4×10^{16}–7×10^{17}
	August 79–November 79	210	3301	1071	
200 m	December–February 80	50	3544	1123	4.5×10^{15}–1.7×10^{17}
100 m	March 1980	20	2657	498	1.0×10^{15}–3.8×10^{16}

Figure 3.4 The frequency distribution of N-fold events recorded by the three array configurations.

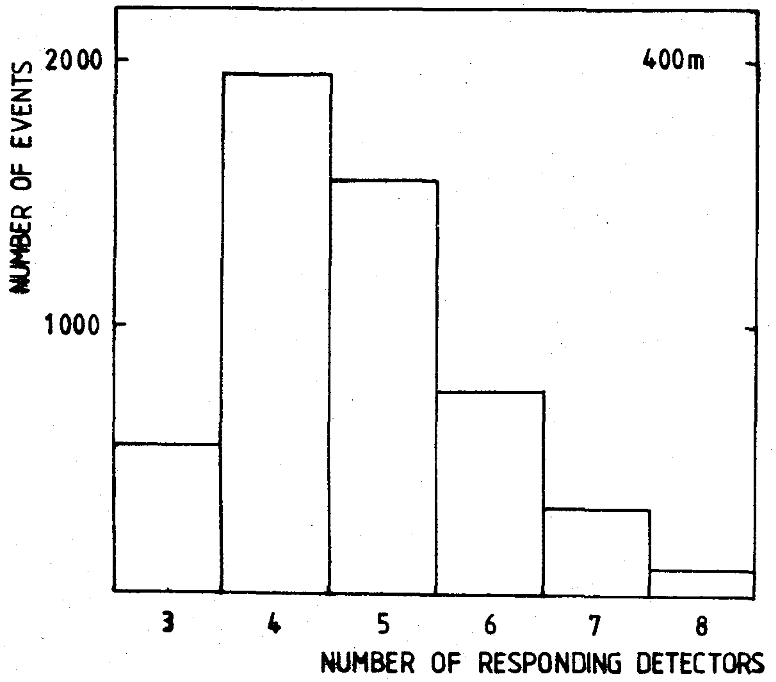
400m
NUMBER OF EVENTS
2000
1000
3
4
5
6
7
8
NUMBER OF RESPONDING DETECTORS

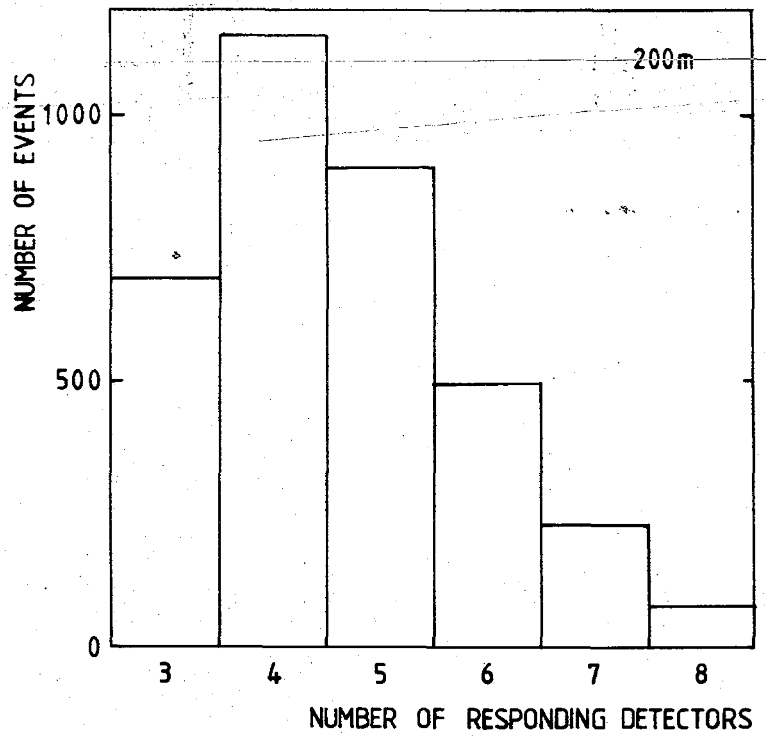
200m
NUMBER OF EVENTS
1000
500
0
3
4
5
6
7
8
NUMBER OF RESPONDING DETECTORS

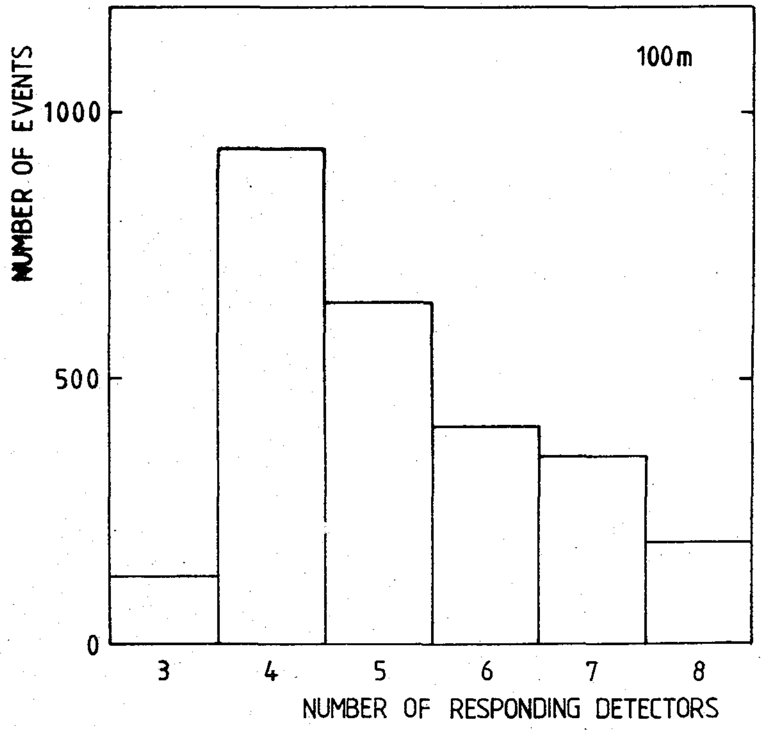
100m
NUMBER OF EVENTS
1000
500
0
3
4
5
6
7
8
NUMBER OF RESPONDING DETECTORS

Figure 3.5 The frequency distribution of the zenith angles of recorded events for the three array configurations.

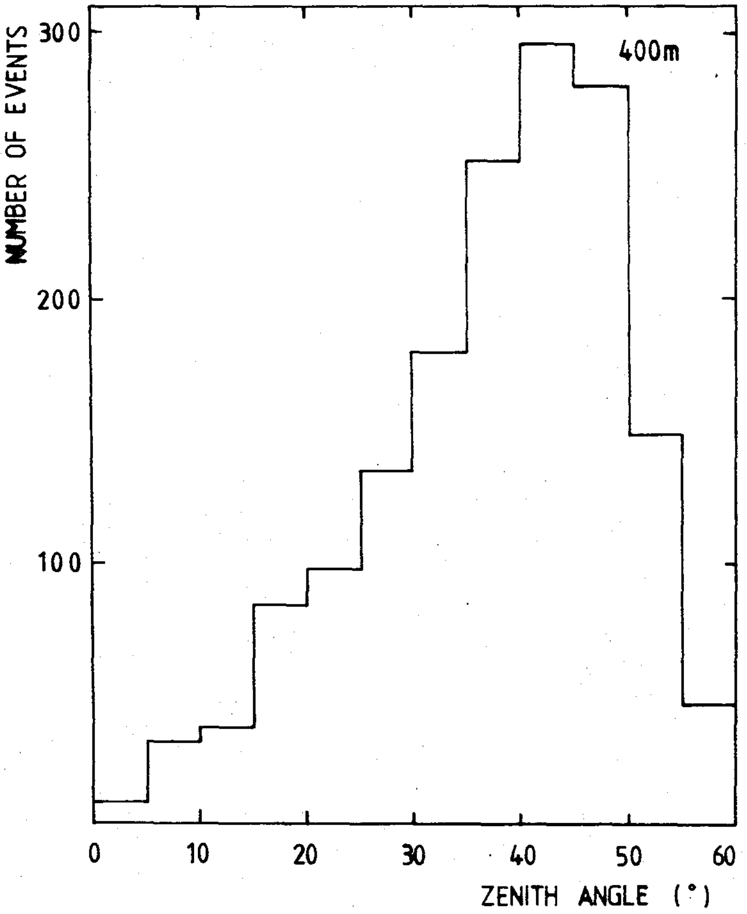
400m
NUMBER OF EVENTS
300
200
100
0
10
20
30
40
50
60
ZENITH ANGLE (°)

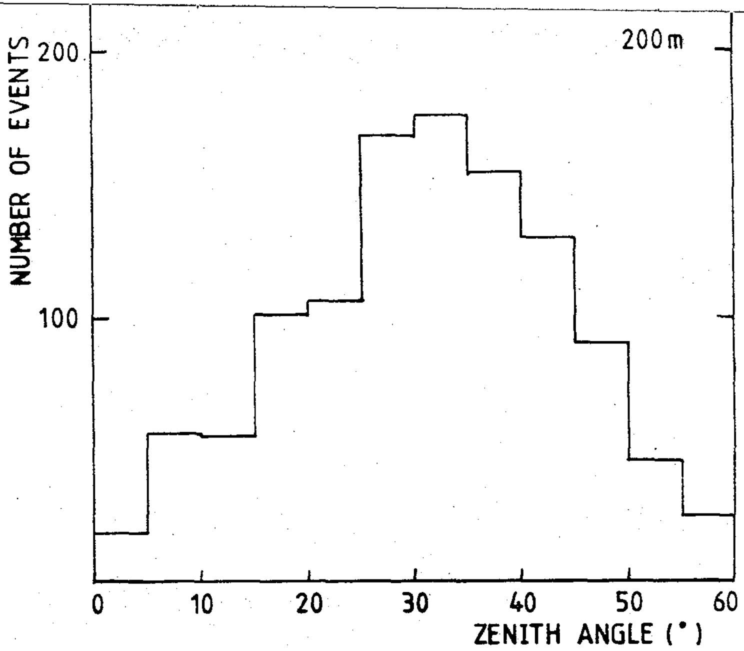
200m
NUMBER OF EVENTS
200
100
0
10
20
30
40
50
60
ZENITH ANGLE (°)

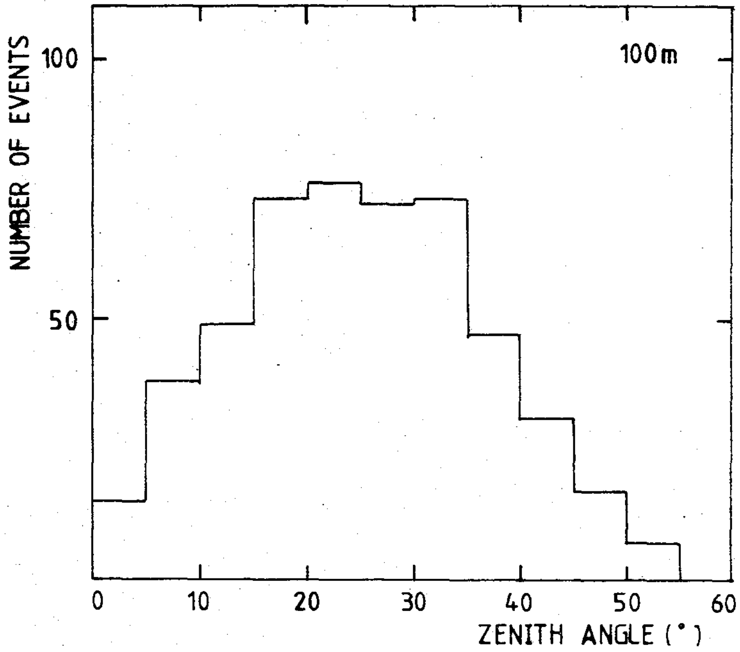
100m
NUMBER OF EVENTS
100
50
0
10
20
30
40
50
60
ZENITH ANGLE (°)

Figure 3.6 The frequency distribution of the energy of the recorded events for the three array configurations.

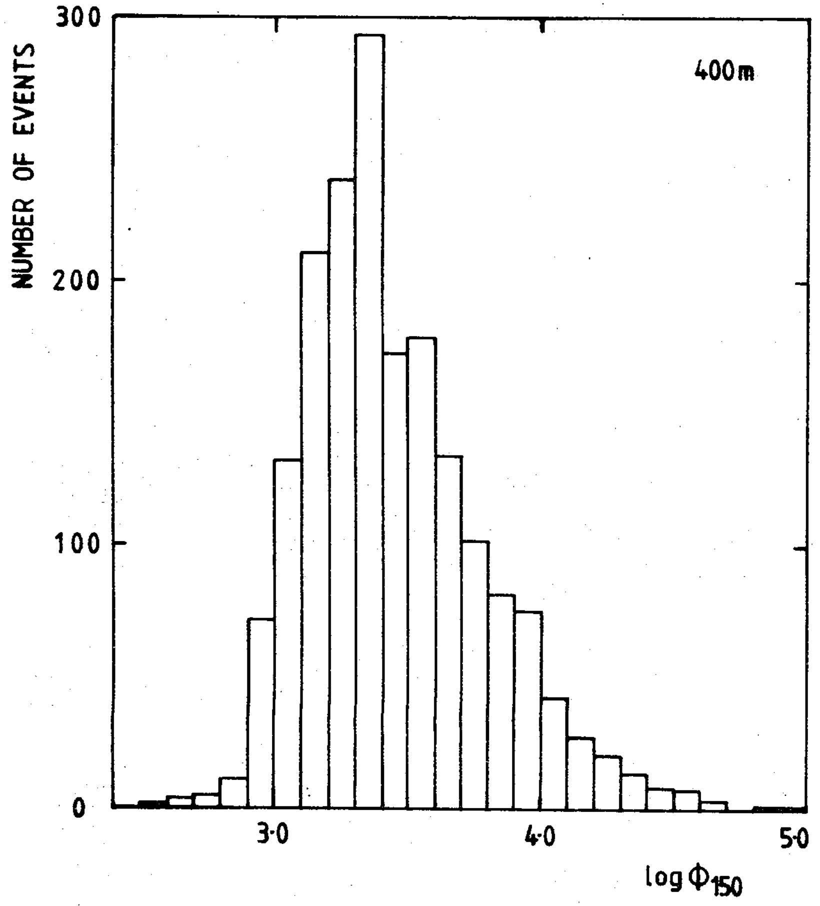
400m
NUMBER OF EVENTS
300
200
100
0
3·0
4·0
5·0
log Φ150

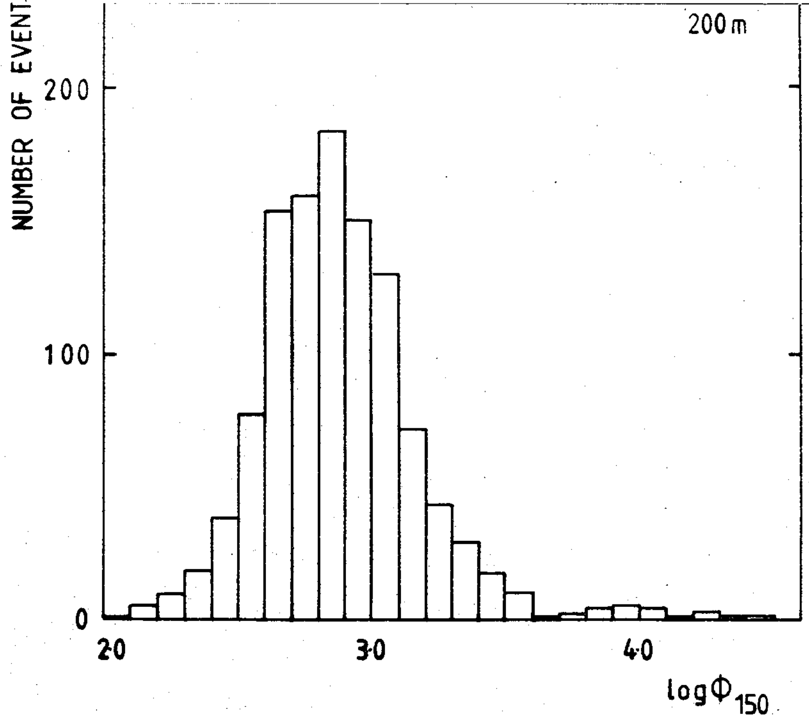
200 m
NUMBER OF EVENT
200
100
0
2·0
3·0
4·0
log Φ150

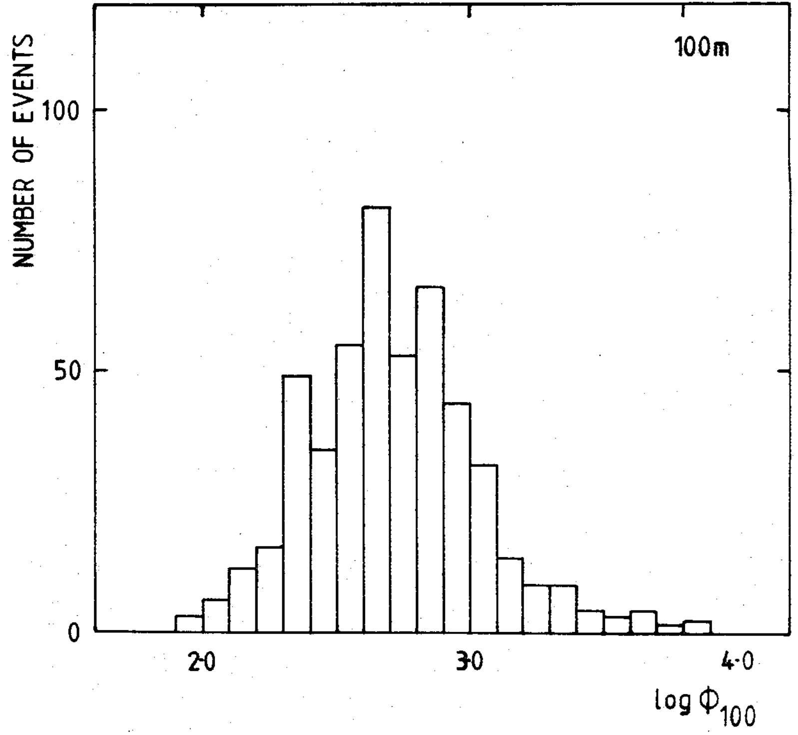
100m
NUMBER OF EVENTS
100
50
0
2·0
3·0
4·0
log Φ100

and 3.6. Energy is determined using the light density at 150 m from the core (Φ_{150}) in the 400 m and 200 m arrays and the density at 100 m in the 100 m array. The use of these parameters is discussed in Section 4.5.

Both the zenith angle and energy distributions show the effect of the array triggering requirement. The threshold for detection is a pulse producing a peak height of 20 mV and this means that the probability of a shower triggering the array is dependent on energy, zenith angle and depth of maximum. The foreshortening of the array dimensions with increasing zenith angle also, of course, affects the triggering rate. Selection probabilities will be discussed in Section 4.7.

3.9 Typical Shower Record

Figure 3.7 shows a typical 7 fold shower record. The signal on detector 1 caused the scalers recording the pulse segments to overflow and this information was irretrievably lost. (Such pulses are close to the core and therefore the pulse shape could provide little information about depth of maximum). The integrator hence contributes the light density measurement. The signal on detector 5 has also overflowed but by using the known characteristics of the Cerenkov pulse and the difference between the integrator record and that calculated from the pulse segments it has been possible to identify and replace the missing signal. (This is only possible if not more than 2 segments have overflowed).

The position of the core and the lateral distribution

Figure 3.7 The record of a typical 7-fold response from the 400 m array showing the pulse segments detected and the lateral distribution of the light density.

Zenith angle = 32.6°

Azimuth angle = 7.3°

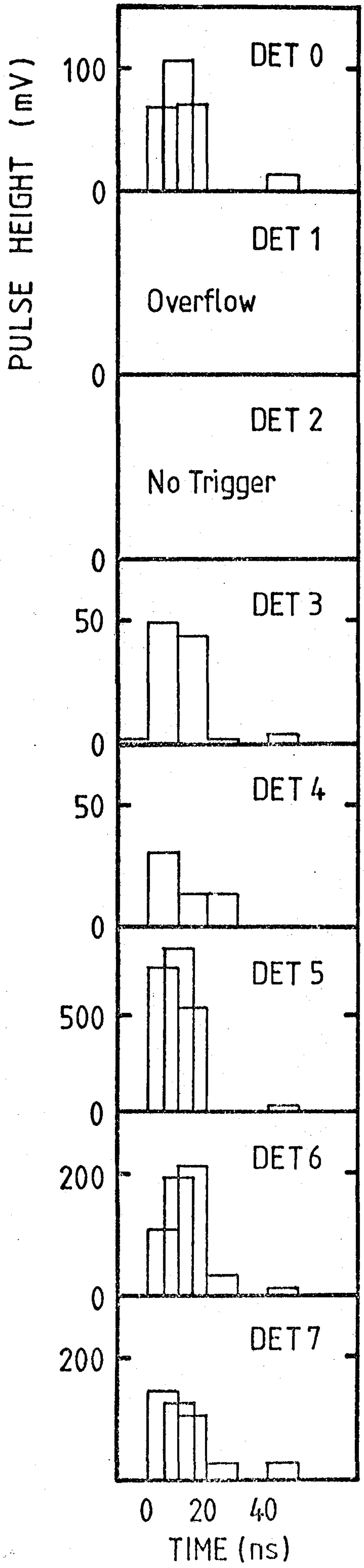

Event 147/231636

13th November 1978

23hr 16min MST

7 fold response

Core Location

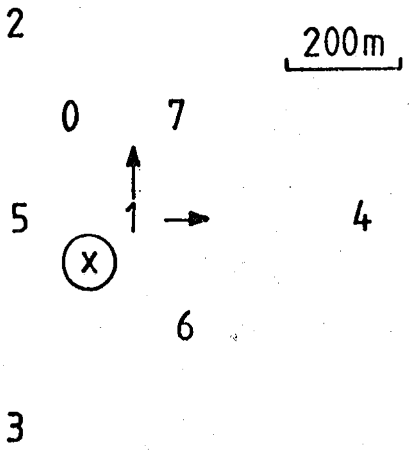

Lateral Distribution

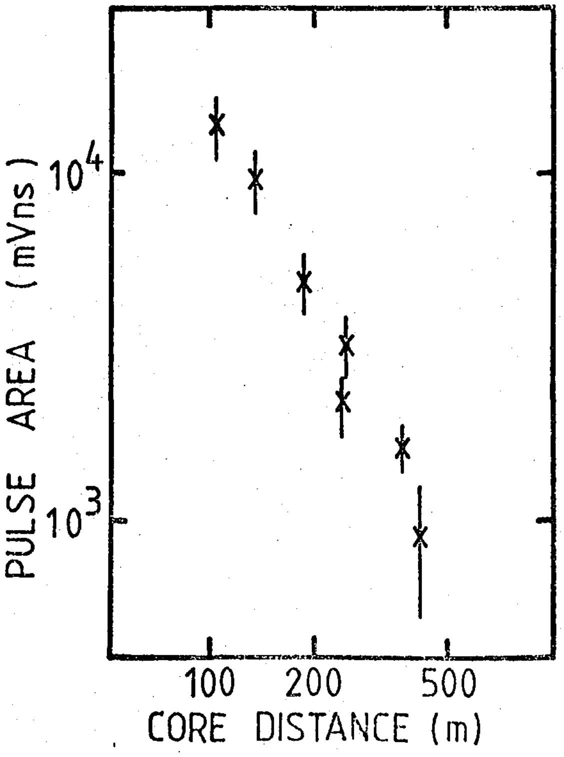

obtained from the analysis are also shown.

3.10 Conclusion

This chapter has provided an outline of the operation of the Dugway Cerenkov Light Detector array over three seasons. The calibration methods for each part of the data collection process have been described and particular emphasis was placed on measurements of the relative gain of the detector photomultipliers - essential to the lateral distribution analysis.

The data recorded by the Tektronix 4051 on magnetic tape was transferred to disc storage on the NUMAC IBM 370 computer for decalibration, sorting and subsequent analysis. This is described in the following chapter.

CHAPTER 4

ANALYSIS PROCEDURES USED IN THE DETERMINATION OF LATERAL DISTRIBUTION

4.1 Introduction

It is the aim of this chapter to explain the analysis procedures used to produce interpretable shower data from event information recorded at the Dugway array. The pre-analysis consistency checks, decalibration procedures and preliminary data sorting are briefly described. A detailed description is given of the allowance made for experimental uncertainties in the subsequent analysis and of the procedure used to obtain the most accurate values of the relative and absolute gains of the detectors. The derivation of both energy-sensitive and depth-sensitive parameters is given and the calculation of their values. Depth sensitivity was investigated both from the average lateral distribution and through a shower by shower analysis. Interpretation of the results from individual events provides the measurement of fluctuations in shower development and therefore careful consideration must be given to possible biasing effects.

A full discussion is given of the sampling problems introduced by the array trigger requirements, which produced bias in the recorded dataset and the Monte Carlo simulation program used in understanding this problem is described. The way sampling errors affect the fluctuations in a dataset - the crucial factor in the interpretation of fluctuations due to primary mass composition - was also investigated using Monte Carlo simulations and the generation of test datasets is outlined in this chapter, while the procedure is more properly explained in Chapter 5.

4.2 Preanalysis Routines and the Preliminary Dataset

The detail of the procedure necessary to convert the digitised information to analysable data was given by Shearer (1980). The intention here is to describe the checks on the quality of the data employed in the work described in this thesis and the status of the dataset from which shower records could be selected for further analysis.

The data were transferred from tape to storage on the main-frame computer and divided into samples of a convenient size which, for the 400 m array, corresponded to the data from a single night of operation. Information for each such sample was scrutinised to check the rate at which the array triggered, the consistency of the responses of each detector and the weather-monitoring information. It was at this point that a quality statement was added to each event signifying the weather conditions and the array reliability; subsequently only good-weather data was used. The appropriate calibration constants from on-site measurements were used to decalibrate the data and a preliminary analysis was produced, as described by Shearer (1980).

The requirement for this procedure was to produce a database containing the necessary information for the analysis routines for each shower measurement (lateral distribution, pulse shape and imaging) to be developed separately. For lateral distribution measurements it was necessary to know the spatial angle of the shower core. This was obtained by fitting a spherical front to the times of arrival of the light pulses where the centre of the sphere lay along the shower axis (see Chantler (1982) who describes this in detail). The photon densities were initially analysed to find the shower core. This core position and the derived detector distances were sufficiently accurate for the derivation of the pulse shape routines. Considerable refinement was to be introduced before development-sensitive lateral distribution information was available, as will be discussed. All non-linear fitting procedures used in this thesis are based on the application of the Minuit multi-parameter minimisation routine (James and Roos, (1975)).

For example, to find the shower core position the photon densities were fitted to a function of the form

$$\Phi(r) = A\,(r + r_o)^{-\eta} \qquad (4.1)$$

where r is the distance from the shower core and $r_o = 50\mathrm{m}$ by minimising the sum

$\sum_i (1 - \frac{\text{observed}}{\text{predicted}})^2$ where i is the number of responding detectors, η is a parameter which gives the shape of the structure function and A is a normalising factor. This was a quick, simple procedure but required considerable improvement before the results could be used for depth sensitive analysis.

The observed photon densities used in the minimisation were routinely derived from the sampled 10ns segments of each pulse. A full reconstruction of all pulse shapes using a spline-fitting procedure (see Chantler (1982)) would be difficult because of the magnitude of the calculation and the instability of the procedure in the measurement of small pulses. However, the difference in resolution between the total photon density measured by the integrator and that derived from summing the 10ns segment meant that these segments provided the more accurate measurement for other than the largest densities. A simple algorithm which summed the values of non-overlapping segments of the pulse and added compensation for the unmeasured portion would give a more accurate density than that available from the integrator measurement. The algorithm, known as Σslices was found empirically and for inner ring detectors was

$$\Sigma\,\text{slices} = \text{sl 1} + \text{sl3} + \text{sl4} + \text{sl5} + \tfrac{1}{2}(\text{sl4}+\text{sl5}) + \text{START} + \text{TAIL} \qquad (4.2)$$

with

$$\Sigma\text{slices} \doteq \text{sl 1} + \text{sl2} + \text{sl3} + \text{sl4} + \text{sl5} + \text{sl6} + \tfrac{1}{3}(\text{sl4}+\text{sl5}) + \tfrac{1}{2}(\text{sl3} + \text{sl4}) \qquad (4.3)$$

for the outer ring where sl n was the area of segment n (see Figure 3.3), START is the area omitted before the pulse reached the discrimination level and is accounted for by a constant factor and TAIL was the area omitted at the end of the pulse approximated by the area under an exponential curve. The results of tests on the accuracy of this method are discussed in 4.3.2.

The high resolution of the segment measurement (2 mV/bit) meant that large, fast pulses produced values beyond the range of the scaler causing it to overflow. This occurrence was easily recognised from the mismatch between the Σslices and integrated density measurements. It was hence possible to recover reliably the information in the overflowed scalers provided overflow had not occurred more than twice in any one pulse; beyond this the appropriate number of overflows could not be identified unambiguously. However such occurrences were only in the very largest pulses where the integrator provided an appropriate, accurate measurement of the photon density.

The fitting procedure used for the lateral distribution of photon density also gave a primary energy estimator for each shower. Densities at a number of core distances were derived, as was the integral of the photon flux between 50 m and 250 m which was investigated by Shearer (1980). The most appropriate value for an energy estimator was later chosen, on the basis of the simulation of showers (McComb and Turver (1981)), to be the flux at 150 m (see 4.6) and this value was used in the sorting of data into primary energy intervals.

The first run of the sorting routine allowed the manual inspection of data. At this point every shower was scrutinised so that overflowed scalers were identified and either the information was reinstated or the segment measurements were suppressed from further analysis, as necessary. The two fitting procedures, timing and lateral distribution, each provided a goodness of fit parameter and this was a valuable indicator of the need for examination of, for example, detectors triggering on noise. (Such records arose by chance on one detector in ten showers). The result of this preliminary analysis was the production of a dataset containing reliable decalibration data, usable values of arrival direction and initial values of core position and primary energy.

4.3 The Refit Procedure

The previous section described the dataset from which information was drawn to develop further analysis procedures. It was observed at this stage that the lateral distribution fitting procedure placed undue weight on the small densities obtained at large distances from the shower core. It was therefore necessary to use a knowledge of the measurement uncertainties for each detector in weighting the structure function i.e. minimising the function

$$\sum_i \left(\frac{\text{observed - predicted}}{\text{error}}\right)^2$$

This is essentially the χ^2 function.

However, such a procedure requires a reasonable estimation of the error term involved and the following describes how the term evolved as a combination of a calculation of the well understood instrumental uncertainties and the less tractable errors caused by the assumptions made about the lateral distribution function. Section 4.3.1 elucidates the sources of error while the calculation of the error term is described in Section4.3.2. Finally, Section 4.3.3 demonstrates the checks which were performed on the refitting procedure.

4.3.1 Sources of Error

Deviations between observed and predicted measurements were derived from two sources - the enforcement of a structure function form on the data and the uncertainties due to the detection system. The main elements which contribute are as follows:-

(a) The true shape of the structure function.

The function chosen to represent the lateral distribution of light density is

$$\Phi(r) = A(r + r_o)^{-\eta}$$

where A, η and the core position were free parameters in the fit and r_o was a constant set at 50 m. In finding the shower core any reasonably steep function relies heavily on the symmetry of the distribution. As an example, Shearer (1980) considered the effect of an exponential function in locating the core position and he concluded that the exact representation of the lateral distribution was not crucial to the accuracy of the core fit. However, a consistent misfit to the data affects the minimisation procedure and the parameter becomes dependent on the distance range over which the shower is sampled. Figure 4.1 shows the result of an investigation of this misfit. The dataset examined was of 8 fold showers and the method used to investigate the misfit of each detector was to calculate the exclusive residual - i.e. the deviation between the measured value and the prediction based

Figure 4.1 The exclusive residuals for events with eight fold detector responses plotted against the distance of the omitted detector.

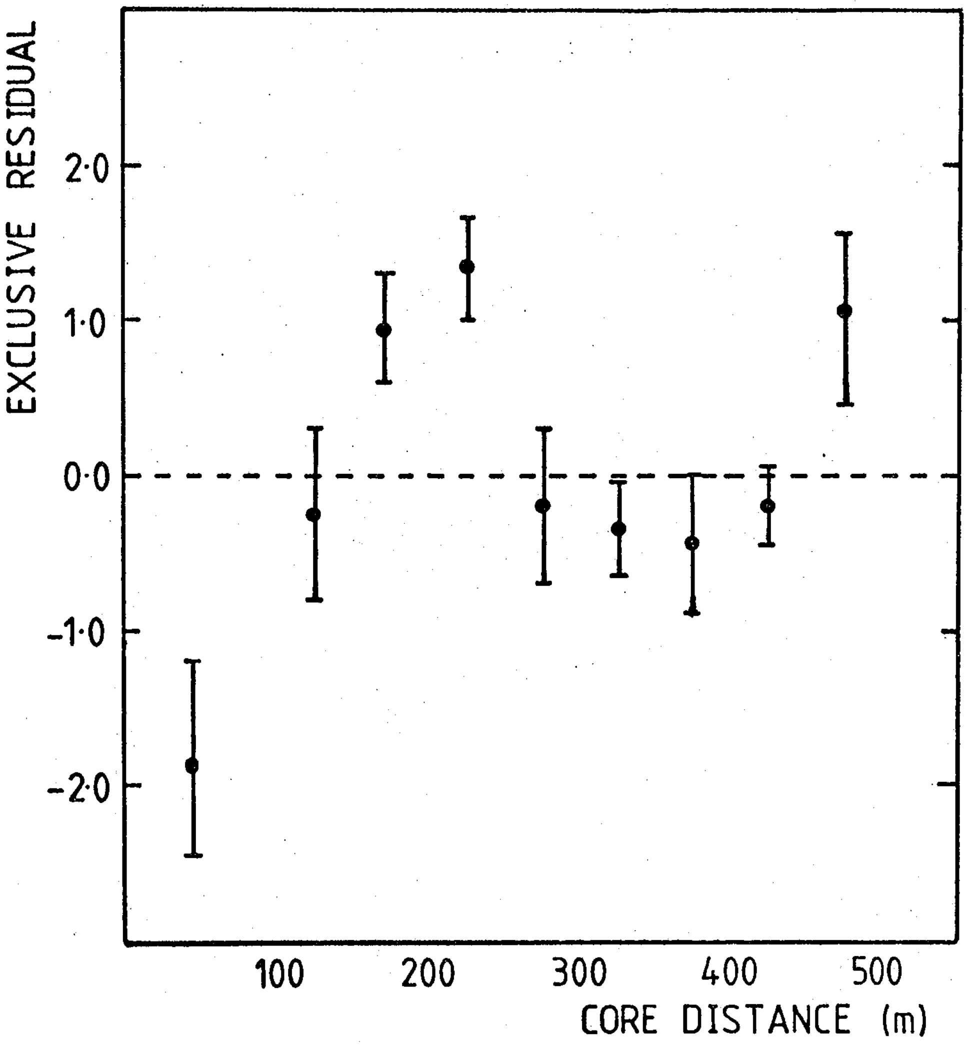
EXCLUSIVE RESIDUAL
2·0
1·0
0·0
-1·0
-2·0
100
200
300
400
500
CORE DISTANCE (m)

on a fit to the other seven detectors only where the deviation is weighted using the error term described in the following section. The average deviation has been plotted and the figure clearly shows that the fitting procedure overestimated the measurement close to the core and underestimated it around 200 m. It was for this reason that the parameter η obtained in the minimisation procedure was not used directly as a depth sensitive parameter (see Chapter 2 for the theoretical discussion and Section 4.6 for the calculation of the depth sensitive parameter).

(b) It has been assumed throughout that each shower had circular symmetry in the plane perpendicular to the shower axis. However the Cerenkov light shower was produced by both electrons and positrons and the symmetry of the shower was broken by the opposite deflection of the charged particles in the geomagnetic field (see Orford et al., (1975)). Indeed the shower should be elliptically not spherically symmetric with the degree of ellipticity dependent on the angle which the shower made with the geomagnetic field lines. No attempt was made to account for the effect on a shower by shower basis at this stage. In Section 4.3.3 the degree of misfit occasioned by the action of the geomagnetic field is demonstrated. The effect however, was regarded as pseudo-random since it was dependent principally on the azimuthal angle of the shower - an essentially random parameter.

(c) Local angle effect.

The measured density at each detector was dependent on the area of the detector presented to the shower in a plane perpendicular to the direction of arrival of the shower photons. In routine analysis a simple correction was made by projecting the area onto the plane perpendicular to the shower axis, i.e. dividing by the cosine of the zenith angle, and therefore made the simplifying assumption that the light travels parallel to the shower core. However, a more suitable correction was found by calculating the local angle of the photons assuming an origin on the shower path at an appropriate atmospheric depth - a constant depth of 550 g cm^{-2} was chosen. This changes the observed density by not more than 3% for the most distant detectors; refitting the dataset with this correction produced no noticeable reduction in the mean value of χ^2.

(d) Random variations in showers.

The statistical nature of the air shower suggests that fluctuations in the interactions in the cascade might combine to give assymmetries in showers. This is an unknown factor since only an extensive, closely spaced array of detectors would measure this effect and the method of averaging used in the simulation study for the present experiment leaves no evidence of the magnitude of any 'lumpiness'. However it is assumed that such deviations from a smooth lateral distribution are proportional to the measured density and is taken account of in this form in Section 4.3.2.

(e) Errors due to digitisation and sky noise.

The major source of error for small densities was caused by the detection system and the magnitude of this error was derived from a knowledge of the response of the detector. For densities measured by the integrator the error is based only on the resolution of the digitisation bit and has a constant value. Shearer (1980) quoted that measurement uncertainty as ± 500 mVns. However the majority of densities were obtained from the 10 ns segments sampled across the pulse. The uncertainty in this measurement was based on the digitisation of each slice and no simple algorithm would calculate the error. The simulation method used to investigate the error is described in the following section and the conclusion is drawn that the effect was largely independent of pulse size and could be represented adequately by a constant value a_i for the ith detector. (The differences in the gains of the photomultipliers mean that the value was different for each detector). The simulation method allowed the effects of background sky noise to be incorporated in the same calculation.

(f) Uncertainty in the detector gains.

Considerable effort was made to determine the relative gain of the light detectors, both from direct calibration and using the improvements described in Section 4.4 but this remained one of the main sources of uncertainty.

The assumption was made that although the error was systematic for each detector the effect operates randomly within the dataset. Since the showers landed randomly within the array no detector sampled consistently at a particular core distance and therefore the error in a measurement due to gain uncertainty was not systematically dependent on the distance at which the measurement was made. The error was represented by a term bd_i where d_i was the measured density at the ith detector and b was a constant to be determined.

Since the contributions to the uncertainty from the effects described in (a) to (d) were also essentially proportional to the measured density (to a first approximation) an error term of the form

$$e_i^2 = a_i^2 + b^2 d_i^2 \tag{4.4}$$

was used where the values of a_i were derived from the calculation outlined in the following section and b was determined by an iterative procedure using the mean χ^2 value, discussed in Section 4.4.

4.3.2 The Error Calculation

The calculation of the error involved in reconstructing the Σ slices response demanded a computer simulation of the sampling procedure used to segment and record the light pulse. The author follows that developed by Chantler (1982) who tested the effect of reconstructing a series of typical Cerenkov light pulses by fitting a quartic B-spline to the recorded segment areas. The test pulses used in both cases were drawn from the simulations of McComb and Turver (1981), described in Chapter 2, which provided a trace of the Cerenkov light pulse at 1ns intervals. Simulated pulses were chosen over a range of widths and scaled over a number of heights. The effect of sky noise was added to the height of the triggering level and to segment measurements using a routine which sampled from a normal distribution with 5mV standard deviation. The randomising effects have varied both the exact time at which the detector triggered relative to the true 20mV height of the Cerenkov pulse and the segment values. The results of the procedure were averaged from 1000 sampling runs giving the mean response and the statistical spread in the measurements. Figures 4.2 and 4.3 display these results over a range of pulse heights and widths for typical inner and outer ring detectors. The range over which the error term would be valid is shown in Figure 4.4 where the distribution of pulse area with full width half maximum within the real dataset is plotted for those measurements where FWHM was available from spline fitting. (Pulses which provided Σslices values but could not be spline fitted were all of small area and large FWHM, and their absence does not affect the conclusions drawn on the basis of this figure).

It was necessary to chose an error of a reasonably simple form which could accommodate the large misfit at small core distances and, taking into account the range

Figure 4.2 Reconstruction of simulation pulses using the Σslices algorithm for a range of pulse heights and FWHMs on a typical inner ring detector. The true pulse areas are represented by open symbols and the reconstructed area by filled symbols. The standard deviation for 1000 "noisy" simulated pulses is displayed. Pulse heights are as follows:-

○	35 mV
▽	50 mV
△	100 mV
□	500 mV

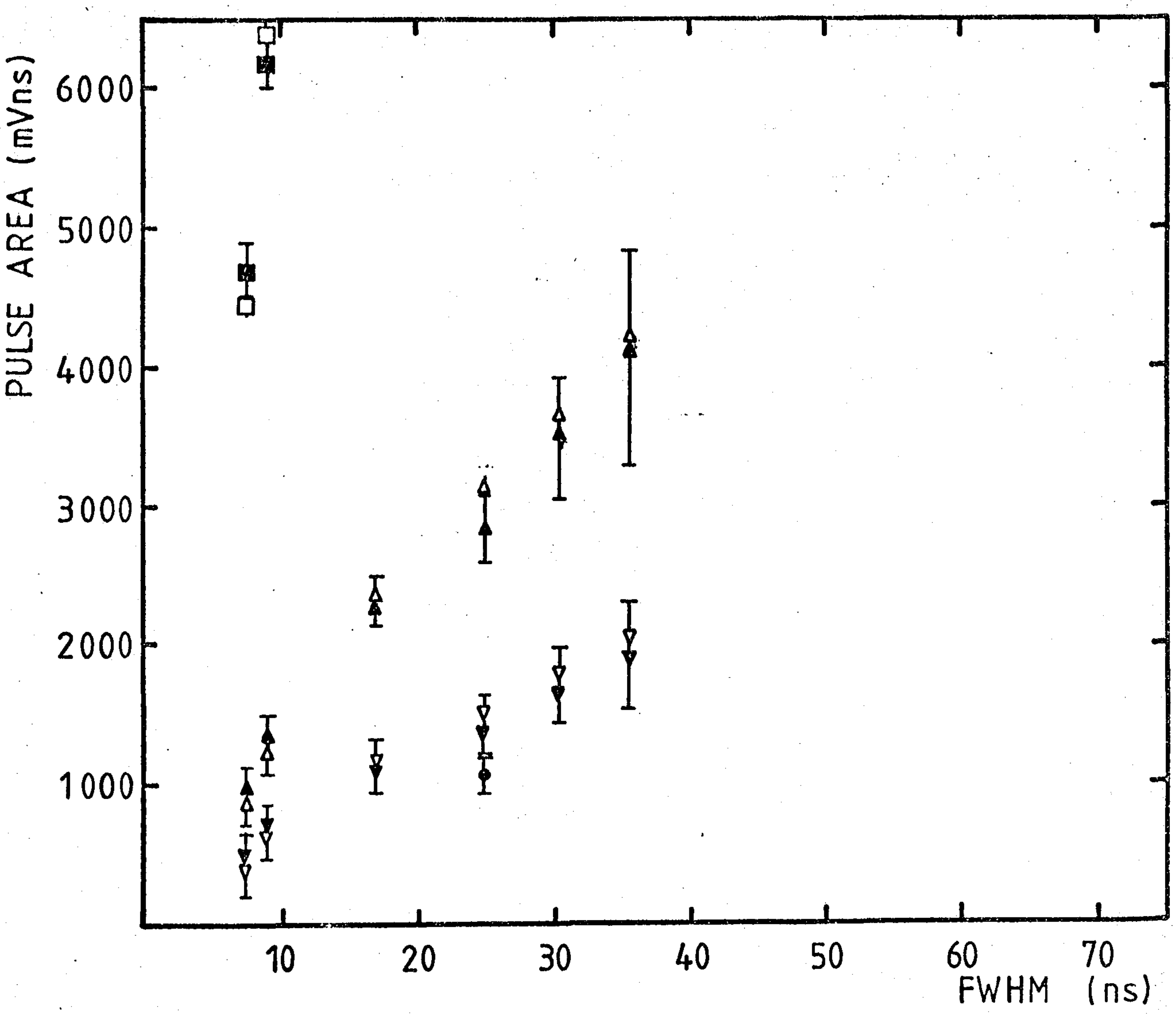
PULSE AREA (mVns)
6000
5000
4000
3000
2000
1000
10
20
30
40
50
60
70
FWHM (ns)

Figure 4.3 Reconstruction of simulation pulses using the Σ slices algorithm for a range of pulse heights and FWHMs on a typical outer ring detector. The true pulse areas are represented by open symbols and the reconstructed areas by filled symbols. The standard deviation for 1000 "noisy" simulated pulses is displayed. Pulse heights are as follows:-

○ 35 mV
▽ 50 mV
△ 100 mV
□ 500 mV

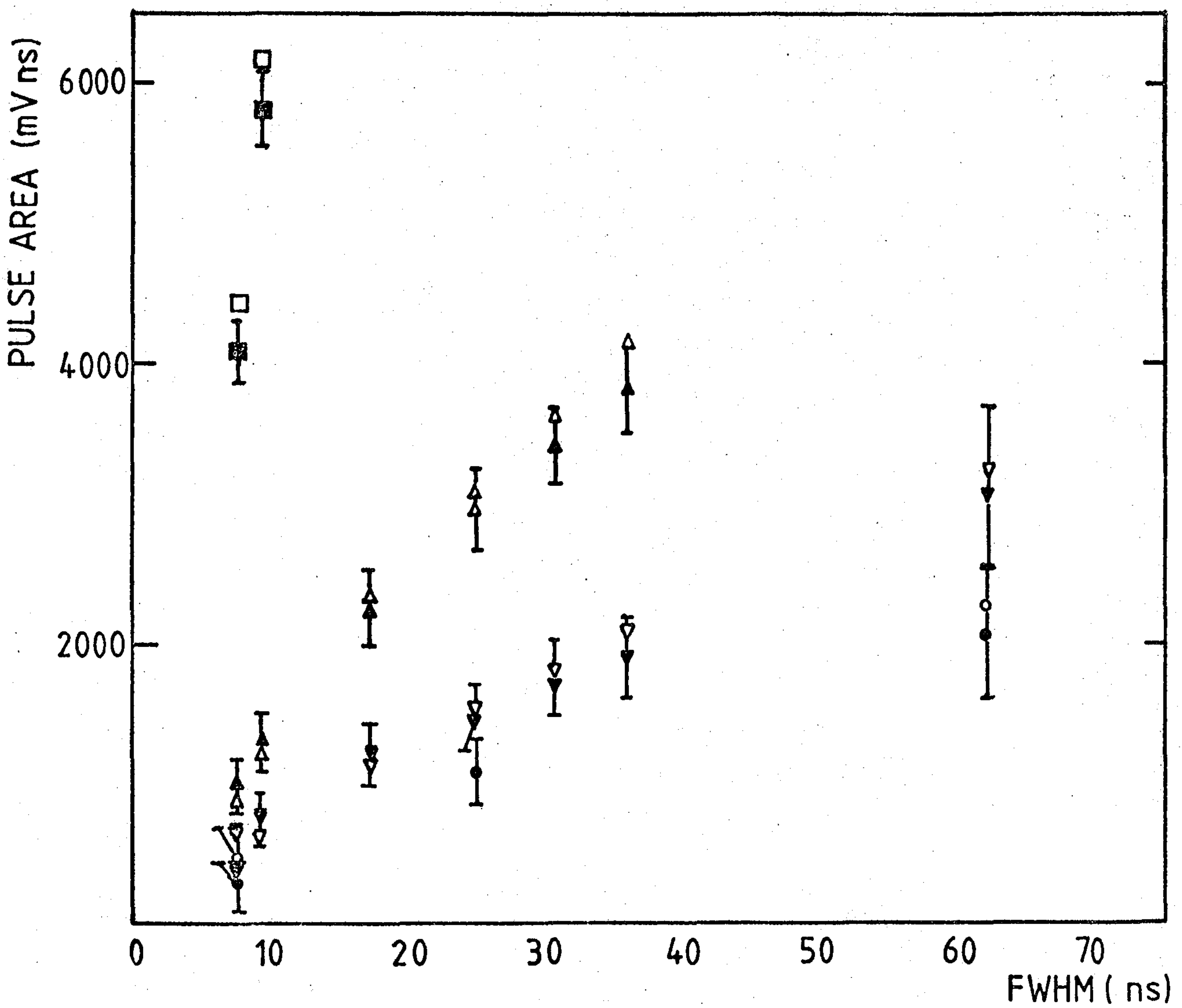
PULSE AREA (mV ns)
6000
4000
2000
0
10
20
30
40
50
60
70
FWHM (ns)

Figure 4.4 Scatter plot of pulse area and FWHM for all pulses which have been reconstructed using spline fitting to demonstrate the range of measurements.

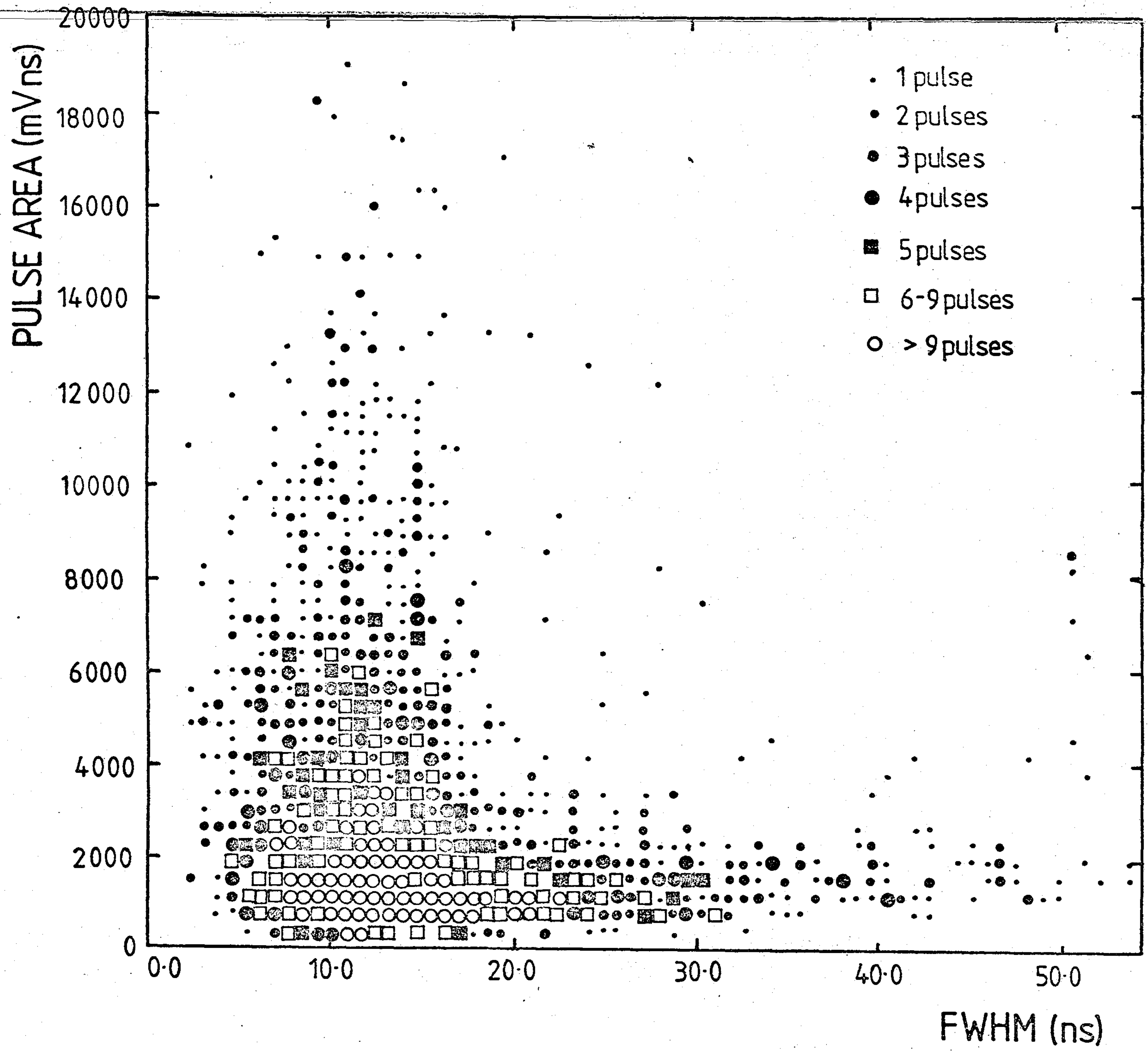
PULSE AREA (mVns)
20000
18000
16000
14000
12 000
10000
8000
6000
4000
2000
0
0·0
10·0
20·0
30·0
40·0
50·0
FWHM (ns)
· 1 pulse
• 2 pulses
● 3 pulses
● 4 pulses
■ 5 pulses
□ 6-9 pulses
○ > 9 pulses

over which the error term operated, Figures 4.2 and 4.3 suggested that a constant error of 200 mVns would satisfy this condition. This value was subsequently modified to take account of the different relative gains of the detectors. This then explains the term a_i in the expression for the error term (4.4).

To calculate the value of b, the well understood behaviour of the χ^2 distribution was used. Since the χ^2 distribution has a mean value equal to the number of degrees of freedom, the present dataset provides four values of χ^2 from showers with five, six, seven and eight fold responses. Thus if the error term has the form $b^2 d_i^2 + a_i^2$ and the constants, a_i, are known, the value of b can be adjusted until the $\overline{\chi^2}$ for the dataset matches that of the theoretical distribution. The dataset was refitted using different values of b until the optimum value of 0.18 was found for six fold responses. The values of χ^2 for five and seven folds using this value of b matched the prediction, though for eight folds the sample was too small to give reliable results. Data from the two seasons of operation were tested separately and gave consistent results demonstrating that the relative gains were accurate throughout. This procedure, using only one piece of information about the χ^2 distribution, the mean value, left a means of testing its validity against the shape of the distribution and this is considered below.

4.3.3 Checks on the Fitting Procedure

Obtaining a reasonable estimate of the measurement error is not only necessary to find an unbiased value of the fitted parameters but it is also essential for estimating the value of fluctuations in the dataset due to measurement uncertainty alone. In Section 4.8 the procedure used to determine these fluctuations is described - Monte Carlo simulation of the array response, where noise is added to each measurement to imitate the effects of the detection system - and it is on the basis of the present analysis that the noise distribution can be sampled. Hence a careful check was made on the validity of the derived error.

Since the value of the mean of the χ^2 distribution is used to determine precisely the error term, it was necessary to demonstrate that the supposed χ^2 distribution of the data was indeed a χ^2 distribution. This was achieved by applying a χ^2 test to the hypothesis that the observed and predicted distributions were the same. In Figure 4.5 the observed and predicted distributions are shown for showers with six responding detectors , i.e. having two degrees of freedom. In Table 4.1 are the results of the χ^2 tests showing that the hypothesis should be accepted and the error term can be used with confidence in the simulation of array response.

However, the discussion of Section 4.3 suggested that a correlation might exist between χ^2 and certain parameters, occasioned, in particular, by the structure function misfit and by the geomagnetic effect. If these effects were significant, correlations should be observed

Figure 4.5 The distribution in Chi-squared for the core fit of events with six fold detector responses. The dashed line indicates the theoretical Chi-squared distribution for two degrees of freedom. There are 27 observations with Chi-squares > 5.25 with a prediction of 23.55).

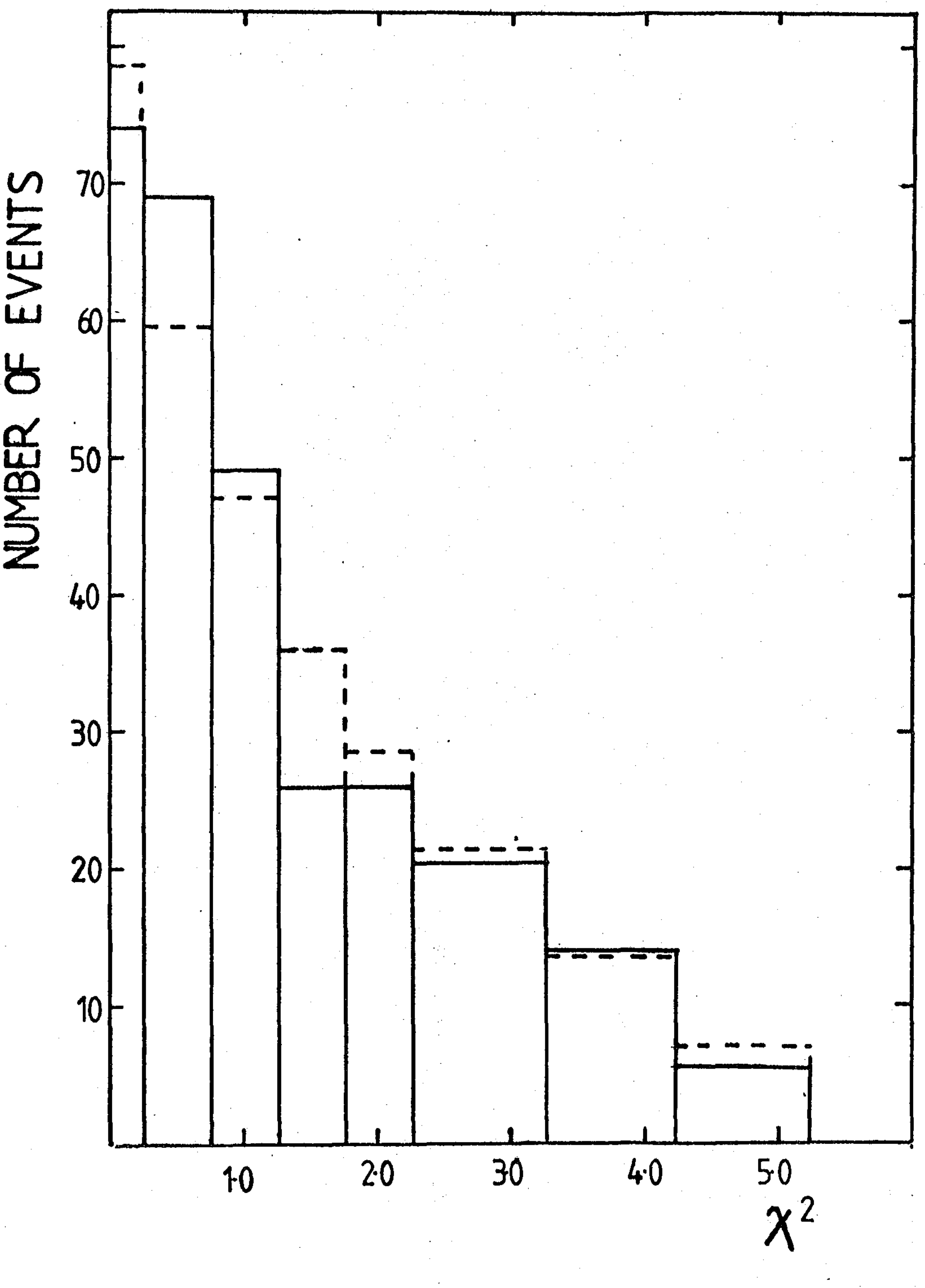
NUMBER OF EVENTS
70
60
50
40
30
20
10
1·0
2·0
3·0
4·0
5·0
χ^2

Table 4.1 The Chi-squared test applied to the distribution of the residuals of the minimisation procedure

Number of responsing detectors	5	6	7	8
Number of events	790	314	108	29
Mean Chi-squared	1.1	2.1	2.9	4.9
Number of degrees of freedom in Chi-squared test	8	8	5	2
Value of Chi-squared	12.94	6.78	3.219	1.275
Probability of obtaining a value at least as large as this	11%	55%	68%	53%

between χ^2 and sinα (the projection of the shower direction perpendicular to the geomagnetic field lines) and between χ^2 and r_{min}, the distance of the closest detector, determining the sampled core distance range. Figures 4.6 and 4.7 show scatter plots of these relationships and demonstrate the effects.

These elements of experimental error have both been treated as pseudo-random. The geomagnetic angle was a function of zenith and azimuth angle (the azimuth range being the larger and therefore the more important factor) and since no preferred azimuthal angle was shown in the data this was reasonable. Similarly the core distance disposition was dependent on the random positions at which the core landed within the array and in obtaining mean characteristics any effect would have averaged out. In fluctuation measurements, the misfit of data to the structure function was overcome by choosing an appropriate depth sensitive parameter (see Section 4.7) which was not dependent on the exact form of the function. Since no attempt was made to remove these effects from the minimisation procedure, the error estimate obtained from the χ^2 distribution still contains the uncertainty caused by them. Hence in using the derived error estimate in the fluctuation analysis in Section 4.8.1 this uncertainty has been accounted for. It does however, leave scope for an improvement in the resolution of the experiment if these pseudo-random effects could be removed from the minimisation procedure.

This discussion has demonstrated that the error term

Figure 4.6 Scatter plot of values of Chi-squared from the core fitting procedure and $\sin\alpha$.

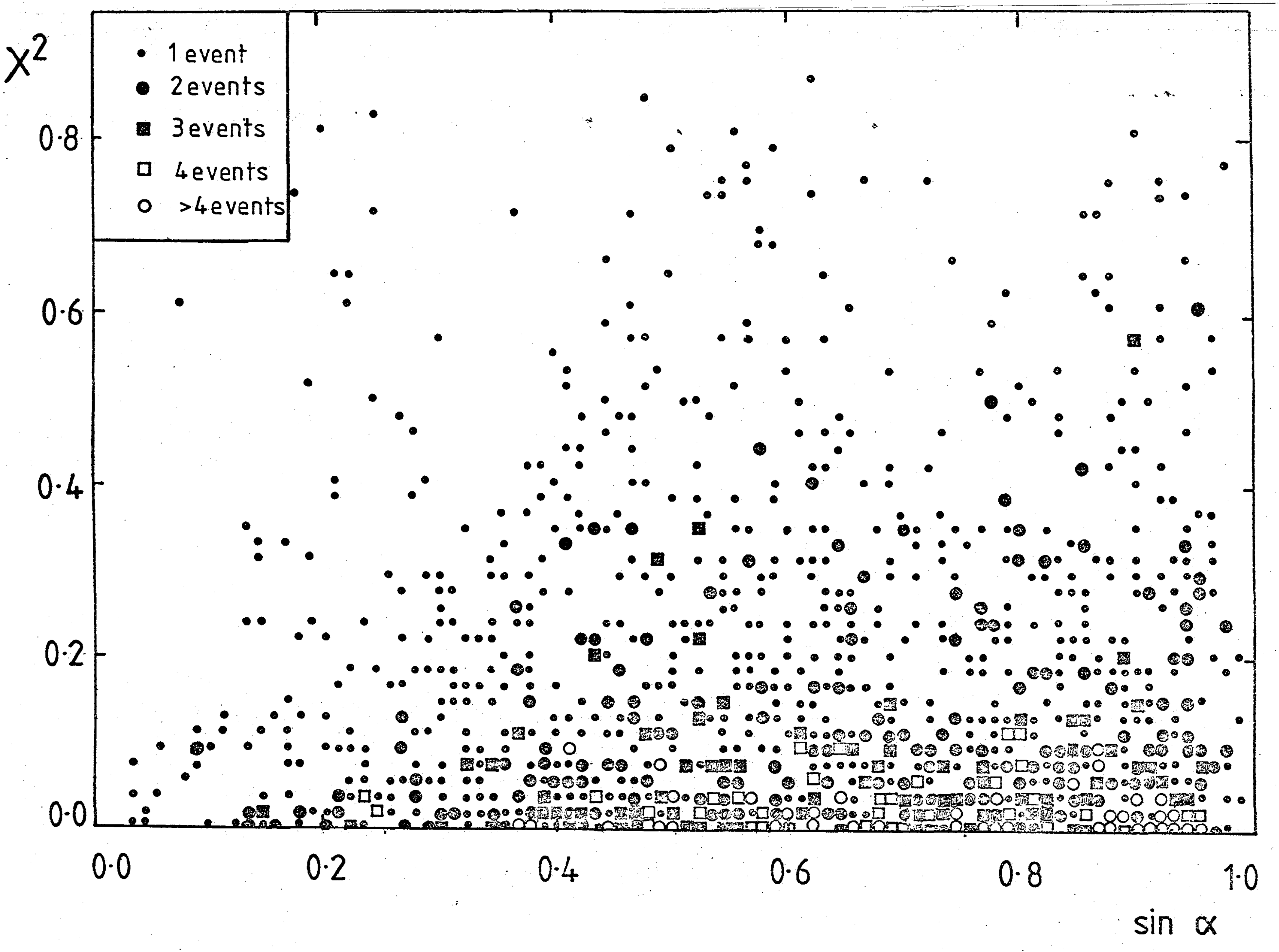
X^2
0·8
0·6
0·4
0·2
0·0
0·0
0·2
0·4
0·6
0·8
1·0
sin α
• 1 event
● 2 events
▨ 3 events
□ 4 events
○ >4 events

Figure 4.7 Scatter plot of values of Chi-squared from the core fitting procedure and the distance of the closest detector for 7 fold detector responses.

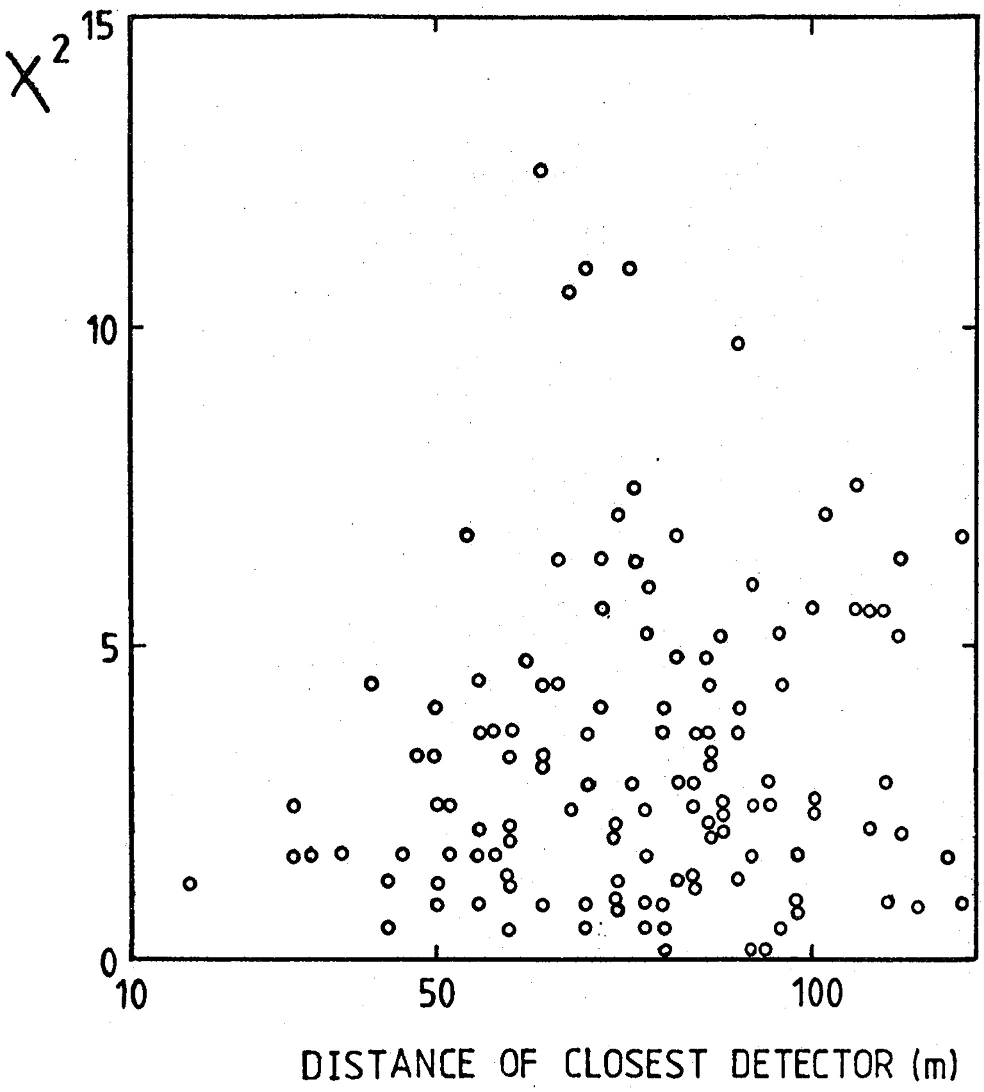

X²
15
10
5
0
10
50
100
DISTANCE OF CLOSEST DETECTOR (m)

used in the calculation of lateral distributions behaves as predicted for a χ^2 distribution and therefore it is justifiable to use that calculation in the simulation of the response of the array to a known air shower.

4.4 Refinement of the Determination of Relative Detector Gain

In the previous section it was pointed out that one of the most important sources of error in obtaining accurate lateral distributions of light density was the uncertainty in the relative gain of the detectors. The field calibration and subsequent laboratory measurements of the detector responses were described in Chapter 3 together with the attendant difficulties in accurate determination which left a residual uncertainty of ~ 20%. The accuracy available from the experimental calibrations was not adequate to extract useful information from the lateral distribution shape and therefore a method of optimising the detector gain measurements was devised.

The method used an iterative procedure to normalise the measurements from each detector at a fixed core distance. A sample of showers was selected from a limited zenith angle and primary energy range and each detector response normalised by Φ_{150m}, the primary energy estimator which was derived from all the densities measured in the shower. The values from individual detectors were then binned in limited core distance ranges in order to produce average lateral distributions for each detector. In theory these distributions should have been identical since they were derived from the same shower sample. However, in practice the errors in gain calibration produced a slightly different shape for each detector caused not only by constant gain discrepancy but also by the attendant error in core distance attribution. The aim therefore, was to derive gain adjustments which produced consistent results on the subset of data and apply them to the whole dataset.

In order not to prejudice the shape of the lateral distribution the adjustments were made on the basis of the response at one point only in the distribution, at 150m from the core. The value of $\Phi_i(150)/\Phi_{shower}(150)$ (where Φ_i is the response from detector i and Φ_{shower} the primary energy estimator for the individual showers), was thus obtained. A gain adjustment was then made to the detector showing the greatest discrepancy and the fitting procedure repeated, leaving all other detector gains the same. The iteration was repeated until the values of $\Phi_i(150)/\Phi_{shower}(150)$ converged to 1 for all detectors. Whereas the correction factor was made only on the basis of the value of the light density at 150 m, the procedure produced consistent lateral distributions over the whole core distance range sampled by each detector. Before the gain correction was made the normalised densities at 250 m differed by 17% whereas afterwards they were consistent to within 6%.

The gain adjustments were, of course, carried out separately for the two seasons' data and the method differed slightly in practice between the two datasets. In the

400 m array the outer ring detectors did not produce a significant number of measurements around 150 m from the core and hence extrapolations could not be made at that point. The outer ring detectors for the second year's data were therefore corrected on the basis of measurements made using the 200 m array where the core distance range sampled by each detector was similar. For the 1978/79 season the response of the outer ring was corrected after the inner ring produced consistent lateral distributions and adjustments were made using measurements as close to 150 m as the core distance distribution allowed.

The refitting procedure was that described in the previous section using a first estimate of the error term. The final term was not of course available until the most accurate detector gains had been determined. Whilst the processes of gain adjustment and error estimation should have been repeated iteratively, in fact the first estimate of the error term was close enough to its optimum value that the change produced no further refinement to the detector gains.

The result of this procedure was to give a relative gain determination correct to ~6% and consistent lateral distributions for each detector. The results from the appropriate subset were used in reanalysis of the whole dataset.

4.5 Primary Energy Attribution for the Dugway Array

The problem of recovering the energy of the primary particle from the information available at ground level effects all extensive air shower arrays and ultimately all must have recourse to simulations of the shower parameters. Thus simulated shower data is searched for a parameter which

(i) shows a simple relationship with increasing primary energy,

(ii) is relatively insensitive to changes in depth of shower maximum due to fluctuations,

(iii) is, at best, invariant or, at least, easily interpretable under changes in the zenith angle of the shower over the energy range being considered,

(iv) is, from an operational point of view, well measured in every shower analysed.

The first consideration demands a primary energy estimator for the Dugway array which should depend solely on the Cerenkov light component but which could be interrelated with estimators used in other longer-established extensive air shower arrays. The only parameter readily available in all showers over all array sizes was the total pulse area as a function of core distance. In practice the total flux density at any fixed core distance is related to the shower size and hence to the primary energy, satisfying the first requirement, but clearly it must also, in general, be depth dependent since the steepness of the lateral distribution function is a depth of maximum measurement. However, by investigating the ratio $\Phi(r)/E_p$ at a range of core distances between 25 m and 1000 m in simulated showers using a range of primary energies, zenith angles and interaction models, it is possible to identify a core distance at which fluctuations due to cascade development are minimised.

Figure 4.8 shows a sample of calculated shower densities normalised by shower energy for a range of primary energies and depths of maximum relevant to the 400 m Dugway array and at a fixed zenith angle. In Figure 4.9 the zenith angle dependence is considered for showers of fixed energy but different depths of maximum. (The value of $\Phi(r) \times r^2/E_p$ is plotted for clarity). It is obvious that no single crossover point exists where the flux becomes independent of cascade development or zenith angle. However, there is a range of core distance over which the fluctuations are considerably reduced, indicating the most promising energy estimator. Figure 4.8 would suggest that a light density between 150 m and 300 m would be an acceptable value for the depth of maximum range appropriate to the present work (600 - 800 g cm^{-2}). Figure 4.9 shows that the best crossover point moves away from the core with increasing zenith angle but that a point within 150 m would be most acceptable. The density at 150 m was hence chosen as a compromise between the cascade development and zenith angle requirements. This core distance was invariably covered in showers recorded by the 400 m array .

It can also be seen from both Figures 4.8 and 4.9 that as the distance between the depth of maximum and the observation level increases (whether by early shower

Figure 4.8 The calculated lateral distributions for a range of depths of maximum at a fixed zenith angle of 35° and observation level of 862 g cm^{-2}.

The models have depth, energy, primary mass, central region multiplicities and cross-sections as follows:

a - 850 g cm^{-2}, 10^{18}eV, A = 1, $E^{0.25}$ constant
b - 800 g cm^{-2}, 10^{18}eV, A = 56, scaling, constant
c - 760 g cm^{-2}, 10^{18}eV, A = 56, scaling, logs
d - 700 g cm^{-2}, 10^{16}eV, A = 1, scaling, logs
e - 650 g cm^{-2}, 10^{17}eV, A = 56, scaling, $\log^2 s$
f - 595 g cm^{-2}, 10^{16}eV, A = 56, scaling, constant
g - 575 g cm^{-2}, 10^{16}eV, A = 56, scaling, $\log^2 s$
h - 500 g cm^{-2}, 10^{15}eV, A = 56, scaling, constant

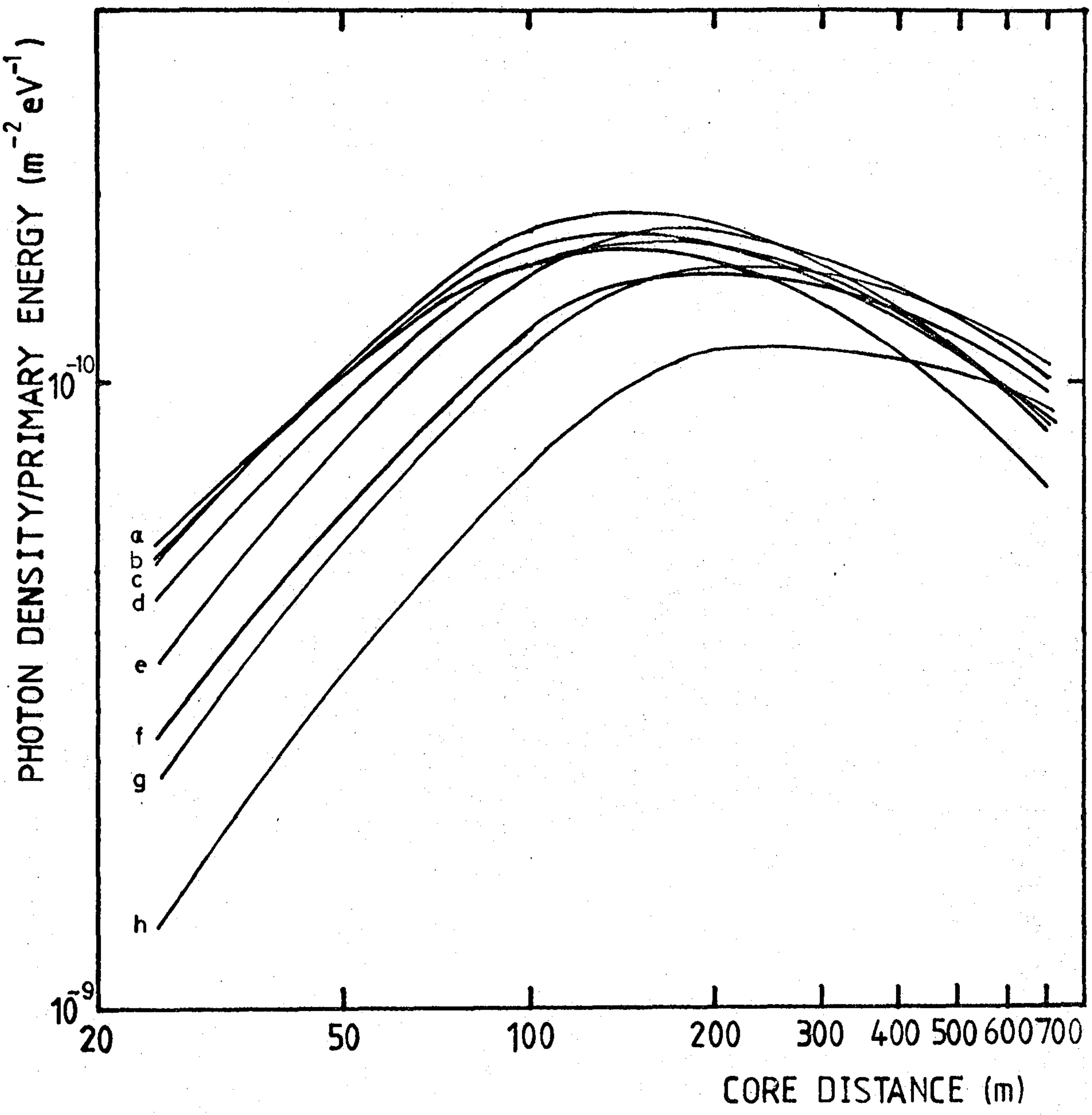
PHOTON DENSITY/PRIMARY ENERGY ($m^{-2}eV^{-1}$)
10^{-10}
10^{-9}
a
b
c
d
e
f
g
h
20
50
100
200
300
400
500
600
700
CORE DISTANCE (m)

Figure 4.9 The calculated lateral distributions for an observation depth of 862 g cm^{-2} for three zenith angles and a range of depths of maximum.

The simulation models used were at 10^{17}eV energy with the following primary masses, central region multiplicities, cross sections and depths of maximum.

a - A = 56, scaling, constant, 690 g cm^{-2}

b - A = 56, $E^{0.33}$, $\log^2 s$, 560 g cm^{-2}

c - A = 1, scaling, logs, 790 g cm^{-2}

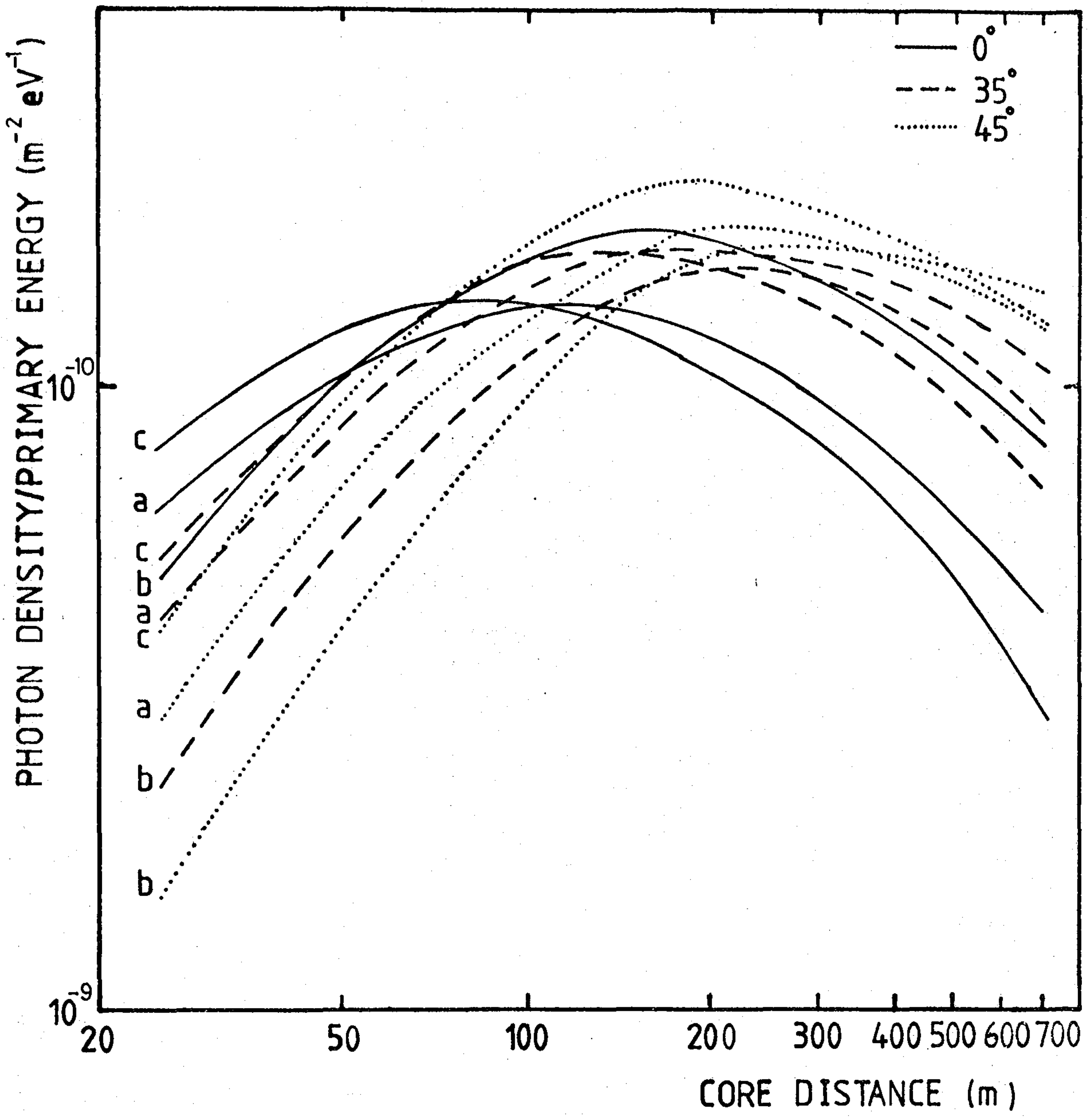

PHOTON DENSITY/PRIMARY ENERGY (m^{-2} eV^{-1})
10^{-10}
10^{-9}
CORE DISTANCE (m)
20
50
100
200
300
400
500
600
700
0°
35°
45°
c
a
c
b
a
c
a
b
b

development or zenith angle effects) the optimal distance for a primary energy estimator increases. Hence the data on lower energy showers obtained by the 100 m array should have a primary energy estimator of, say $\phi(400\text{m})$. Clearly a compromise had to be evolved between this requirement and the available measurement and since the density at 100 m was the furthest distance routinely available this was chosen as the primary energy estimator.

Using a Cerenkov light density as a primary energy estimator was investigated by Wellby (1977) for the Haverah Park Cerenkov Light experiment when he compared the relation between the light density at a series of core distances with the established primary energy estimator ρ_{500}, the deep water tank signal at 500 m from the core measuring a combination of the local density of hard and soft components. (The choice of ρ_{500} derives from the calculations of Hillas et al. (1971).) It was found that $\Phi_{(200\text{ m})}$ correlated more strongly with the Haverah Park primary energy estimator ρ_{500} than the density at other core distances. The suitability of $\Phi_{(150\text{ m})}$ at Dugway (862 g cm^{-2}) and $\Phi_{(200\text{ m})}$ at Haverah Park (1016 g cm^{-2}) accords with the simulation evidence that the increased distance from the shower maximum requires a more distant density as primary energy estimator. This experiment demonstrated that the Cerenkov light density at a fixed distance from the core could be used as a reliable primary energy estimator.

Having established that a simple linear relationship can be assumed, it was necessary to calibrate the primary energy estimator absolutely. Two approaches were available

- either to use simulation data together with the absolute calibration of the detectors against a standard light source where the photon output had been calculated, or to relate the measurements to the Haverah Park primary energy estimator by using the known response of the Dugway and Haverah Park Cerenkov light detectors to the same light source and making allowance for the difference in altitude of the two arrays. The latter method was enhanced by the availability of measurements made by an array of four Cerenkov detectors, similar to those used in the Haverah Park and Dugway arrays, operating in conjunction with the scintillator array at Volcano Ranch (Linsley, Orford, Turver and Waddoup, unpublished). This allowed another calibration against an established primary energy estimator, that obtained from measurements of N_e, the number of electrons in the shower at the observation level of 835 g cm^{-2} - which corresponds approximately to the maximum development of showers in the energy range considered here.

It was thus possible to convert the detector response at 200 m from the core in units of the standard light source to a primary energy measurement at two atmospheric depths, 1130 g cm^{-2} and 835 g cm^{-2} - the depths appropriate to inclined showers at Haverah Park and vertical showers at Volcano Ranch (Wellby, (1977) and Waddoup, unpublished). By interpolating at the Dugway depth of 865 g cm^{-2}, Φ_{200} was found in terms of standard light units and using a reasonable lateral distribution function the density at 150 m was predicted giving a primary energy conversion which was directly related to that used in other air shower experiments and which was independent of any absolute calibration of the output of the radioactive standard light source but demanded only that it was constant.

In obtaining the value of Φ_{150} for each shower it was decided, in consideration of the misfit of the structure function, to limit the core distance range over which detectors contributed to the measurement. However, it was desirable that a primary energy should be assigned to each shower and too restricted a core distance range would result in the rejection of a large amount of data at this early stage in the analysis. On the basis of Figure 4.1 all detector densities within 90 m of the core were omitted and the remaining information was used in a weighted regression of the observed densities and the core distances obtained from the Minuit minimisation to interpolate a light density at 150 m.

4.6 Choice of Depth-Sensitive Parameter

The discussion in Chapter 2 showed the need for an appropriate depth sensitive parameter based on the lateral distribution of light in the shower which is independent of the core distance range sampled. The data analysis procedure has shown the expected deviation from the structure function $(r + r_o)^{-\eta}$ and confirms that η is not the best available parameter. No other simple function produced a marked improvement over the whole dataset and it was undesirable to increase the number of free parameters in the function, reducing the number of degrees of freedom in the fit and hence the minimum number of detector responses in a shower necessary for analysis.

Direct comparison with simulation data would be possible if the ratio between densities at two fixed core distances $R(r_1, r_2)$ was estimated. Furthermore direct deduction of the depth of maximum from the $R(r_1, r_2)$ would be obtained using the relation shown in Figure 2.6.

It is then necessary to choose the most appropriate distances r_1 and r_2 to define the ratio. The sensitivity of the parameter $R(r_1, r_2)$ to depth of maximum is increased by maximising the difference between r_1 and r_2 consistent with the ability to make a good measurement. The outer distance r_2 presents an important problem of biasing data since the effective radius of the shower (the distance at which the pulse peak just reaches the discrimination level) is dependent on the shower size, measured by Φ_{150}, and the steepness of the structure function given by $R(r_1, r_2)$ which is the fluctuating parameter being measured. A full discussion of the energy and depth dependence of the relative collection probability of a given shower is shown in Section 4.8 and here it is merely pointed out that the outer distance r_2 is chosen taking this into consideration to minimise biases which would favour broad lateral distributions (corresponding to high developing showers). The biasing effect can be corrected using Monte Carlo simulations provided enough information is left from the original input distribution.

The distribution of the core distances of responding detectors is given in Figure 4.10 for the energy range $1.2 \times 10^{17} - 3.6 \times 10^{17}$eV (specified by log Φ_{150} at 3.7 - 4.2), and it can be seen that densities are well measured at 100 m and 250 m in this energy range. At lower energies the loss of the more distant detector responses is observed. Figure 4.11 shows the dependence of the effective radius of the shower on the depth of shower maximum found using data from the simulation of McComb and Turver (1981) discussed in Chapter 2. (Since there are slight differences in the discrimination level of each detector due to the different photomultiplier gain, the figure shows the results for a typical detector).

Different methods were used to find distributions of R(100m,250m) on average and in individual events. The philosophy of measuring local densities (see e.g. Craig et al. (1979)) demands that there should be a reasonable number of detector responses in a limited range about the chosen distance allowing accurate interpolation of the local behaviour. In order to find the ratio $R(r_1, r_2)$ on a shower by shower basis it is necessary to select only showers satisfying certain requirements of core distance disposition.

This selection is thus essentially on core location, a parameter independent of shower depth of maximum and hence it does not introduce any further selection bias. The crucial, additional requirements in the data selection which can produce a bias are:

(i) that at least one detector lies at a distance

Figure 4.10 The distribution of the core distances of responding detectors in energy range 1.2 x 10^{17}eV - 3.6 x 10^{17}eV.

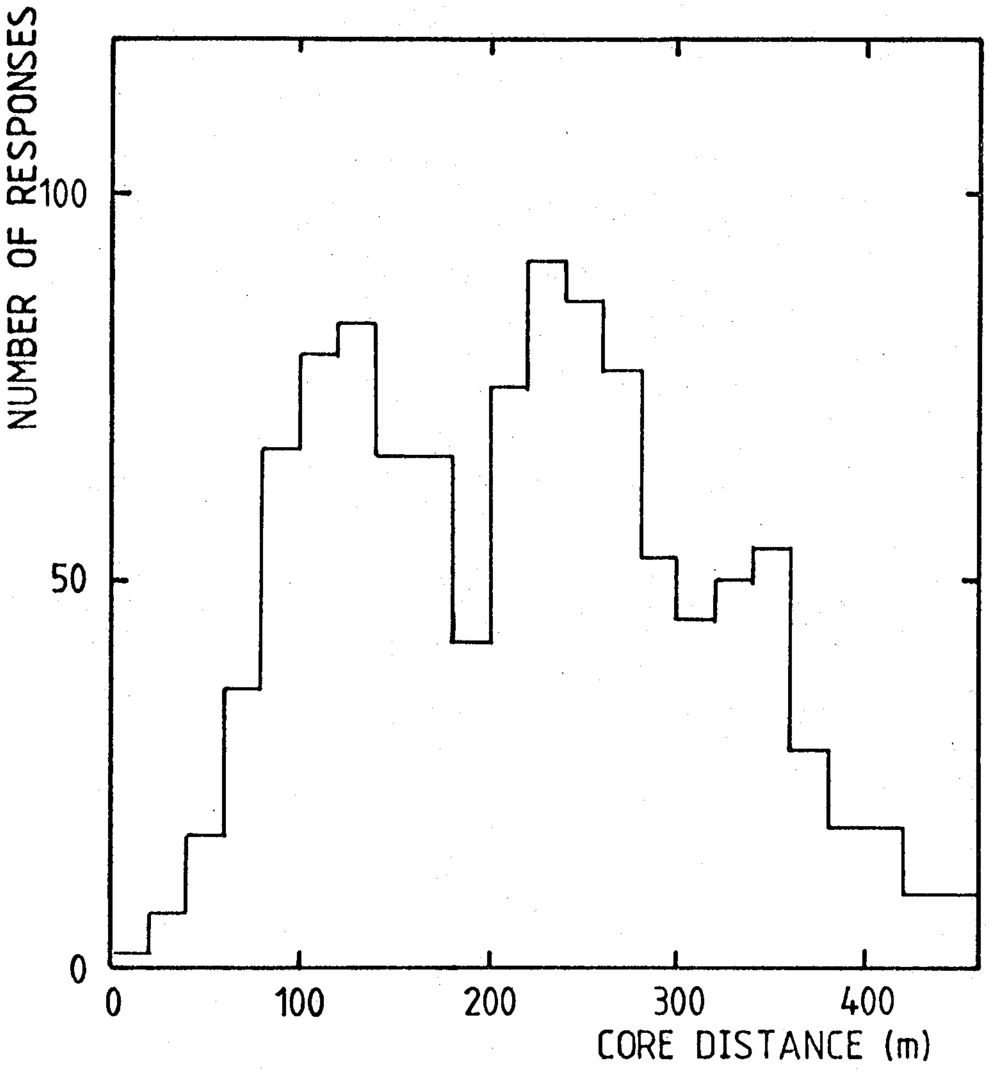
NUMBER OF RESPONSES
100
50
0
0
100
200
300
400
CORE DISTANCE (m)

Figure 4.11 The effective radius of showers (i.e. the maximum distance at which a detector triggers) for a typical detector with a range of zenith angles, and two different energies (log Φ_{150} of 3.4 corresponds to a primary energy of 6 x 10^{16}eV and 3.7 corresponds to 1.2 x 10^{17}eV).

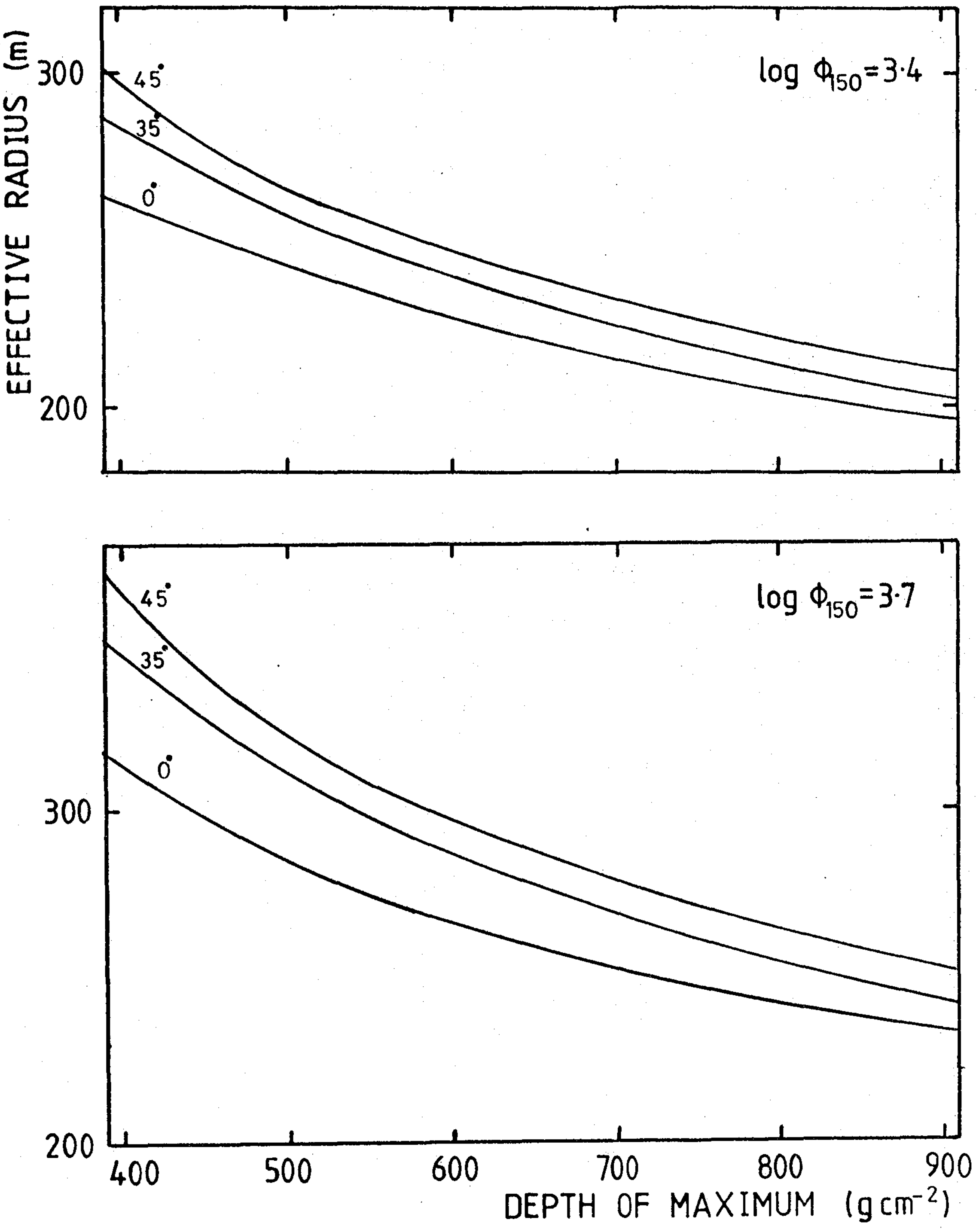
EFFECTIVE RADIUS (m)
300
200
log Φ_{150}=3·4
45°
35°
0°
log Φ_{150}=3·7
45°
35°
0°
300
200
400
500
600
700
800
900
DEPTH OF MAXIMUM (g cm^{-2})

in excess of r_2 and

(ii) that at least six detector responses are available for analysis.

Thus the selection procedure involves in this experiment, as in others, the rejection of a large proportion of the data for fluctuation analysis.

In contrast when measuring the average value of $R(r_1, r_2)$ it is desirable to use all the data available which satisfy the following criteria (common to both datasets);

(a) at least five detectors responded giving a reliable core fit measurement,

(b) the shower core landed within the triangle defined by the outer ring detectors,

(c) the value of χ^2 is acceptable at the 5% confidence level,

(d) the shower has a zenith angle of $< 45°$,

(e) clear skies were viewed on the night of operation.

Average lateral distributions were then obtained by dividing the detector responses into limited zenith angle and energy bins (bin widths were selected to have similar predicted $R(r_1, r_2)$ variations in zenith angle and energy) and reconstructing the lateral distribution of densities normalised by the primary energy estimator (Φ_{150}) and averaged over limited core distance bins.

For both the average lateral distributions and the reconstruction of individual events a weighted least squares regression was used to interpolate densities at 100 m and 250 m using only measurements in the region adjacent to these core distances. The weights used in the regression were the standard error for each averaged density in the former case and the calculated measurement error, already used in the core fit, in the latter. In choosing the range of distances to use in the interpolation a balance must be sought between the reduction in the size of the dataset and the accuracy of interpolation and the ranges 75 m - 200 m and 150 m - 300 m were selected as leaving an acceptable dataset whilst allowing minimal imposition of the theoretical structure function.

Thus the depth sensitive parameter R(100m,250m) was provided both as an average measurement and, on a more limited dataset, as a fluctuating measurement which includes experimental uncertainties and the true statistical fluctuation in shower development.

4.7 Array Response Simulations

The Monte Carlo simulation of the array response was undertaken to investigate two elements of the measurement process:-

(i) the biasing of the dataset due to preferential selection of showers initiated high in the atmosphere, and

(ii) the uncertainties in reconstruction of the depth sensitive parameter $R(r_1, r_2)$ due to the instrumental uncertainties and the sampling procedure.

The need for these simulations and the method employed is described below.

4.7.1 The Effect of Sample Selection Criteria

The biasing effect of the selection of a well measured dataset was present in each of the analysis procedures used in this experiment and since each analysis imposed different selection criteria the effects operated differently in each case.

The selection of each dataset started with the triggering requirement of the array - that three detectors, not including the central detector or the assymmetric detector (detectors 1 and 0) recorded light signals in coincidence. However in order to obtain well measured values of the various shower parameters it was necessary to impose severe criteria on the quality of the measurements and these criteria depended on the parameter being measured. It was found, for example, that five measurements were required to give a reliable determination of the shower core provided that the core lay within the array boundary. This meant that if the core position was required in determining a shower parameter five detector responses were a minimum criterion for the inclusion of the shower in the dataset.

The factors which determined whether a shower was recorded, in the first place, were the geometry and size of the array and the level at which detectors discriminated a light pulse from the sky background. The zenith angle of the shower affected both these factors because the array was foreshortened in the plane normal to the shower and the sensitive area of the detector was similarly reduced. Each detector triggered when the signal from the photomultiplier amplifier reached 20 mV and this meant that the minimum light signal which could be recorded was slightly different for each detector because of the different detector gains. The probability of a given shower being detected was principally dependent on the way the maximum height of the light pulse fell away as the distance from the shower core increased - the lateral distribution of peak height. Since the height of the pulse was determined by the pulse shape scaled by the total pulse area and the lateral distribution of both these quantities, at fixed primary energy, was strongly correlated with the depth of shower maximum, the core distance at which the shower just attains the discrimination level is a depth dependent quantity. Thus the probability of selection of a shower was related to the parameter being measured (t_{max}). The effect was to introduce a spurious enhancement of the relationship between primary energy and depth of shower maximum because at low energy, high developing showers were preferentially selected while the bias reduced as the primary energy increased.

The problem could be solved in two ways. Firstly, given a particular array size and geometry, there is a lower energy limit above which all showers from the input dataset will trigger the array. (A threshold must exist similarly for each subsequent selection criterion). In fact, finding this threshold demands some knowledge of the original depth distribution or at best an upper limit to the steepness of the lateral distribution function. This need not be an insurmountable problem and a reasonable estimate could be obtained by considering an extreme simulation model. Furthermore where the onset of a biasing effect is sudden it is usually possible to see it directly in the data and impose a suitable threshold.

A simple energy cut was not identifiable in the Dugway data however, since measurements were required beyond the distance at which the primary energy estimator, Φ_{150}, was measured. (This can be compared with the Haverah Park Infilling Experiment (Craig et al.,(1979) where the particle density at 500 m, ρ_{500}, was both the primary energy estimator and the distant measurement required). The triggering requirement of the Dugway array in fact showed the progressive onset of the bias which minimised the energy dependence of the depth of maximum leading to a spuriously large elongation rate. In addition to the problem of identifying a suitable energy threshold, the main drawback of such a course was the loss of data involved. Figure 4.12 shows that this threshold must be above $\log\Phi_{150}$ of 4.5 ($E_p \sim 7 \times 10^{17}$eV) for the $R(r_1, r_2)$ measurement of depth of maximum. This would reduce the data set before further quality selection to 27 showers.

The second possible solution was to attempt to correct for the progressive effect of the array bias allowing a much greater proportion of the collected data to be used. This demanded a detailed simulation of the array triggering biases using appropriate shower data and examining the probability of selection. Thus different sets of selection criteria were tested and the probability of inclusion in any analysed dataset obtained. Events selected

Figure 4.12 The selection probabilities for inclusion in the dataset for the determination of the mean lateral distribution parameter R(100m, 250m) for a range of zenith angles and values of log Φ_{150}.

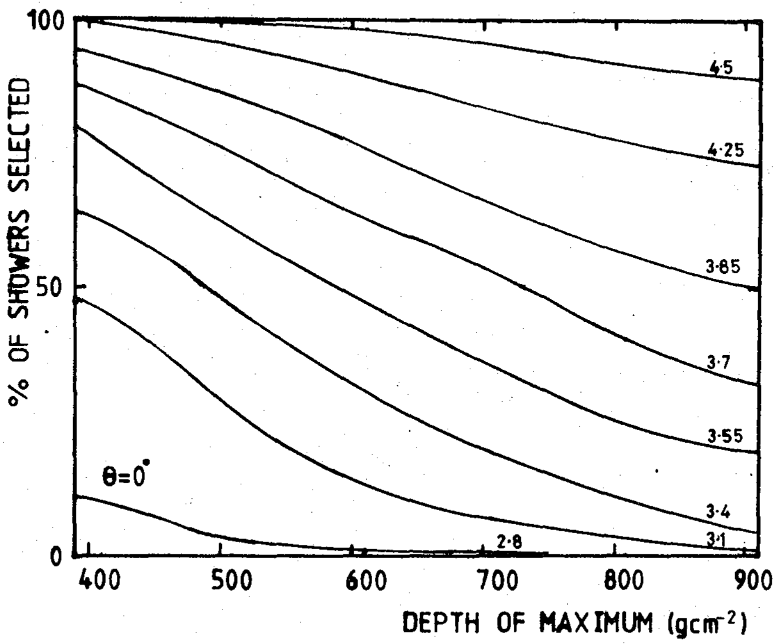
100
50
0
% OF SHOWERS SELECTED
θ=0°
4·5
4·25
3·85
3·7
3·55
3·4
3·1
2·8
400
500
600
700
800
900
DEPTH OF MAXIMUM (gcm^{-2})

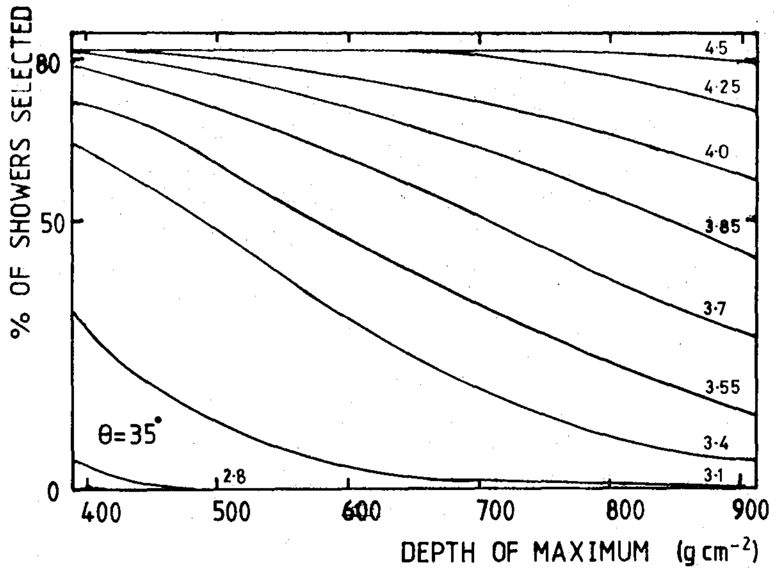
80
50
0
% OF SHOWERS SELECTED
θ=35°
4·5
4·25
4·0
3·85
3·7
3·55
3·4
3·1
2·8
400
500
600
700
800
900
DEPTH OF MAXIMUM (g cm^{-2})

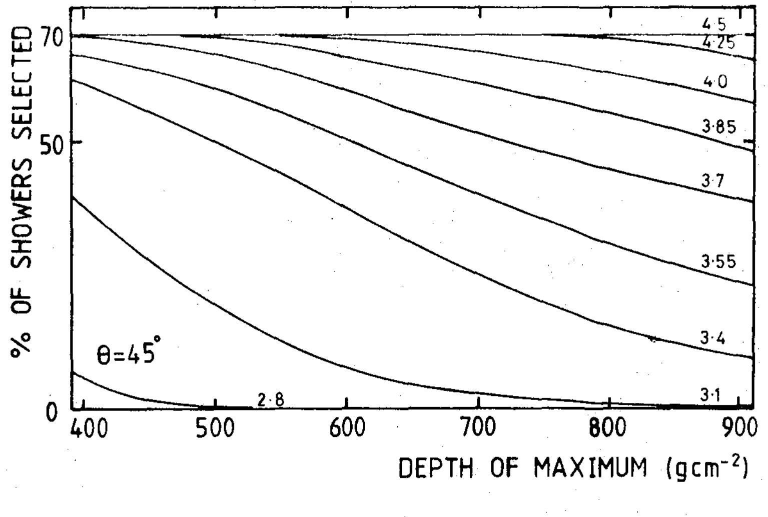
70
50
0
% OF SHOWERS SELECTED
θ=45°
4·5
4·25
4·0
3·85
3·7
3·55
3·4
3·1
2·8
400
500
600
700
800
900
DEPTH OF MAXIMUM (gcm^{-2})

with a reduced probability could then be weighted such that their contribution to the data analysis was appropriate to their representation in the incoming cosmic ray flux. The limit to this procedure is imposed when the input distribution is not sufficiently represented in the selected data to allow unambiguous reconstruction. With that proviso in mind this latter solution was used to account for selection bias in the Dugway experiment.

4.7.1.1. The Simulation Method. In Figure 4.13 a flow chart shows the procedure used to investigate selection probabilities. Simulated showers were generated to land randomly across the array and the showers which would have triggered the array were recorded. Data for this was obtained from the full shower simulation of McComb and Turver (1981) described in Chapter 2 and the result that certain shower parameters are dependent essentially on the depth of maximum was used. By labelling showers by depth of maximum independent of model, energy and primary particle it was possible to obtain the pulse height variation with core distance over a range of t_{max}. Since it was only necessary to test whether the detectors triggered or not an accurate reconstruction of the peak height was required only over the core distance range 200 m to 500 m. An interpolating function was chosen which fitted well over that limited range. The function used was

$$pk(r) = \alpha(r + 100)^{-\beta}$$

where pk was the peak height

Figure 4.13 Flow chart of the program used to investigate the triggering probabilities of different showers for the 400 m array configuration.

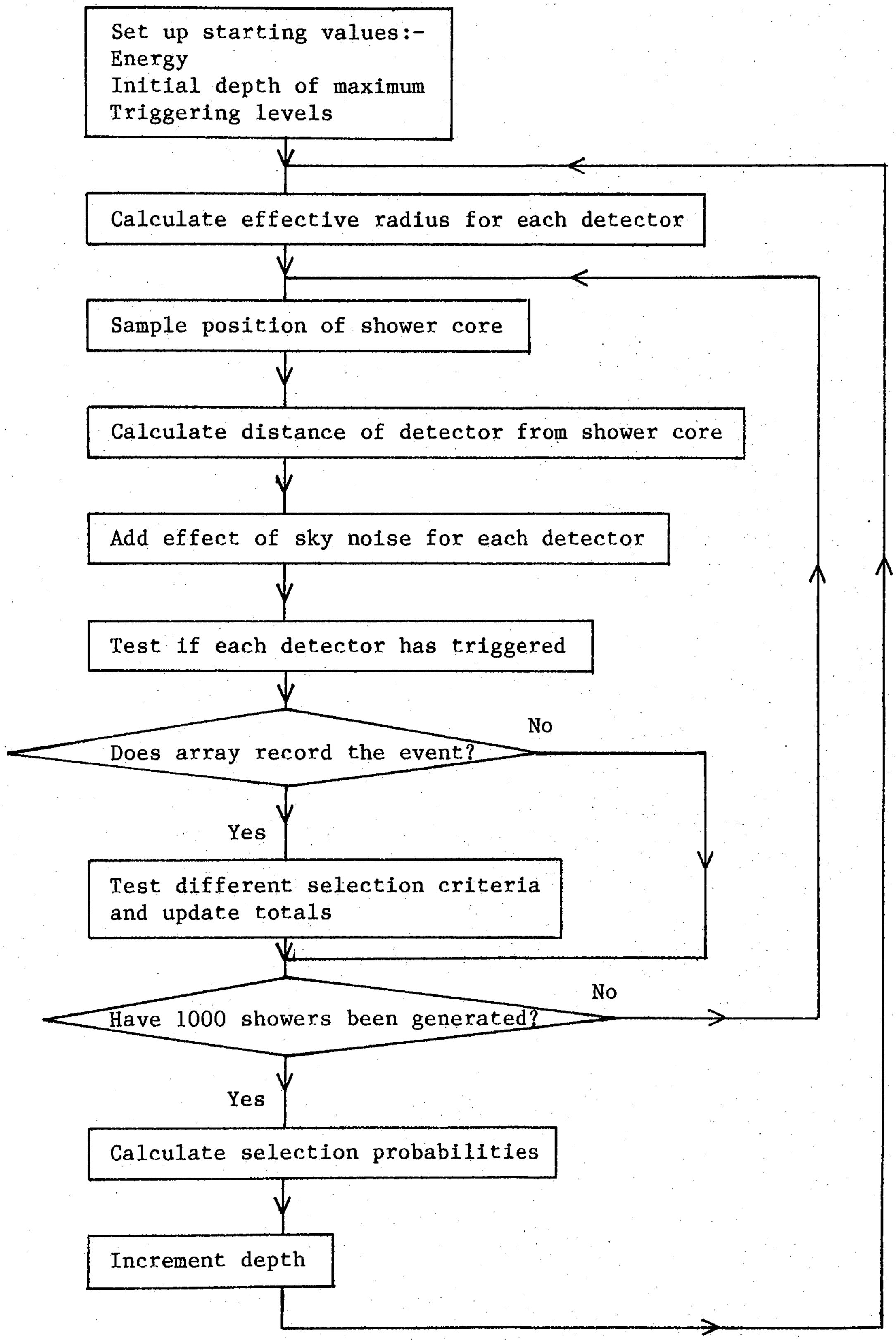
Set up starting values:-
Energy
Initial depth of maximum
Triggering levels
Calculate effective radius for each detector
Sample position of shower core
Calculate distance of detector from shower core
Add effect of sky noise for each detector
Test if each detector has triggered
Does array record the event?
No
Yes
Test different selection criteria and update totals
Have 1000 showers been generated?
No
Yes
Calculate selection probabilities
Increment depth

r was the core distance

β was a function of t_{max} and zenith angle which was found empirically from the data of Mc Comb and Turver (1981),

and α was a normalising factor. The normalising factor was calculated from the ratio between the peak height at 150 m and the total light density, Φ_{150}. This ratio was energy independent but varied with zenith angle and t_{max} and was obtained in the same way as β above.

Triggering probabilities were those calculated for a series of depths of maximum and a series of primary energies. The primary energy was set as a value of Φ_{150} measured in mVns so that it was not necessary to convert the 20 mV triggering level to an equivalent light signal before testing whether a detector had triggered. Thus the interrelation between these array response simulations and measured data was not dependent on the absolute gain calibration of the detectors.

For showers of fixed primary energy, zenith angle and depth of maximum an "effective radius" could be calculated from the peak height structure function above. This was the distance at which the light signal just attained the detector discrimination level and was different for each detector because of their different relative gains. The simulation program selected core positions and taking account of distortion of the array due to zenith angle effects tested to see whether each detector was within the effective radius. Finally a 5mV jitter was added to the pulse height before a decision was made whether the detector had triggered. This was to take account of background sky noise.

Calculations were made for three zenith angles 0°, 35° and 45° and the resultant probabilities adjusted to take account of the reduced collecting area of the array for inclined showers. Of more interest than simply whether the shower had triggered the array was whether the shower was selected for data analysis in any of the different aspects of this experiment. Therefore each shower was also tested to see whether it met the more stringent criteria imposed before it was included in lateral distribution or pulse shape measurements, (see Section 4.6 and Chantler (1982)). The results for different triggering criteria are shown in Figures 4.12 and 4.14.

The same simulation procedure was readily adapted to the lower energy measurements of the smaller arrays by changing the array coordinates. In addition it was necessary to recalculate the zenith angle and depth of maximum dependence of the peak height structure function parameters because the core distance range of the smaller arrays was significantly different.

4.7.2 The Effect of Sampling Errors

A further series of simulations investigated the effects of experimental error and of the sampling procedure on the results obtained from the experimental analysis. One of the results required from this experiment was the magnitude of fluctuations in the depth of shower maximum due to the mechanism of shower production. In order to

Figure 4.14 The selection probabilities for inclusion in the dataset for R(100m, 250m) fluctuation analysis for three zenith angles and a range of values of log Φ_{150}.

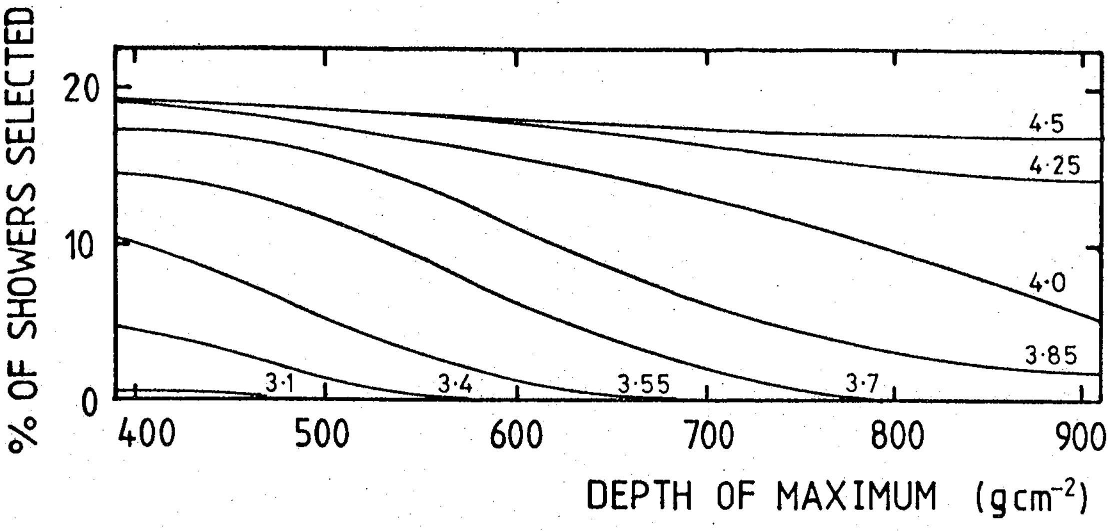
% OF SHOWERS SELECTED
0
10
20
400
500
600
700
800
900
DEPTH OF MAXIMUM (gcm⁻²)
4·5
4·25
4·0
3·85
3·7
3·55
3·4
3·1

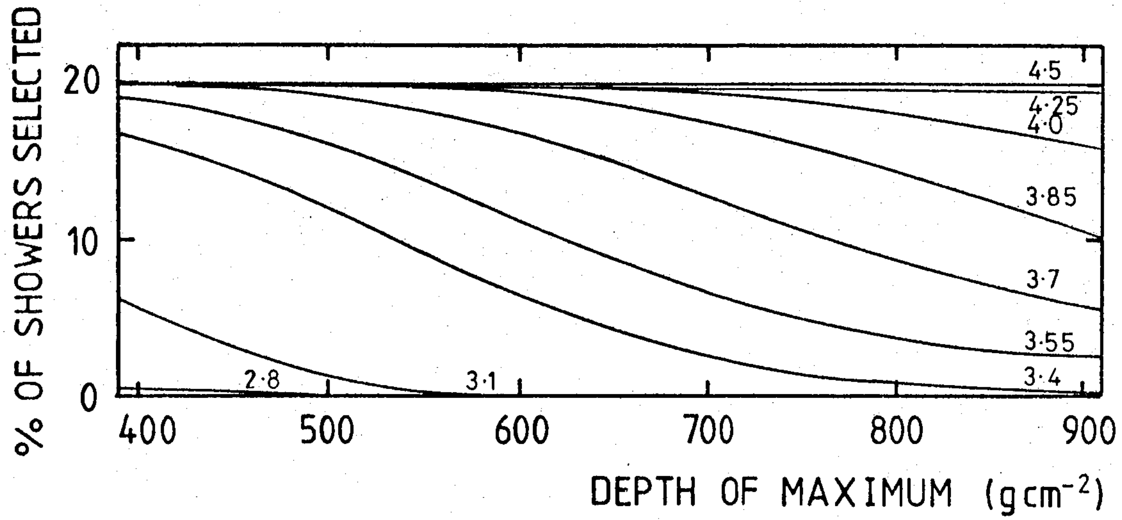
% OF SHOWERS SELECTED
0
10
20
400
500
600
700
800
900
DEPTH OF MAXIMUM (gcm⁻²)
4·5
4·25
4·0
3·85
3·7
3·55
3·4
3·1
2·8

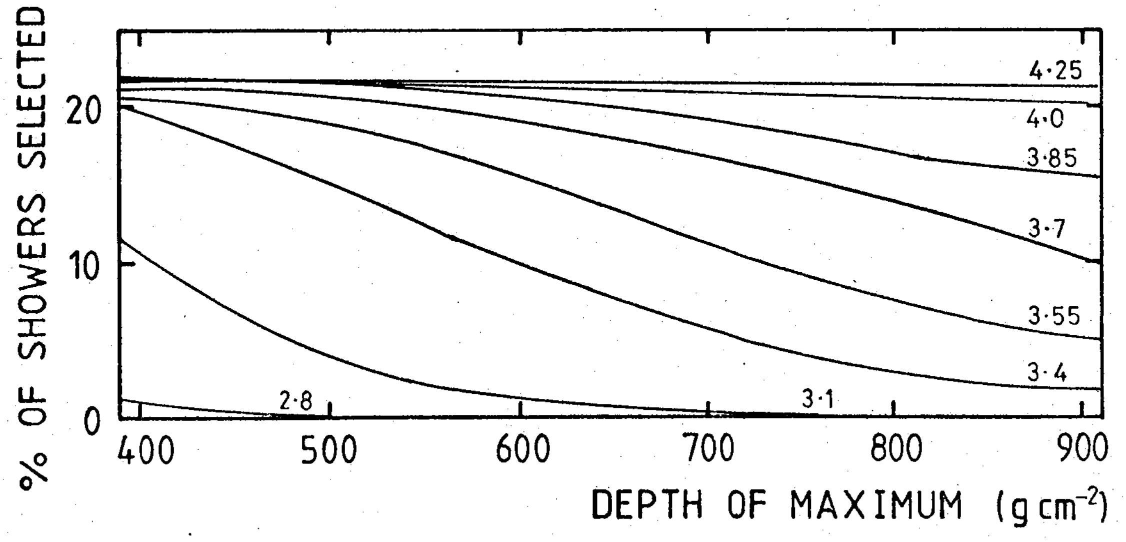
% OF SHOWERS SELECTED
0
10
20
400
500
600
700
800
900
DEPTH OF MAXIMUM (gcm⁻²)
4·25
4·0
3·85
3·7
3·55
3·4
3·1
2·8

find this it was necessary to take account of the fluctuations in the measured shower parameters due simply to the experimental procedure.

The elements which contributed to measurement uncertainty have been described in Section 4.3. However, the method used to obtain the best estimate of the depth sensitive parameter R(100m,250m) did not allow this experimental uncertainty to be used to obtain an estimate of error on that parameter for each shower. (The method used to obtain R(100m,250m) should be compared with that used to find the pulse shape parameters described in Chantler (1982)). It was therefore decided to use the knowledge of instrumental uncertainties to produce a series of sets of simulated showers each assuming a different magnitude of fluctuations in the depth of maximum. This data was then submitted to precisely the same analysis as the true showers and the real data could be matched with the simulated data to obtain an estimate of the residual fluctuations due to particle interactions in the shower.

Figure 4.15 shows the method used to generate data simulating the true measurements. The only information about individual shower characteristics not used in the previous simulations was the depth of maximum and zenith angle dependence of the parameter R(100m,250m). To simulate detector measurements it was necessary to use a theoretical structure function and the function

$\Phi(r) = A(r + 50)^{-\eta}$ as in Section 4.3.1

was used. This was the relationship used in finding the

Figure 4.15 Flow chart for the program used to investigate the effects of sampling errors in the determination of R(100m, 250m).

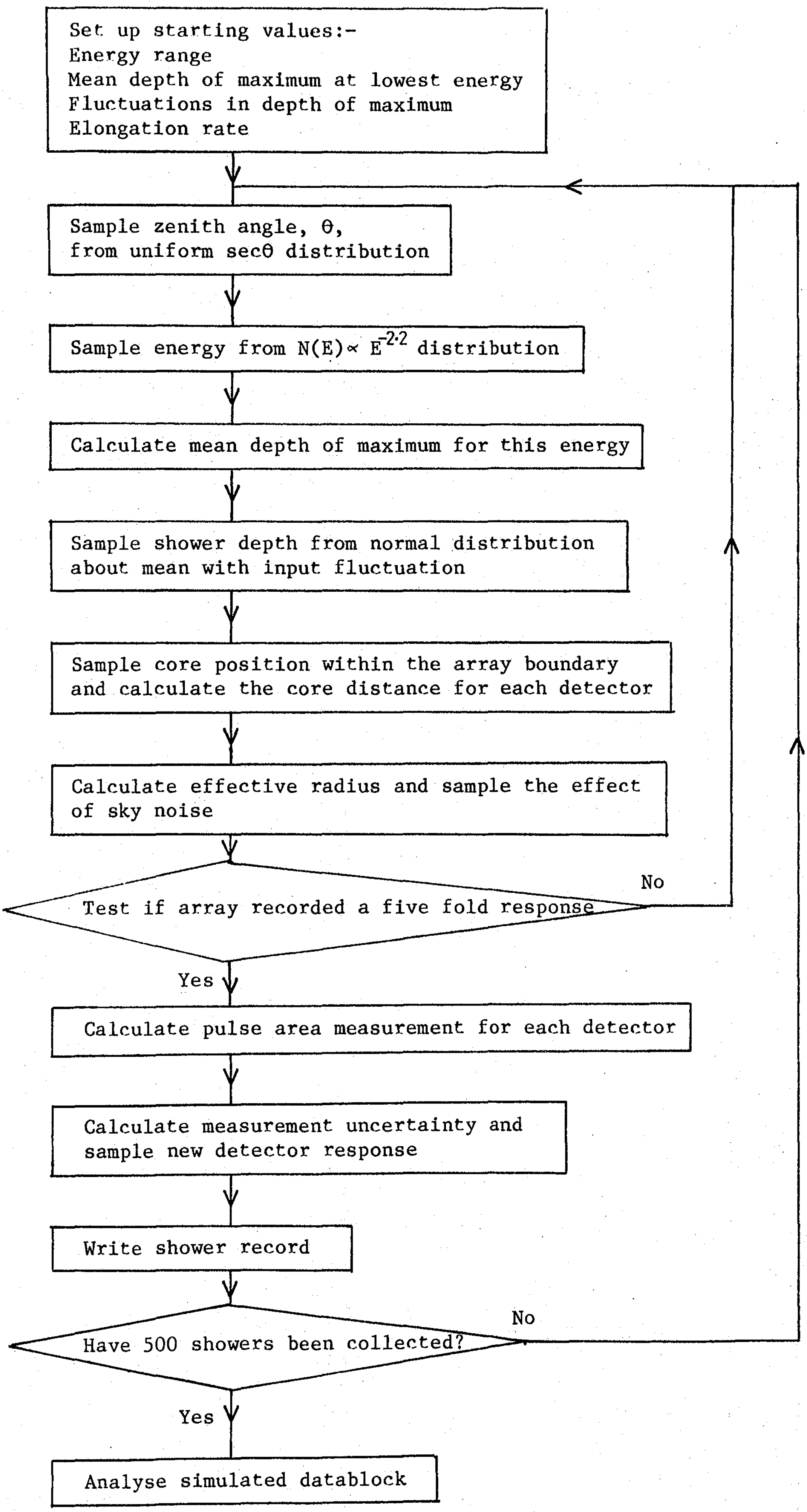
Set up starting values:-
Energy range
Mean depth of maximum at lowest energy
Fluctuations in depth of maximum
Elongation rate
Sample zenith angle, θ, from uniform secθ distribution
Sample energy from N(E)∝ E^{-2·2} distribution
Calculate mean depth of maximum for this energy
Sample shower depth from normal distribution about mean with input fluctuation
Sample core position within the array boundary and calculate the core distance for each detector
Calculate effective radius and sample the effect of sky noise
Test if array recorded a five fold response
No
Yes
Calculate pulse area measurement for each detector
Calculate measurement uncertainty and sample new detector response
Write shower record
Have 500 showers been collected?
No
Yes
Analyse simulated datablock

shower core.

Whilst this has been shown to be inadequate in finding a good measurement of the lateral distribution because the steepness parameter, η , depended on the core distance range over which the measurement was made, the misfit was treated as noise on the individual detector responses and was included in the error attributed to each measurement. The error term used was that calculated in Section 4.5 using the χ^2 distributions of the dataset. The simulated detector responses were found by sampling a value from a normal distribution with the predicted value as mean and the calculated error as standard deviation.

The distribution of primary energy used was from the primary energy spectrum

$$N(E) \propto E^{-2.2}.$$

The zenith angle distribution sampled was uniform in $\sec\theta$. This was a reasonable approximation of the distribution of the true dataset . Finally, the dependence of R(100m, 250m) on zenith angle and depth of maximum was necessary. This was estimated from the full shower simulation of McComb and Turver which led to a relationship

$$R(100m,250m) = -0.01945 \sec^{0.5}\theta\ (t_{max}-590) + 0.0305\ (t_{max}-590) + 5.946 \sec^{-2}\theta + 1.$$

This was a good approximation in the zenith angle range $\theta°$ to 45° and the t_{max} range 390 to 800 g cm^{-2}. It was not appropriate beyond a zenith angle of 45° and it overestimated the value of R(100m, 250m) at 60°.

This outlines the method used to generate the simulated data. The results of the fluctuation analysis are given in Chapter 5.

In addition to investigating the fluctuations in the parameter R(100m, 250m), the procedure also provided useful information on the accuracy of reconstruction of the showers' core positions and primary energy estimators. Errors in the recovered distances from detectors were typically 12 m and Φ_{150} could be recovered to better than 10%.

4.8 Conclusion

This Chapter has given a detailed account of the analysis procedures used in obtaining the results presented in the following chapters. This includes the philosophy behind the selection of R(100m, 250m) as the depth sensitive parameter and its calculation. The analysis procedures allowed an accurate assessment of the measurement errors inherent in the detection system. This then has been used in the Monte Carlo simulations of the array response which provided a framework for determining the effect of the measurement fluctuations in augmenting the true fluctuations in depth of shower maximum.

CHAPTER 5

THE LATERAL DISTRIBUTION OF CERENKOV LIGHT IN EXTENSIVE AIR SHOWERS

5.1 Introduction

In the previous chapter the analysis procedure to obtain distributions of Cerenkov light from the shower records of the Dugway Cerenkov Light Detector Array was described. It is the aim of this chapter to demonstrate the characteristics of the lateral distribution shape parameter $R(r_1, r_2)$ which was derived. This involved interpreting the dependence of the average value on energy and zenith angle and the fluctuations of the individual measurements from average behaviour. These data were then interpreted as measurements of the depth at which the shower maximised.

The dataset used for analysis is first described and reasons for imposing the selection criteria discussed. From this dataset the zenith angle and energy dependence of the average lateral distribution were derived. This analysis used the parameter R(100m, 250m) as the measurement of lateral distribution shape. The ratio R(100m, 200m) was also investigated as a depth of maximum measurement. This showed that any choice of r_1 and r_2 was equally valid and allowed consistency to be demonstrated between the depth of maximum measurements of the 400 m array and the two smaller arrays where different values of r_1 and r_2 were used. It also provided one measurement of depth of cascade maximum at an energy below that available from

R(100m, 250m).

More stringent requirements of data quality meant that a reduced dataset was available for analysis of shower fluctuations. For each of these showers a value of R(100m,250m) was available and the deviation of these points from the average value was interpreted as a measurement of fluctuations in depth of maximum.

Finally an attempt was made to investigate the behaviour of the shape parameter η, obtained from the core fit procedure described in Section 4.3. Despite its low quality as a depth sensitive measurement it is a lateral distribution parameter which was routinely available from a large enough dataset to allow investigations of correlations between different depth sensitive measurements from the Dugway experiment, e.g. the lateral distribution of light density and pulse shape. This investigation was to demonstrate its suitability for correlation studies.

5.2 Data Selection

Before attempting to analyse the shower information it was necessary to select data which was both reliable and amenable to interpretation using the theoretical knowledge available. The first criterion imposed has already been discussed in Section 4.3 - that five detector responses were required to provide a reliable core position. A further requirement on the quality of the core fit was that the core should have landed inside the boundary of the array.

In the present study, data were considered only in the zenith angle range 0° to 45°. This limitation was imposed because although inclined shower simulations were available for interpretation up to zenith angles of 60° the primary energy estimator Φ_{150} became increasingly inappropriate at large zenith angles (see Section 4.6). Since large zenith angle simulations suggest that the magnitude of changes in R(100m,250m) due to changes in depth of maximum alone decreases rapidly beyond 45° and since only a small number of showers were detected at zenith angle beyond 45° this limit was chosen. This made the interpretation of data simpler and represented a marginal loss of information.

The problem of rejecting those showers of low energy recorded because of extreme bias in array triggering has already been discussed in Section 4.8.1. A lower energy threshold had to be imposed below which it was fruitless and unreliable to attempt to interpret measurements. This was the level at which detected showers could no longer be said to represent the distribution of primary particles. Figure 5.1 shows the energy distribution of showers with cores landing within the array at zenith angle of less than 45° and giving at least five detector responses one of which was beyond 250 m. (This was the dataset from which results are presented). Superimposed on this is the primary energy spectrum of

$$N(E) \propto E^{-2.2},$$

which has been normalised to fit the observed distribution in the range of log $_{150}$ of 4.1 to 4.3 (primary energy 2.9×10^{17}eV - 4.5×10^{17}eV). This comparison, together

Figure 5.1 The primary energy distribution of showers selected for the determination of the mean value of R(100m, 250m). The dashed lines represent a primary energy spectrum of $N(E) \alpha E^{-2.2}$ normalised to the observed data between 2.9×10^{17}eV and 4.5×10^{17}eV.

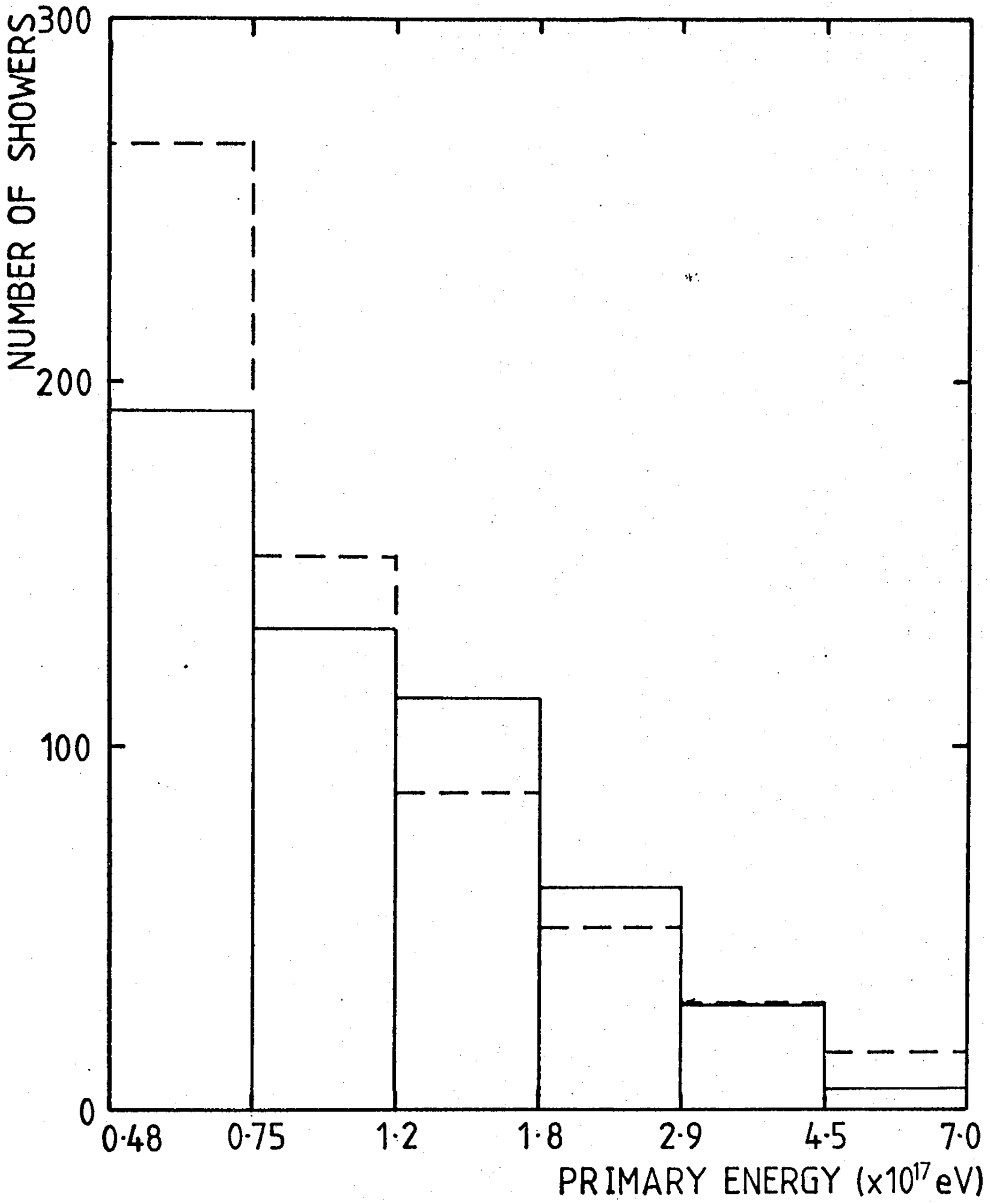
NUMBER OF SHOWERS
300
200
100
0
0·48
0·75
1·2
1·8
2·9
4·5
7·0
PRIMARY ENERGY (x10^{17} eV)

with the energy dependence of selection probabilities displayed in Figure 4.13, suggested that a lower energy limit of 1.2×10^{17}eV ($\log\phi_{150}$ of 3.7) was suitable. The choice of a conservative limit was influenced by the fact that showers with energies below this were within the range of data available from the 200 m and 100 m arrays (Walley, private communication).

A final quality check was placed on the data to ensure that no residual data errors were included in the final analysis. This check was carried out by rejecting from the dataset any shower producing a χ^2 value for the core fit analysis with a significance level of less than 5%. In addition no data were included from nights with other than good sky clarity.

These requirements lead to a reliable dataset of 200 showers spanning the energy range 1.2×10^{17}eV to 7×10^{17}eV (mean energy 2×10^{17}eV) with zenith angles between 0° and 45° from which mean lateral distribution of light density could be built up, providing measurements of R(100 m,250m) at different energies and zenith angles. In creating this dataset a further requirement was imposed - that there should be at least one responding detector beyond 250 m from the shower core. Although this produced a biasing effect on the dataset its inclusion can be interpreted using array response simulations. Were this distance requirement not introduced, the interpolated density at 100 m would be based on measurements from all showers in the sample whereas the density at 250 m would be influenced only by those showers with a broad enough lateral distribution to trigger detectors at that distance. This would mean that the parameter R(100 m,250 m) would not be a true representation of the average behaviour of the showers in the sample and could not be interpreted as a measure of depth of maximum.

5.3 The Dependence of R(100m, 250m) on Cascade Development

Before attempting to interpret R(100m, 250m) as a measure of depth of cascade maximum it was necessary to show that the parameter displayed a dependence on the factors which determined cascade development. Firstly a strong zenith angle dependence was predicted reflecting changes in the total depth of atmosphere above the array and the density distribution of the air through which the shower developed. The other dominant factor in shower development which should be displayed in the variation of R(100m,250m) was primary energy since the depth at which the electron shower maximises moves deeper into the atmosphere with increasing energy. In this dataset the effects of changes in R(100 m,250 m) due to zenith angle were expected to dominate over those due to primary energy. The simulation study of McComb and Turver (1981) described in Section 2.5.4 predicted that the change in the average value of R(100m,250m) due to zenith angle effects was four times greater than that caused by primary energy between the extremes of energy and inclination in this dataset.

Average lateral distributions of detector response were collected for a series of zenith angle and energy intervals. These intervals were chosen to have an approximately similar variation of R(100m, 250m) due to primary energy and zenith angle effects. Before contributing to the average lateral distribution each detector response was normalised using the primary energy estimator Φ_{150} for the shower. Errors were attributed to each response corresponding to the measurement uncertainty of the value combined with the uncertainty in estimating Φ_{150}.

Figures 5.2 and 5.3 show examples of mean lateral distributions of detector response for the two extreme zenith angle intervals ($\sec\theta$ of 1.0 - 1.05 and 1.40 - 1.45) at fixed primary energy (1.1×10^{17} - 2.3×10^{17}eV). The figures clearly show the broadening of the lateral distribution as the zenith angle of the shower increased. Simulated shower lateral distributions have been added to these figures to show that the shape of the distribution over the whole core distance range accords very well with the simulation predictions. No particular significance is attached to the model chosen - it was selected because the value of R(100m, 250m) was approximately the same as that of the measured value and the zenith angle is the nearest to the mean of the zenith angle interval which was available from simulations. It is not intended to act as an interpretation of R(100m, 250m) as a depth of shower maximum.

Measurements of R(100m, 250m) were calculated in each of the energy and zenith angle intervals by interpolating

Figure 5.2 The composite lateral distribution of the normalised detector responses from showers in the zenith angle interval $\sec\theta$ of 1.0 - 1.05 and primary energy 1.1×10^{17} - 2.3×10^{17} eV. The dashed line is the simulation prediction for a vertical shower maximising at 570 g cm^{-2}.

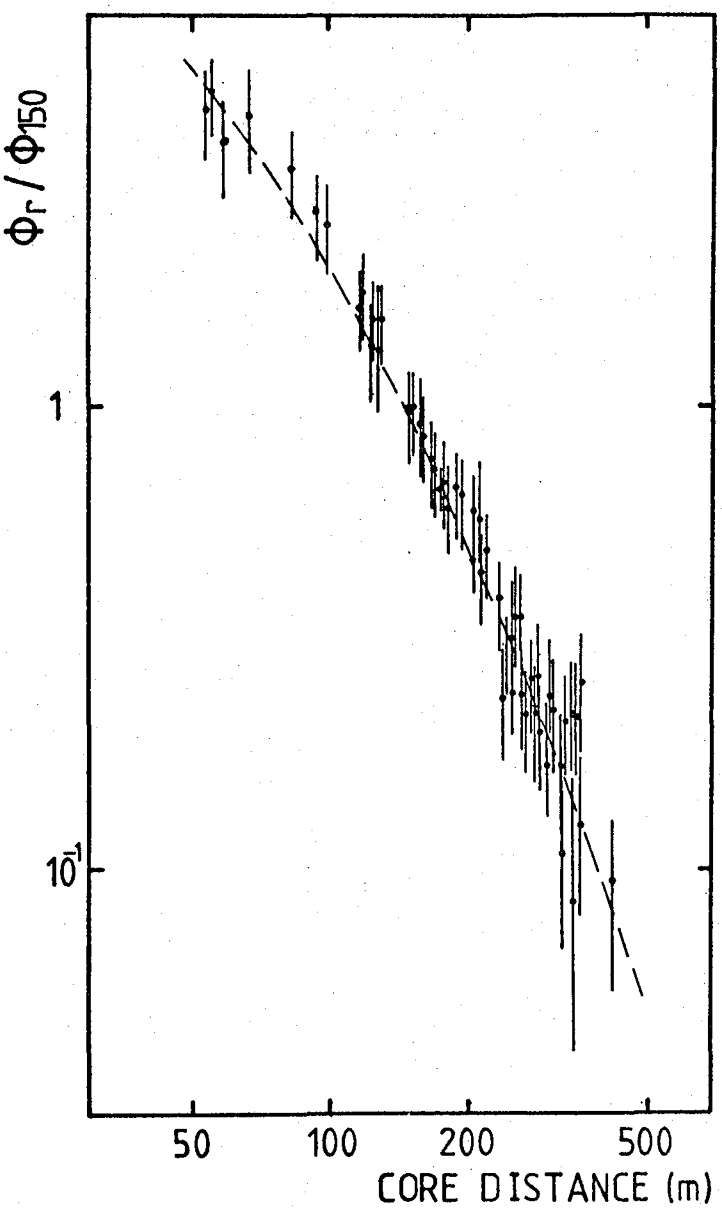

Φ_r / Φ_{150}
1
10^{-1}
50
100
200
500
CORE DISTANCE (m)

Figure 5.3 The composite lateral distribution of the normalised detector responses for showers with $\sec\theta$ of 1.40 - 1.45 and primary energy 1.1×10^{17} - 2.3×10^{17} eV. The dashed line is the predicted lateral distribution for a shower at 45° maximising at 570 g cm^{-2}.

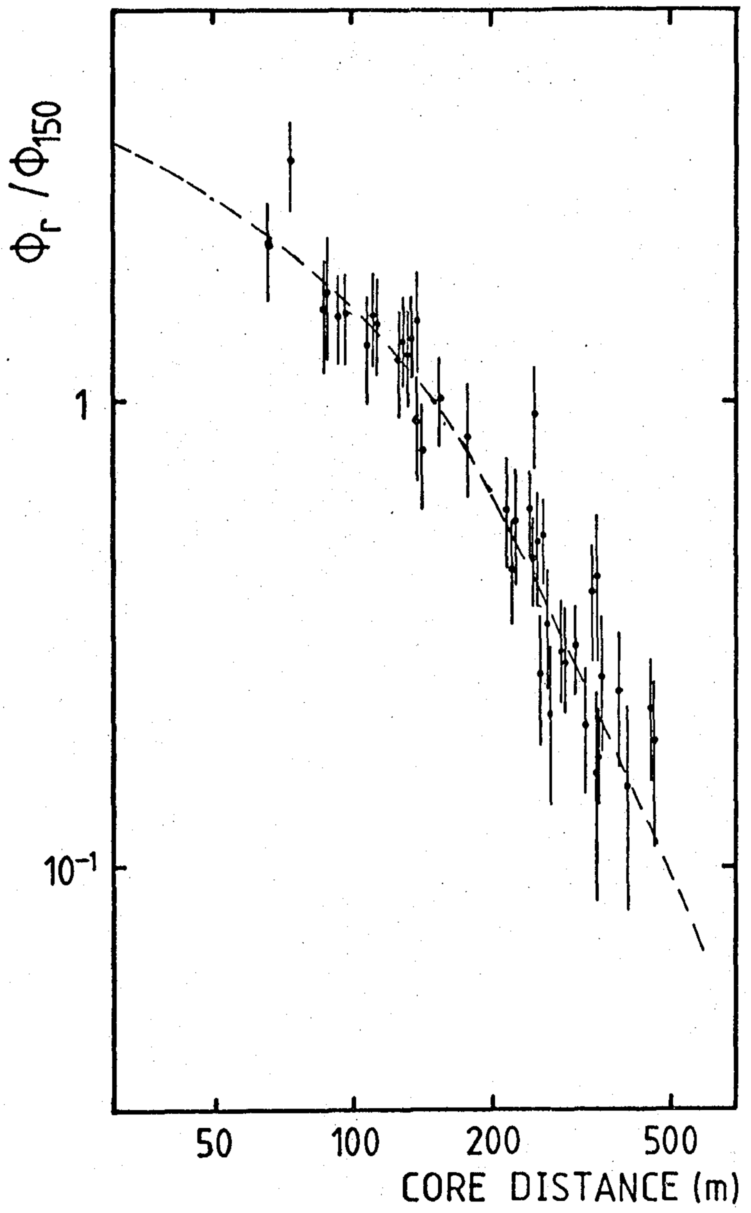
Φ_r / Φ_{150}
1
10^{-1}
50
100
200
500
CORE DISTANCE (m)

TABLE 5.1

Measurements of R(100m, 250m)

Zenith Angle (secθ)	Primary Energy (log Φ_{150})		Zenith Angle secθ
	3.7 - 4.0	4.0 - 4.5	
1.00 - 1.05	7.00 ± 0.13	7.92 ± 0.64	1.00 - 1.10
1.05 - 1.10	7.03 ± 0.27		
1.10 - 1.15	6.22 ± 0.23	6.73 ± 0.64	1.10 - 1.20
1.15 - 1.20	5.93 ± 0.24		
1.20 - 1.25	5.31 ± 0.30	5.46 ± 0.35	1.20 - 1.30
1.25 - 1.30	4.39 ± 0.15		
1.30 - 1.35	4.72 ± 0.10	5.18 ± 0.49	1.30 - 1.40
1.35 - 1.40	4.77 ± 0.20		
1.40 - 1.45	3.63 ± 0.30		

between detector responses averaged over limited core distance ranges. Figure 5.4 displays a set of such measurements with densities interpolated at 100 m and 250 m. The resultant ratio values are presented in Table 5.1.

Figure 5.5 shows the measured ratio values compared with the simulation predictions of the variation of R(100m,250m) with zenith angle for showers with constant depth of maximum. This figure displays the strong dependence of R(100m,250m) on zenith angle but also clearly shows the expected small increase in the parameter between the two energy intervals.

A functional dependence of R(100m,250m) on zenith angle and primary energy was not calculated for each measurement since each value could be interpreted directly as a measurement of depth of maximum as described in the next section.

5.4 Interpretation of the Mean Characteristics of R(100m,250m)

The sensitivity of the average value of the parameter R(100m,250m) to changes in cascade development due to primary energy and zenith angle effects was demonstrated in the previous section. This parameter can be interpreted directly as a measure of depth of cascade maximum using the results of the model calculations of Mc Comb and Turver (1981) described in Section 2.5. These shower simulations indicate that the mean characteristics of the Cerenkov light shower were principally dependent on the depth at which the shower maximised in the atmosphere. The mass of the primary particle and the nature of the interaction model used in the simulation defines the depth of shower

Figure 5.4 The mean lateral distributions for showers with mean energy 3.2 x 10^{17}eV. The crosses (+) represent the interpolated values of ϕ_{100} and ϕ_{250}.

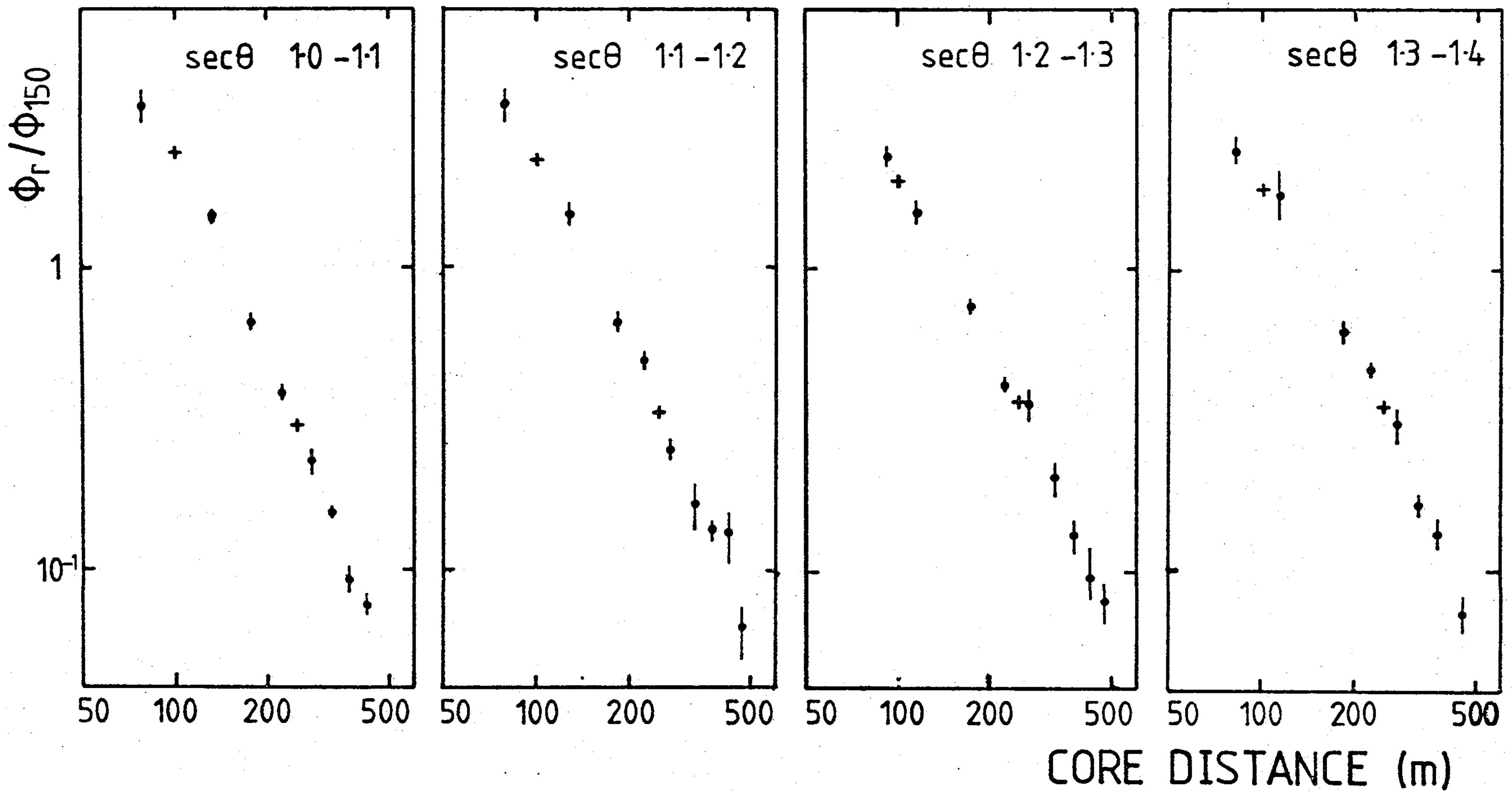
Φ_r / Φ_150
1
10⁻¹
secθ 1·0 – 1·1
secθ 1·1 – 1·2
secθ 1·2 – 1·3
secθ 1·3 – 1·4
50
100
200
500
CORE DISTANCE (m)

Figure 5.5 The measured mean values of R(100m, 250m) for two energy intervals and a range of zenith angles. The open circles represent showers of mean energy 3.2×10^{17}eV and the crosses, an energy of 1.6×10^{17}eV. The simulation lines are the predictions for showers of fixed depth of maximum observed at 862 g cm^{-2}.

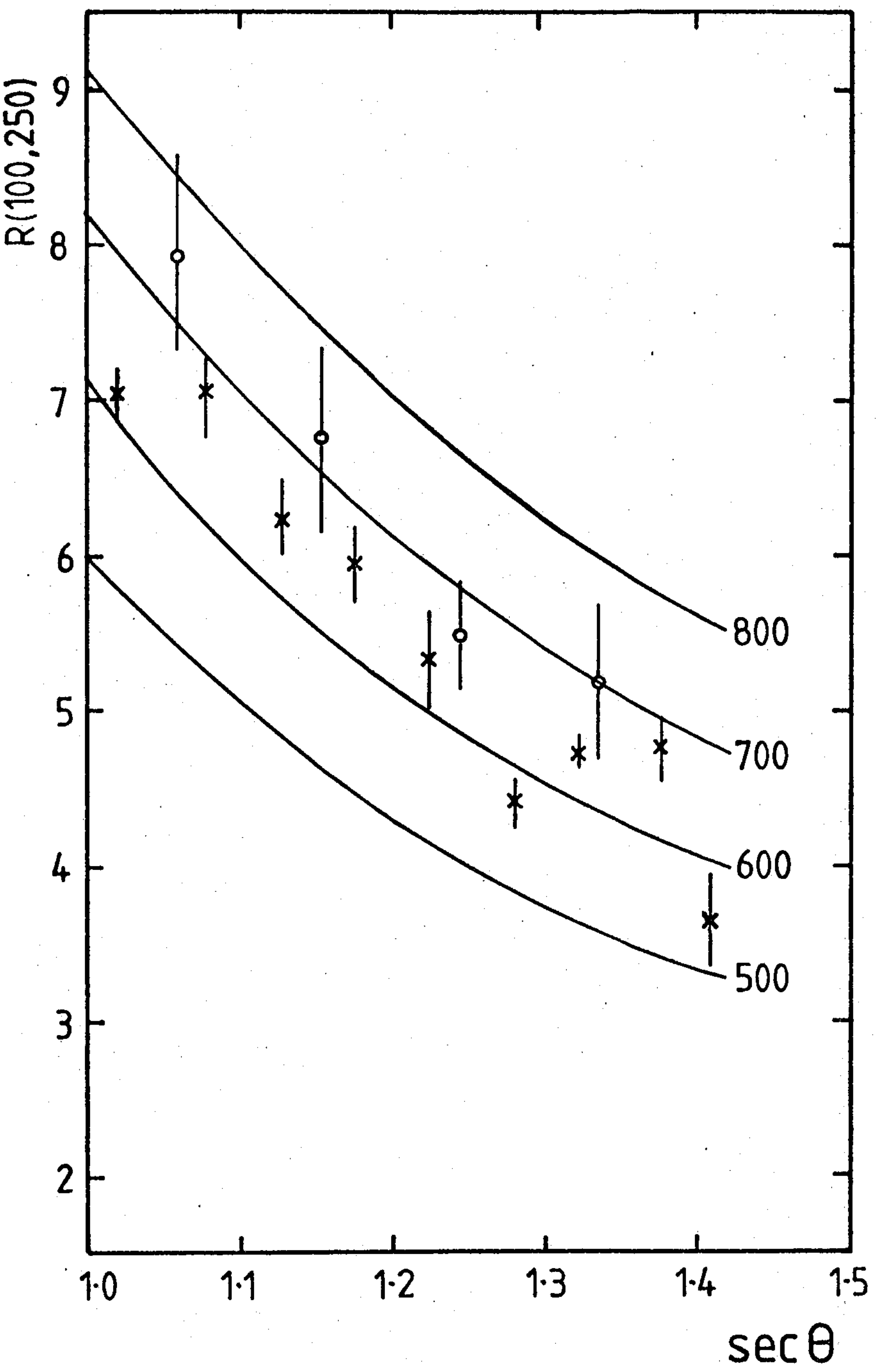
R(100,250)
9
8
7
6
5
4
3
2
1·0
1·1
1·2
1·3
1·4
1·5
sec θ
800
700
600
500

maximum but does not further influence the measurable features of the shower. By using this result it was possible to relate the parameter R(100m,250m) directly to a depth of cascade maximum without making assumptions about the nature of the primary particle.

An empirical expression was derived from the data of Figures 2.4 and 2.6 to calculate depth of maximum as a function of zenith angle and R(100m,250m). This relation

$$t_{max} = 590 + \left(\frac{R(100m,250m) - 5.946 \sec^{-2}\theta - 1}{- 0.01945 \sec^{0.5}\theta + 0.0305}\right) g\ cm^{-2} \qquad (5.1)$$

was applicable in the zenith angle range 0° to 45° for showers with depths of maximum between 390 and 790 g cm^{-2}. Table 5.2 shows the results of transforming the R(100m,250m) values of Table 5.1 to values of depth of maximum using equation 5.1.

These measurements however were subject to the selection biases described in Section 4.7.1. The showers which contributed to these measurements were not directly representative of the primary particle flux but depended also on the acceptance criteria of the analysis procedure which preferentially selected showers with higher depths of maximum. It was therefore necessary to apply the calculation of selection probabilities from Section 4.7.1.1. A first order correction was applied to each value of Table 5.2 by calculating the displacement of the mean depth of maximum of the measured showers from the mean of the original distribution. For this calculation the original distribution was taken to have the mean depth of maximum

TABLE 5.2

R(100m, 250m) interpreted as Depth of Maximum

Zenith Angle ($\sec\theta$)	Primary Energy ($\log \Phi_{150}$)		Zenith Angle ($\sec\theta$)
	3.7 - 4.0	4.0 - 4.5	
1.00 - 1.05	619 ± 12	778 ± 74	1.00 - 1.10
1.05 - 1.10	678 ± 26		
1.10 - 1.15	645 ± 23	722 ± 67	1.10 - 1.20
1.15 - 1.20	656 ± 26		
1.20 - 1.25	629 ± 33	659 ± 40	1.20 - 1.30
1.25 - 1.30	562 ± 18		
1.30 - 1.35	630 ± 12	696 ± 61	1.30 - 1.40
1.35 - 1.40	672 ± 26		
1.40 - 1.45	540 ± 40		
Weighted Mean	624 ± 12	694 ± 24	
Primary Energy (eV)	1.6×10^{17}	3.2×10^{17}	

as in column II of Table 5.2 and a standard deviation of 80g cm^{-2}. (The calculation was not sensitive to small changes in these assumptions). The corrections applied to each value of R(100m,250m) in Table 5.2 are shown in Table 5.3.

By applying these corrections the lower energy mean depth of maximum measurements became

633 ± 16g cm^{-2} at mean energy of 1.6 x 10^{17}eV

which should be compared with the higher energy measurement, not requiring correction, of

694 ± 26g cm^{-2} at mean energy of 3.2 x 10^{17}eV.

The error quoted is a combination of the standard error on the mean of the measurements and a 10g cm^{-2} uncertainty in the values of t_{max} attributed to computational error in the shower simulations, (McComb and Turver, private communication).

5.5 Further Depth Sensitive Lateral Distribution Measurements

The lateral distribution measurement discussed throughout the chapter has been the ratio R(100m,250m) which was chosen to be appropriate to the geometry of the 400 m Dugway array. The core distance range sampled by the array meant that the ratio was well measured and it provided the maximum sensitivity to changes in the depth of shower maximum. However the ratio of any two spot densities would provide a parameter which could be interpreted as a measure of depth of maximum and for arrays of different geometry the distances r_1 and r_2 chosen to calculate $R(r_1, r_2)$ would be different. The 100 m and 200 m Dugway arrays

TABLE 5.3

Corrections to depth of maximum measurements on the basis of selection probabilities

Primary Energy $\log\Phi_{150}$)	Depth of maximum (g cm^{-2})	Correction (g cm^{-2})		
		0°	35°	45°
3.7	630	18	12	10
3.85	640	13	8	5
4.0	660	7	5	3
4.25	680	2	-	-

used ratios R(50m, 100m) and R(75m, 150m) respectively. The detailed analysis of these measurements was undertaken by Walley (unpublished).

This meant that although a single analysis technique was used for showers at different energies measured by different arrays the parameter being interpreted was not the same in each case. It was therefore important to investigate a second R(r_1, r_2) ratio for one of the arrays to show consistency within the same energy range between different ratio measurements.

The ratio R(100m,200m) was also well measured by the 400 m array though the fact that r_1 and r_2 were closer than for R(100m,250m) meant that it was less sensitive to changes in depth of maximum and was therefore, not the optimum parameter. It could however, be interpreted at lower energies than R(100m,250m) because showers only needed to be able to trigger detectors beyond 200 m rather than 250 m to be included in the analysis. Thus the selection bias did not affect the data irrecoverably beyond an energy threshold of log Φ_{150} of 3.5 (7.5 x 10^{16}eV). (The selection probabilities displayed in Figure 4.14 are appropriate to this dataset and show that a shower with log Φ_{150} of 3.7 has approximately the same probability of inclusion in the dataset for R(100m,250m) analysis as a shower with log Φ_{150} of 3.5 in the R(100m,200m) analysis). This lower energy threshold therefore provided an additional reason for analysing the ratio R(100m,200m).

The calculation of R(100m,200m) proceeded in exactly the same way as R(100m,250m) and Figure 5.6 shows the zenith angle dependence of this parameter for different energy intervals together with the appropriate simulation predictions for R(100m,200m) at fixed depth of shower maximum. 364 showers were used in this analysis. Figure 5.6 should be compared with Figure 5.5 where similar results were shown for R(100m,250m) for a dataset of 200 showers.

The R(100m,250m) values were interpreted as measurements of depth of cascade maximum using the appropriate relationship from shower simulation data and the results are displayed in Table 5.4. Only the lowest energy measurement required to be corrected for the selection bias which allowed high developing showers to be recorded preferentially.

It is important to note that the two highest energy points show excellent agreement with the values obtained from R(100m,250m) and demonstrate the essential consistency in the analysis technique. The lowest energy point provides a further measurement of mean depth of maximum of $\underline{624\pm 11\text{gcm}^{-2}\text{ at an energy of }9.5\times 10^{16}\text{eV.}}$

5.6 Fluctuations in Depth of Maximum

The accurate determination of values of R(100m,250m) in individual showers is possible only for a subset of the data used in measuring the average characteristics, since strict requirements on the core distance distribution of the responding detectors must be satisfied before the light densities at 100 m and 250 m from the core can be accurately interpolated. The selection of these showers is described in Section 4.6.

The fluctuation in the depth sensitive parameter

Figure 5.6 The mean value of R(100m, 200m) for three energy intervals and a range of zenith angles. The filled circles represent showers of mean energy 3.5 x 10^{17}eV, the open circles have mean energy 1.5 x 10^{17}eV and the crosses a mean energy of 9.5 x 10^{16}eV. The simulation lines show the predictions for showers with fixed depth of maximum observed at 862 g cm^{-2}.

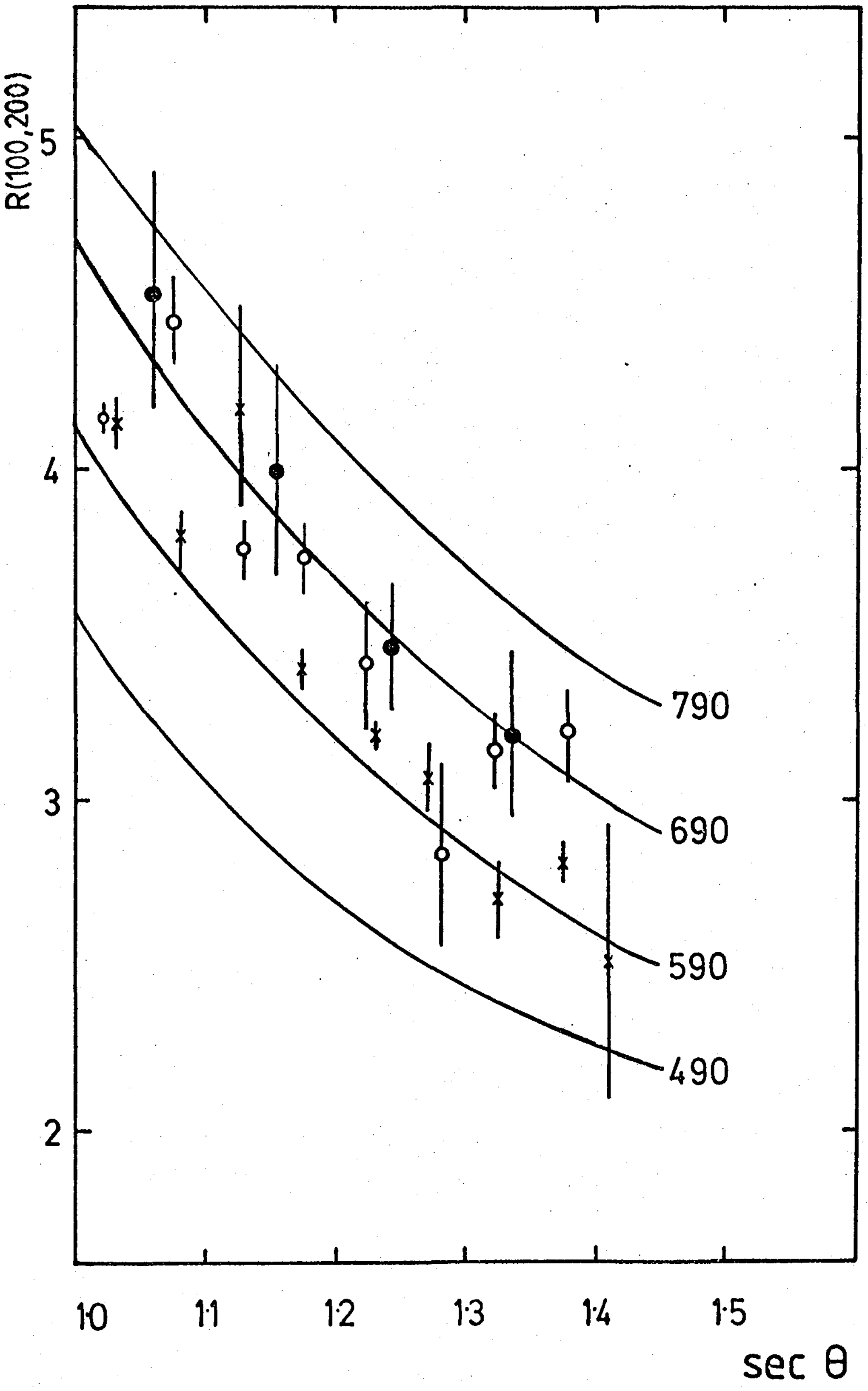
R(100,200)
5
4
3
2
790
690
590
490
1·0
1·1
1·2
1·3
1·4
1·5
sec θ

TABLE 5.4

R(100m, 200m) interpreted as Depth of Maximum (g cm^{-2})

Zenith Angle ($\sec\theta$)	Primary Energy ($\log \Phi_{150}$)			Zenith Angle ($\sec\theta$)
	3.5-3.7	3.7-4.0	4.0-4.5	
1.00 - 1.05	621 ± 13	612 ± 7	737 ± 95	1.00 - 1.10
1.05 - 1.10	605 ± 17	735 ± 34		
1.10 - 1.15	732 ± 74	643 ± 15	720 ± 79	1.10 - 1.20
1.15 - 1.20	611 ± 12	680 ± 21		
1.20 - 1.25	615 ± 8	657 ± 40	682 ± 42	1.20 - 1.30
1.25 - 1.30	620 ± 22	573 ± 67		
1.30 - 1.35	572 ± 32	674 ± 27	690 ± 55	1.30 - 1.40
1.35 - 1.40	628 ± 14	722 ± 38		
1.40 - 1.45	569 ±124			
Weighted Mean	600 ± 7	631 ± 12	695 ± 55	
With correction for selection bias	624 ± 4			
Primary energy (eV)	9.5×10^{16}	1.5×10^{17}	3.5×10^{17}	

is quantified by the standard error on a multiple regression of R(100m,250m) with primary energy and zenith angle. The form of zenith angle dependence and the interaction term between primary energy and zenith angle is that suggested by Figure 2.6. This value measures the statistical fluctuations when the systematic dependence of the depth of maximum on primary energy and zenith angle has been removed. However the fluctuation is a combination of the true distribution of depth of maximum due to the randomness of collisions in shower development and the uncertainty caused by the measurement process. These effects must be distinguished.

Initially the data was examined for correlation between R(100m,250m) and atmospheric pressure, since this factor causes changes in the atmospheric depth through which the shower develops. No significant dependence was observed on the reduced dataset. However it was decided to remove the small correlation before the multiple regression with zenith angle and energy was performed.

The multiple regression of R(100m,250m) with $\log \Phi_{150}$ and $\sec\theta$ used the form

$$R(100m,250m) = a + b\sec^{-2}\theta + c(\log \Phi_{150}-3.7) + d(\log \Phi_{150}-3.7)\sec^{0.5}\theta$$

which fitted well with the results of Figure 2.6.

In order to distinguish the true fluctuations from the measurement uncertainty, the simulation of array response was expanded to investigate the full analysis procedure used to produce this set of measurements of R(100m,250m). This procedure and the reasons for its adoption are described in Section 4.7.2. Datasets of approximately 50 showers were generated, each from a distribution of primary particles sampled from the same energy and zenith angle distribution as the measured data and with the depth of maximum fluctuating about the measured average value (see Section 5.4) with a different standard deviation for each dataset.

The multiple regression of the reconstructed R(100m,250m) on zenith angle and the reconstructed value of Φ_{150} was then performed to calculate the standard error, σ_R, appropriate to the intrinsic fluctuations of that dataset (Δt_{max}). Thus it is possible to produce a calibration of fluctuations in depth of maximum against the standard error on the multiple regression. Figure 5.7 shows the results of the simulation exercise. The errors on the value of σ_R are calculated as $\frac{1}{2\nu}$ where ν is the number of degrees of freedom in the regression. The calculated points are fitted to a curve

$$\sigma_R{}^2 = \sigma_c{}^2 + B(\Delta t_{max})^2$$

where σ_c is the error due to the measurement process.

Imposing the conservative lower energy threshold of 1.2×10^{17}eV used in calculating the average characteristics of R(100m,250m) (see Section 5.2) left only 47 showers for the regression analysis of the true data.

This gives a standard error of 1.30 ± 0.14.

Interpreting this from the relationship of Figure 5.7 produces

$\Delta t_{max} = 68\text{g cm}^{-2}$ with 68% confidence limits of

$0 < \Delta t_{max} < 95$ at a mean energy of 1.8×10^{17}eV.

Figure 5.7 The relationship between the residual fluctuations in the parameter R(100m, 250m) and the fluctuations in depth of maximum of the original distribution of showers obtained from simulations of the array response. The curve represents a quadratic curve fitted to the data.

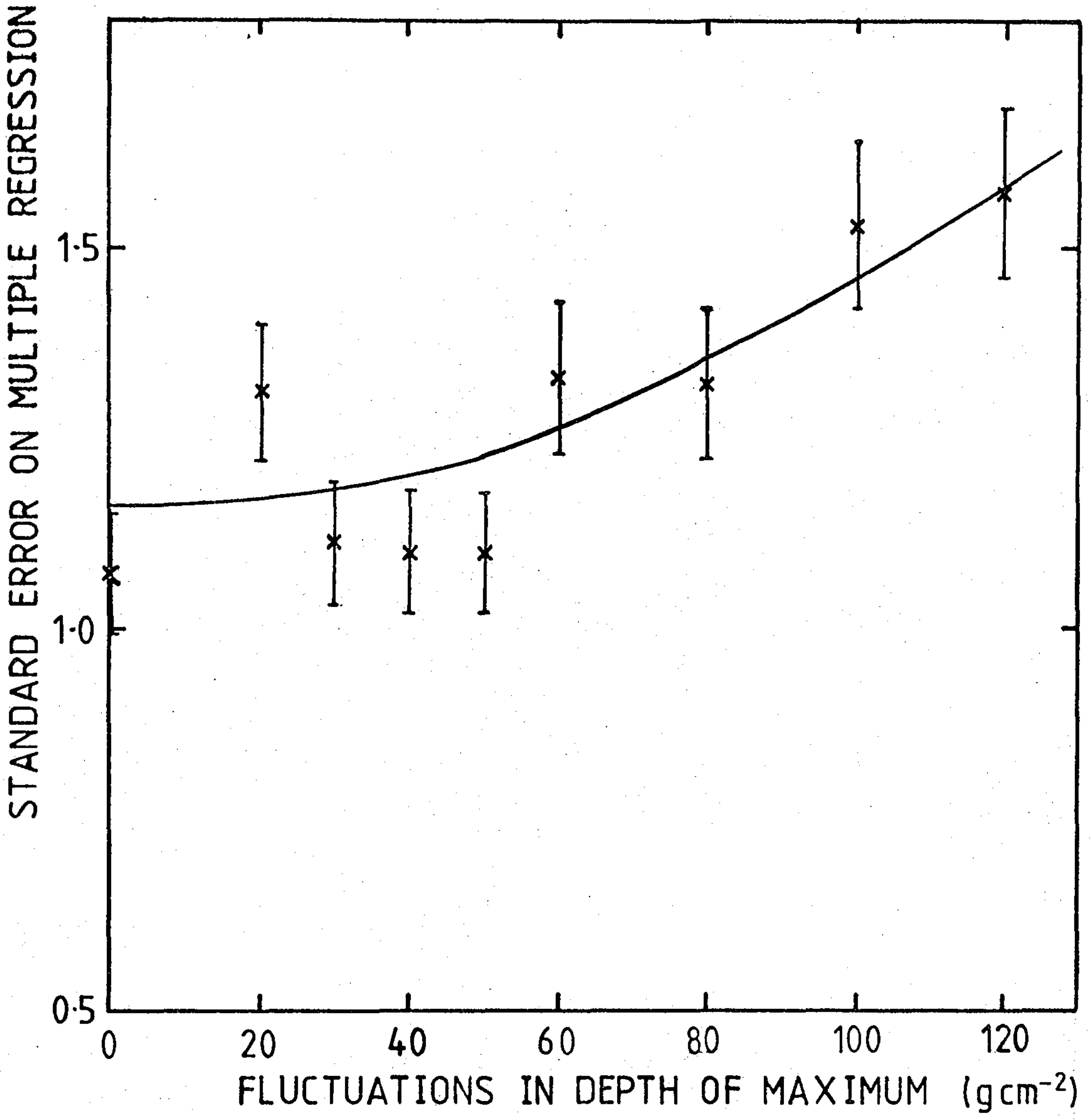
STANDARD ERROR ON MULTIPLE REGRESSION
1·5
1·0
0·5
0
20
40
60
80
100
120
FLUCTUATIONS IN DEPTH OF MAXIMUM (gcm^{-2})

The result simply provides an upper limit to the fluctuations in depth of maximum. This is due to the fact that the calibration curve flattens off rapidly at approximately Δt_{max} of 50g cm^{-2}. Beyond this point the measurement uncertainty completely masks the intrinsic fluctuation in the data. The only way to improve the measurement was to increase the dataset by relaxing the lower energy threshold until a large enough sample was obtained. (It should be noted that the triggering bias is the same for both the real and simulated data). By choosing showers with energies greater than log Φ_{150} of 3.4 (6.0×10^{16}eV) a total of 95 events were included in the dataset.

The error on this regression line was

$$\underline{\sigma_R = 1.27 \pm 0.09}$$

which translated to

$$\underline{\Delta t_{max} = 62\text{g cm}^{-2}}$$

with 68% confidence limits of $\underline{29 < \Delta t_{max} < 79}$ at a mean energy of 1.3×10^{17}eV.

In the following chapter this result is compared with the fluctuation measurements obtained from 200 m and 100 m arrays using the same method as described in Section 4.7.2 and above. The information which these results gives about the mass of the primary particle and the interaction model appropriate to the energies in high energy cosmic ray showers is discussed.

5.7 The Structure Function Exponent as a Measure of Depth of Maximum

The strict criteria for the selection of data for the density ratio analysis described means that it is possible to attribute high quality depth-sensitive measurements only to a limited proportion of showers recorded in the energy and zenith angle range considered. However a lateral structure shape measurement is available for all showers with 5 or more detector responses, viz. the exponent η in the function

$$\Phi(r) = A(r + r_o)^{-\eta}$$

to which the detector responses were fitted to find the shower core (see Section 4.3). The uncertainties in this parameter which make it unsuitable for fluctuation measurements have already been discussed in Section 4.3.1(e). This low grade measurement has previously been used in presenting preliminary results from the Dugway array (Chantler et al.,(1979)) and it is therefore of interest to compare this parameter with R(100m,250m). In addition its justification as a reliable but imprecise indicator of depth of maximum presents the possibility of investigating correlations between the deviations from the average behaviour of the lateral structure shape and similar deviations in other depth sensitive parameters from the Dugway array. As with the R(100m,250m) measurements, very strict quality requirements restrict the dataset used for analysis of other depth sensitive parameters to the extent that there is little overlap between the selected datasets, so that a parameter available in every shower, though of relatively poor quality, presents the only method of testing correlated fluctuations. Though it is not within the scope of the present work to attempt to demonstrate correlated fluctuations it is desirable to establish the validity of η for the investigation of such correlations.

The relationship between η and the parameter R(100m,250m) is shown in Figure 5.8. The energy and zenith angle dependence of both lateral structure shape measurements has been removed and the residual fluctuations in each parameters plotted. This demonstrates clearly that changes in the parameter η do indeed indicate changes in depth of maximum though it is impossible to interpret η accurately as an absolute measure of depth of maximum. Thus, since η is a measurement available in all showers with a well-determined core position, it is a suitable parameter to use to study correlated fluctuations.

5.8 Conclusion

The measurements of the development of the cascade of extensive air showers around 10^{17}eV provided by the shape of the lateral distribution of Cerenkov light density measured by the largest configuration of the Dugway Cerenkov Light Array have been described.

The average characteristics of the depth sensitive parameters R(100m,250m) and R(100m,200m) and their dependence on the primary energy and inclination of the shower were displayed. Three measurements of average depth of cascade maximum were derived using the results of the shower simulation of Mc Comb and Turver (1981) to interpret $R(r_1, r_2)$ as values of depth of maximum. A measurement of the fluctuations

Figure 5.8 Scatter plot of the residuals in R(100m, 250m) and η after the energy and zenith angle dependence has been removed from each parameter.

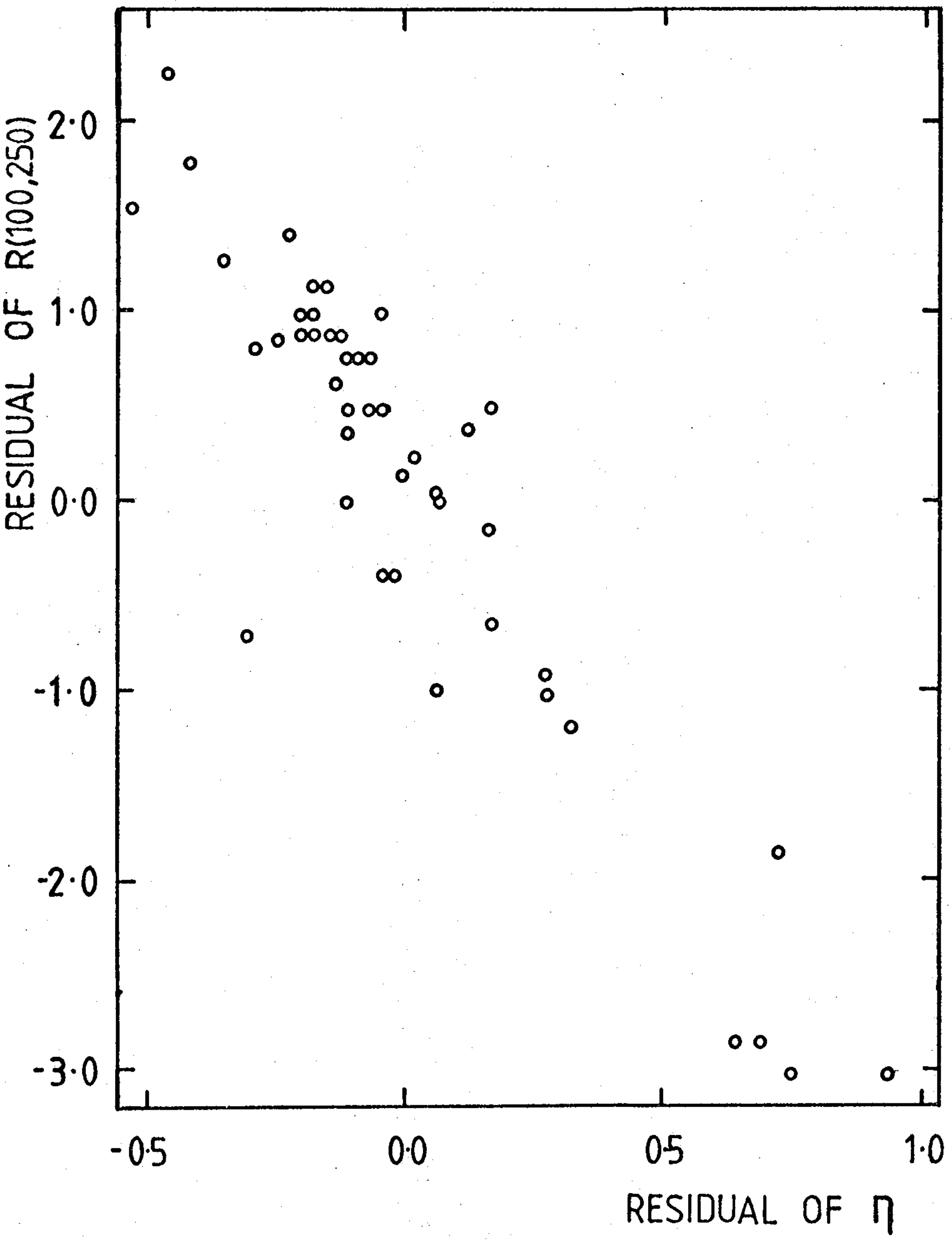
RESIDUAL OF R(100,250)
2·0
1·0
0·0
-1·0
-2·0
-3·0
-0·5
0·0
0·5
1·0
RESIDUAL OF η

in the depth of maximum was also provided from measurements on individual showers. These measurements, of mean depth of maximum and fluctuations about the mean, provide the evidence on which to assess models of the primary mass composition at 10^{17}eV based on different prediction of high energy interactions in the shower.

Finally, a low grade depth-sensitive parameter, which would be available for all showers, was identified and this allows the investigation of correlations between lateral distribution and other depth-sensitive measurements in the same shower.

CHAPTER 6

COMPARISON OF LATERAL DISTRIBUTION MEASUREMENTS WITH OTHER DATA FROM THE DUGWAY EXPERIMENT AND WITH COMPUTER SIMULATIONS

6.1 Introduction

This chapter seeks to place the measurement of the lateral distribution of Cerenkov light in large cosmic ray showers into a context with other measurements from the Dugway Cerenkov Light Detector Array. In Chapter 5 results were presented for the mean depth of maximum, $\overline{t}_{max}$, and fluctuations in depth of maximum, Δt_{max}, which arose from the analysis of one part of the Dugway data. This approach has been expanded in two ways - firstly the same techniques of lateral distribution measurement, but with smaller array spacing, were used to provide measurements of $\overline{t}_{max}$ and Δt_{max} at primary energies down to 6×10^{15}eV and secondly, a different technique, measurements of the time structure of the Cerenkov light signal, was used to calculate independent results in the same 10^{16}-10^{17}eV energy range.

The mean depth of maximum has been measured using various techniques by the Dugway array in the energy range 6×10^{15}-$2\text{x}10^{17}$ eV and these results are compared with computer simulation predictions of the $\overline{t}_{max}$ dependence on primary energy. From this, certain initial conclusions can be drawn about the appropriate interaction model and the primary mass composition. However, the greatest value of the results from the Dugway experiment is the simultaneous determination of both $\overline{t_{max}}$ and Δt_{max} based on measurements of the lateral distribution shape and time-structure of pulses. These have been interpreted as a measure of the ratio of light to heavy mass particles (using a simple binary model with proton and Fe nuclei components) over the same primary energy range - 6×10^{15} to 2×10^{17}eV.

6.2 Lateral Distribution Measurements from the 100 m and 200 m Configurations of the Dugway Cerenkov Light Detector Array

The most rewarding aspect of the lateral distribution shape as a measure of depth of shower maximum is the wide range of energy over which the same technique can be successfully applied. By altering the size of the Dugway array to be sensitive to even lower primary energy cosmic rays in the last few months of observation, data were obtained at a high event rate for lower energy showers. The measurement and analysis techniques applied to the lateral distribution data were essentially the same as those described in Chapter 4 although certain adaptations were necessary. The most significant was the change in ground parameter $R(r_1, r_2)$. For the 200 m configuration, sensitive to energies 9×10^{15} to 3×10^{16}eV, the ratio of densities at 75 m and 150 m was chosen and the corresponding distances for the 100 m array sensitive to 3×10^{15} - 3×10^{16}eV were 50 m and 100 m. The justification for these choices is, as far as possible, the same as for the 400 m array - that the densities at these core distances are well measured and that the ratio gives good sensitivity to t_{max}. Again, the observations were interpreted directly using the equivalent density ratios produced by simulations. The consistency of interpretation between different density ratios in showers of the same energy has already been demonstrated in the 400 m array data in Section 5.5 by comparing $\overline{t_{max}}$ derived from R(100m, 250m) and R(100m, 200m).

It should also be noted that for the 100 m array the core distance range over which the shower is sampled does not in general include samples to distances as large as 150 m. Thus it is not possible to use Φ_{150}, the density at 150 m (or greater distance as would be more appropriate), as the primary energy estimator for this array configuration. The most distant well measured density was typically at 100 m and this has been used as the best compromise in determining the primary energy of the shower (see Section 4.5).

The error estimation procedure for each detector (see Section 4.3) was also repeated for the measurements made with the 100 m and 200 m configurations, to allow for possible changes in the size of random fluctuations within showers of different primary energy.

As was the case when analysing the data from the 400 m array, the mean depth of maximum measurements were obtained by averaging over normalised detector responses in specified zenith angle and energy intervals. In

Figure 6.1 an example is shown of one such result based on data from the 200 m array where R(75m, 150m) is plotted against secΘ at an energy of 2.3×10^{16}eV. (This should be compared with Figures 5.5 and 5.6 where equivalent results for R(100m, 250m) and R(100m, 200m) for the 400m array are shown). Each data point was interpreted as a value of $\overline{t_{max}}$ and the resulting estimates for each primary energy interval are displayed in Table 6.1.

Rigorous selection criteria, similar to those used for the 400m array data were applied to showers in the lower energy data sets before they were included in the analysis, and only values interpolated from local detectors were used to calculate the densities making up the ratio R(75m, 150m) or R(50m, 100m). The results of an analysis of fluctuations in these data are discussed later in Section 6.2.4.

Finally it should be pointed out that one of the advantages of measuring the lateral distribution in showers of lower energy is that because the showers generally have a broader lateral distribution the probability of selection is less dependent on the depth of shower maximum. Thus the selection biases are significantly less important (c.f. Section 4.7). However, at the lowest energies accessible to the 100m detector array, when the signals at each detector are near threshold there is a sudden onset of bias, giving preferential selection of showers developing high in the atmosphere. For this reason the lowest energy

Figure 6.1 The measured variation of R(75m, 150m), and zenith angle for showers with mean energy 2.3 x 10^{16}eV measured by the 200 m array configuration. The simulation lines for showers with fixed depth of maximum are also shown.

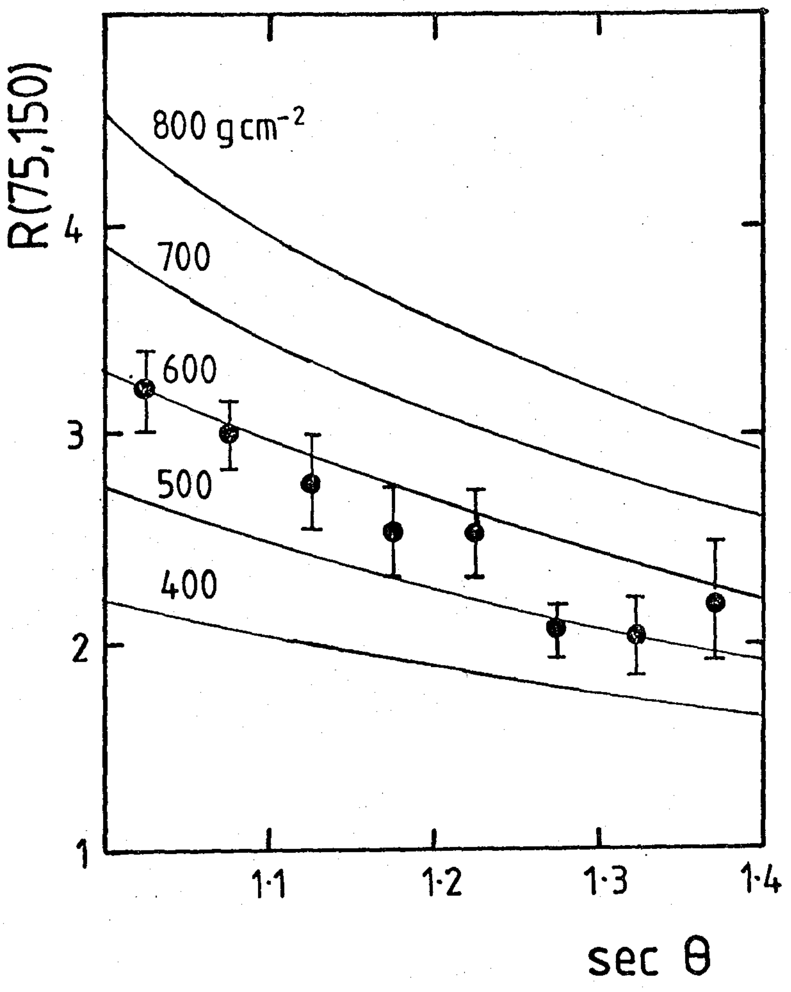
R(75,150)
800 g cm^{-2}
700
600
500
400
4
3
2
1
1·1
1·2
1·3
1·4
sec θ

TABLE 6.1 Mean Depth of Maximum Derived From Lateral Distribution Measurements

Mean Energy (eV)	t_{max} (g cm^{-2})	Array Size
3.2×10^{17}	694 ± 26	400 m
1.6×10^{17}	633 ± 16	
9.5×10^{16}	624 ± 11	
3.4×10^{16}	555 ± 40	200 m
2.3×10^{16}	548 ± 15	
1.5×10^{16}	520 ± 12	
9×10^{15}	490 ± 20	
3.1×10^{16}	555 ± 60	100 m
1.2×10^{16}	482 ± 16	
6.3×10^{15}	472 ± 18	
3.0×10^{15}	520 ± 20	

measurement of t_{max} at 3×10^{15}eV must be regarded as an upper limit estimate.

6.3 Pulse Shape Measurements

One particular feature of the Dugway experiment is that it produced, for the first time in Cerenkov light studies, two independent techniques to measure the depth of shower maximum in one dataset of showers - lateral distribution measurements and the time structure of the Cerenkov light signal. The fact that the synchronised time of arrival measurements and the time structure of the Cerenkov light signal contain information about the development of the shower through the atmosphere has already been discussed (see Section 2.5.4 and Section 2.6). This was on the basis of the results of computer simulations and the pioneer work of the Haverah Park Cerenkov Light Detector Array.

Two methods of determing t_{max} using the timing of pulses were used for the reconstruction of the depth of Cerenkov maximum - using the synchronised time of arrival of the shower front and the dependence of the full width at half maximum of the signal on core distance. The detailed analysis of these measurements has been described by Chantler (1982) but a brief discussion will be appropriate here.

6.3.1 Pulse Shape (FWHM) Measurements

The analysis of pulse shape information proved a fruitful ground for depth of maximum measurements in the data obtained from the 400 m and 200 m array configurations giving results for showers of energy between 3×10^{16} – 2×10^{17}eV. The first step in analysis of all the fast timing measurements was to reconstruct the time profile of the light signal from the sampled segments recorded by each detector. A quartic B-spline was chosen as the best approximating function to facilitate the recovery of the pulse shape parameters. This technique was only suitable for reasonably large pulses and so measurements in low energy showers, in particular, were not amenable to this analysis. However for measurements at distances appropriate to small showers ($r < 100$ m) simulations suggest that the pulse shape is very narrow and displays little sensitivity to the depth of maximum in any case.

The pulse shape parameter chosen to measure t_{max} was the full width at half maximum (FWHM). Although other parameters, say rise time, are also sensitive to depth of maximum, FWHM was chosen not only because it displays a strong coupling to t_{max} but also because it is most accurately recovered from the spline fitting procedure. The average behaviour of FWHM with core distance, r_1 was shown to be entirely consistent with the prediction from simulations, viz.

$$\mathrm{FWHM}(r) = a + br^2 \qquad (6.1)$$

where a and b are dependent on t_{max}, by considering the average response with core distance of signals from showers in limited zenith angle and primary energy intervals. As with the lateral distribution parameter $R(r_1, r_2)$, the interpretation of results involved invoking the simulation prediction that a near-unique relationship exists between FWHM at fixed core distance and the depth of shower maximum (see Section 2.5.4). Thus each measurement of $\overline{\mathrm{FWHM(r)}}$ at fixed core distance could be interpreted directly as a measure of $\overline{t_{max}}$ for showers in the energy and zenith angle interval under consideration. Figure 6.2 shows the measurement of FWHM from the 400 m array configuration for a range of secθ intervals at mean energy 2.1 x 10^{17}eV. Using this method one measurement of $\overline{t_{max}}$ was obtained from the data recorded by the 400 m array and two from the data of the 200 m array. It was found, as expected, that measurements of showers detected by the smallest array could not benefit from this analysis.

For shower-by-shower analysis to investigate fluctuations in depth of maximum, a FWHM value was interpolated at fixed core distance (250 m for the 400 m array data) using all acceptable detector responses in the shower. This value was then interpreted as a depth of maximum measurement and an appropriate error estimate was obtained based on the uncertainty in the FWHM (250 m) estimate from this interpolation. This fluctuation analysis was only undertaken for data from the 400 m array configuration and the results are presented in Section 6.5.

6.3.2 Depth of Cerenkov Light Maximum Measurements

The measurement of D_{100}, the depth of Cerenkov light maximum contributed an additional measurement of $\overline{t_{max}}$ to the results available from the Dugway project. The

Figure 6.2 The variation of FWHM with core distance for a range of secθ intervals at a mean energy of 2.1×10^{17}eV measured by the 400 m array.

(from Chantler (1982)).

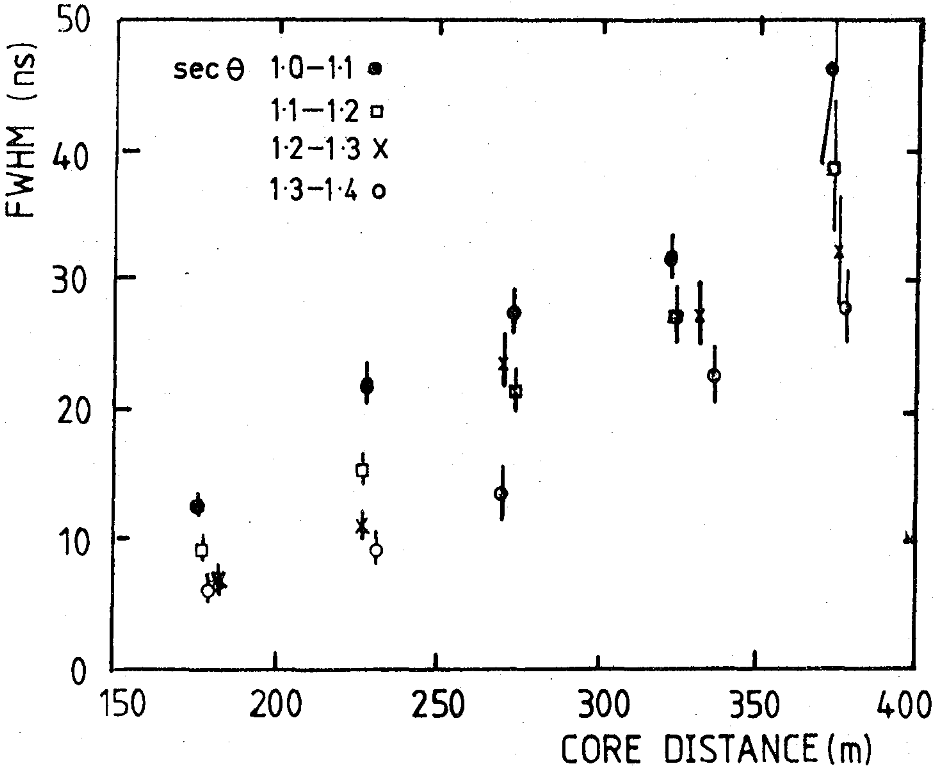
FWHM (ns)
50
40
30
20
10
0
150
200
250
300
350
400
CORE DISTANCE (m)
sec θ 1·0−1·1 ●
1·1−1·2 □
1·2−1·3 X
1·3−1·4 o

measurement used the synchronised time at which the Cerenkov light pulse reached its peak on each detector. The data confirmed the simulation prediction that the Cerenkov light shower has a spherical front. By fitting the time of arrival of percentage levels of rise and fall in the pulse on each detector to a sphere, a series of points corresponding to the centres of each sphere would be found to map out the growth and decay of the light shower (see Orford and Turver (1976)). (The geometrical argument supporting this is an extension of that which predicts that FWHM will reflect the depth of shower maximum). In the current experiment only the time of arrival of the peak of the pulse was analysed since the measurement accuracy was not sufficient to allow a full reconstruction of the development of individual showers. The reconstructed depth D_{100} is uniquely related to the depth at which the electron shower maximises though the interpretation is not trivial. The principal problem with interpretation concerned the biasing of results not only from preferential selection, a subject discussed in Section 4.7.1, but also from the fact that the uncertainty in reconstruction correlated strongly with the inferred depth of cascade maximum.

Because of the stringent selection criteria which ensured that enough well-fitted pulses were available in each shower and that they were sufficiently well spaced to give a large baseline for reconstructing the spherical front, only a small number of high energy showers were available for this analysis. The problem of inferring the distribution of t_{max} from the observed distribution in D_{100} was solved using a Monte Carlo simulation of observed values of D_{100} obtained from a known distribution of t_{max}. This succeeded in giving a value of $\overline{t_{max}}$ but it was insensitive to changes in the spread Δt_{max}.

Table 6.2 summarises the mean depth of maximum measurements from the analysis of measurements of the timing of Cerenkov light pulses.

6.4 Comparison of Depth of Maximum Measurements with the Predictions of Computer Simulations

Until this point the results of computer simulations have been used only to interpret the ground parameters of the Cerenkov light shower as a measure of depth of maximum, relying on the fact that the detailed structure of the Cerenkov light signal in a shower is virtually independent of primary energy (beyond a scaling factor), primary mass and the model used to describe hadron interactions. In essence, the depth of shower maximum alone determines the value of ground based measurements. Having obtained the measurement of mean depth of shower maximum over a range of primary energy it is here necessary to compare the observations with the energy dependence of $\overline{t_{max}}$ which is predicted by different combinations of mass and interaction model.

Figure 6.3 shows all the measurements of the mean depth of maximum obtained from the Dugway experiment together with nine different interaction models spanning a wide range of reasonable extrapolations of the known behaviour

TABLE 6.2

Depth of Maximum Measurements from Timing of Cerenkov Light Pulses

Mean Energy (eV)	Mean Depth of Max. (g cm^{-2})	Method
2.1×10^{17}	678 ± 25	FWHM 400 m array
6.5×10^{16}	646 ± 44	FWHM 200 m array
3.1×10^{16}	581 ± 26	
1.7×10^{17}	730 ± 35	D100 400 m array

Figure 6.3 Measurements of the depth of maximum from the Dugway Cerenkov Light Detector Array together with simulation predictions.

Measurements

○	lateral distribution	400 m array
●		200 m array
X		100 m array
□	FWHM	400 m array
■		200 m array
▲	D100	400 m array

Simulation models

————————	scaling	multiplicity in the central region
— — — — — — —	$E^{0.25}$	
—·—·—·—·—·	$E^{0.33}$	

a	constant	cross-section
b	logs	
c	$\log^2 s$	

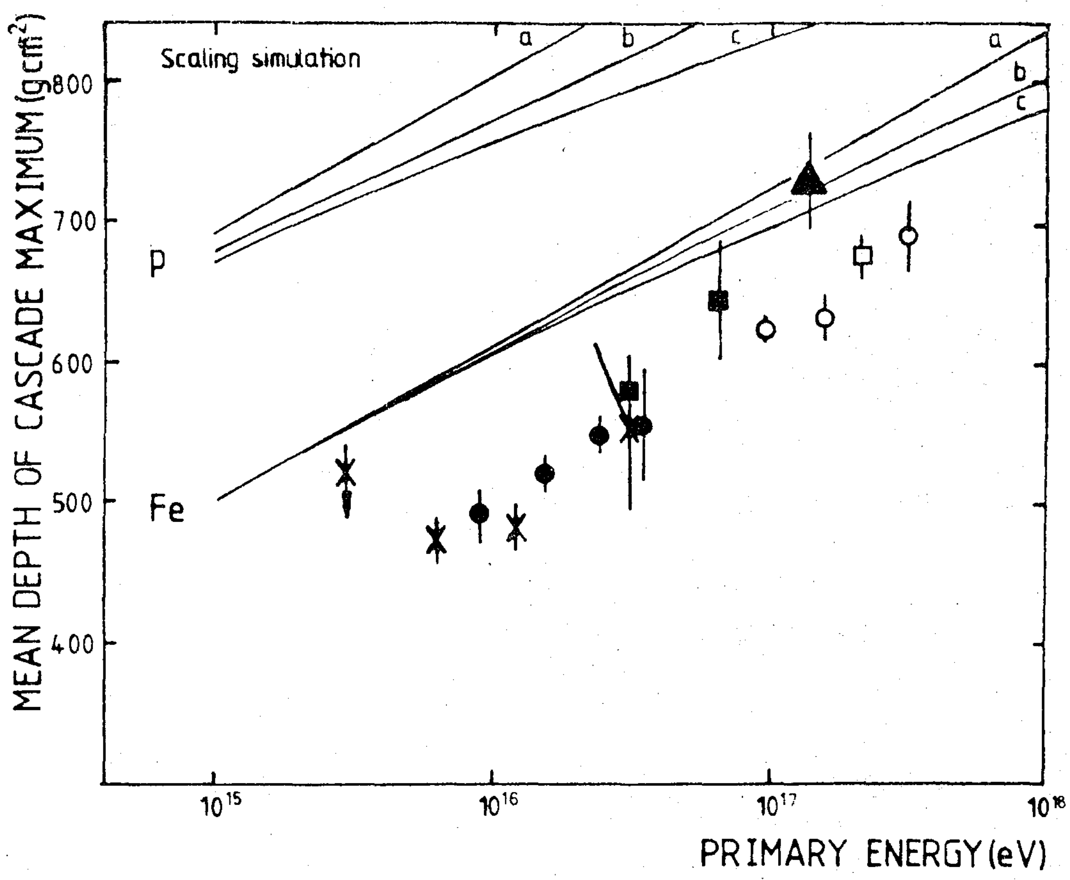
Scaling simulation
a
b
c
a
b
c
p
Fe
400
500
600
700
800
MEAN DEPTH OF CASCADE MAXIMUM (g cm-2)
10^15
10^16
10^17
10^18
PRIMARY ENERGY (eV)

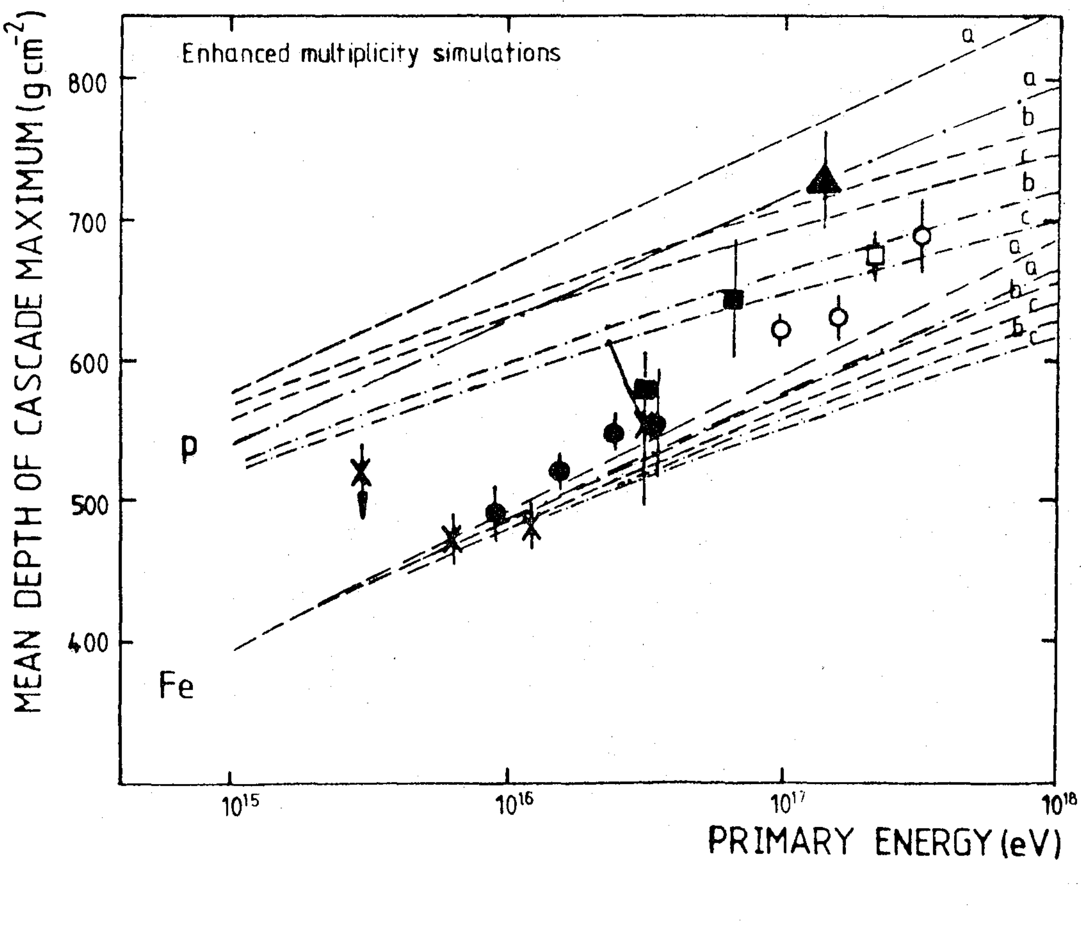
Enhanced multiplicity simulations
a
a
b
c
b
c
a
a
b
c
b
c
p
Fe
400
500
600
700
800
MEAN DEPTH OF CASCADE MAXIMUM (g cm-2)
10^15
10^16
10^17
10^18
PRIMARY ENERGY (eV)

of hadron interactions. All use scaling in the fragmentation region but three different treatments of the multiplicity in the central region have been considered - scaling and multiplicities rising as $E^{0.25}$ and $E^{0.33}$. These have been combined with cross-sections which remain constant, rise as ln s or increase as $\ln^2 s$ (see Gaisser et al.(1978) for further details). It is evident that the data are entirely inconsistent with a scaling model without enhanced particle production regardless of the primary mass composition; only at 10^{17}eV could the Dugway data be considered a reasonable fit were the flux of primary particles all iron nuclei. It is interesting to note that most of the experimental data leading to mean depth of maximum measurements have been in this energy region before the Dugway experiment. Only by considering the results of reducing the primary energy can the pure scaling model be rejected so firmly.

The other two models for multiplicity in which the number of secondaries increases as $E^{0.25}$ or $E^{0.33}$ are consistent with the observed depth of maximum dependence provided that the primary mass composition is predominantly iron-like at 10^{16}eV and changes in the following decade of primary energy to have a higher protonic component, though each model would predict a different mixture of light and heavy primaries. In either case however, a model with a constant cross section would be difficult to justify on the basis of the present results. (Current accelerator data at 10^{11} - 5 x 10^{13}eV also indicate that the cross-section rises with increasing energy).

It is only by considering also the fluctuations in the depth of maximum that any more significant conclusion can be drawn. This is undertaken in the following section.

6.5 Fluctuation Measurements from the Dugway Array

The principal measurements of fluctuations in depth of maximum which arise from the stochastic process governing the production of the air shower and the distribution of mass of the primary particle flux are derived from the lateral distribution analysis conducted on data from the three different array configurations. The Monte Carlo simulation technique used to quantify the fluctuations in depth of maximum corresponding to the observed variation in the ground parameter $R(r_1, r_2)$ for the 400 m array data has been described in detail in Section 4.7.2 and Section 5.6. This was readily adapted to calculate the fluctuations in lower energy showers. In all, the lateral distribution measurement produced four values of the fluctuation Δt_{max} in a range of energies 5.9×10^{15}eV to 1.3×10^{17}eV, although once again one result, at an energy of 1.1×10^{16}eV is, in fact, only an upper limit. The advantage of the lateral distribution technique over pulse timing is not only that the parameter retains sensitivity at lower shower energies but also that there is a high data collection rate whereas the pulse shape measurements both lose sensitivity to depth of maximum and the quality of reconstruction deteriorates.

The most precise estimate of Δt_{max} however was produced by pulse shape measurements from the data of the 400 m array configuration. Further fluctuation measurements could not be calculated because the pulse shape data from the 200 m array was not of sufficient quality to provide a reliable value of Δt_{max} although measurements could be interpreted to give a worthwhile value of $\overline{t_{max}}$. The determination of Δt_{max} from the FWHM measurements of the 400 m array was effected using a different technique from the lateral distribution measurements although a Monte Carlo simulation of the system response was conducted for comparison. The technique was as follows:- for each shower, selected according to rigorous criteria of data quality, the FWHM at 250 m was interpolated and converted to t_{max}. Because the functional form of FWHM(r) was well established and of a simple form it was possible to attribute an unbiased error estimate to each of the values of FWHM (250 m). Thus where the multiple regression of FWHM (250 m) on primary energy and zenith angle was conducted (c.f. Section 5.6), the variance attributable to measurement uncertainty and that derived from the intrinsic fluctuations in $\overline{t_{max}}$ could be identified directly.

In Table 6.3 a summary of all Δt_{max} measurements from the Dugway Cerenkov Light Detector Array is presented. This gives a range of measurements in showers of energy from 6 x 10^{15}eV to 2.1 x 10^{17}eV allowing investigation of any significant changes with energy.

The potential of the fluctuation result as a measure of primary mass composition is greatly enhanced by considering it in conjunction with the mean depth of maximum

TABLE 6.3

Fluctuation Estimates from Dugway

Mean Energy (eV)	Mean Depth of Max. (g cm^{-2})	Fluctuation (g cm^{-2})	Confidence Interval g cm^{-2}	Method
1.3×10^{17}	629 ± 12	62	29 - 79	Lat. Dist. 400 m
2.3×10^{16}	544 ± 14	87	69 - 105	Lat.Dist. 200 m
1.1×10^{16}	504 ± 16	0	0 - 50	
5.9×10^{15}eV	486 ± 10	75	50 - 95	Lat.Dist. 100 m
2.1×10^{17}eV	678 ± 25	79	68 - 90	FWHM
1.7×10^{17}eV	730 ± 35	120	0 - 190	D_{100}

measurement at the same energy. This composite Δt_{max}, $\overline{t_{max}}$ data can be compared with simulation predictions using different primary mass composition and interaction models. Such results are presented in Figure 6.4. The simultaneous measurement values of $\overline{t_{max}}$ and Δt_{max} together with experimental uncertainties are plotted and compared with predicted ($\overline{t_{max}}$, Δt_{max}) curves from simulation results. Each curve traces the change in $\overline{t_{max}}$ and Δt_{max} as the primary mass composition changes from purely protonic to purely Fe assuming a binary mass composition model. Each observation must be plotted separately since the set of simulation curves is, of course, distinct for each primary energy. The curves produced by pure scaling and constant cross-section interaction models have been omitted since they are inconsistent with measurements of $\overline{t_{max}}$ alone and current accelerator data at lower energy.

Before considering what these figures determine about the primary mass composition it is first necessary to state any conclusions about the most appropriate model for hadron interactions in this energy region. The three low energy measurements can provide little information about interaction models since between 10^{15} - 10^{16}eV only a predominantly proton flux displays any sensitivity to the details of the hadron physics employed in the simulation. The measurement derived from FWHM at 2.1 x 10^{17}eV, being the most precisely measured and also located at a position of reasonable sensitivity to interaction model, clearly rejects the model incorporating a multiplicity in the

Figure 6.4 The simultaneous measurement of $\overline{t_{max}}$ and Δt_{max} from the Dugway array:

Measurements are derived from

Lateral distribution 100 m array (a)
200 m array (b)-(c)
400 m array (d)
FWHM 400 m array (e)

The crosses (x) represent the simulation predictions for iron and proton primaries and the curves trace the relationship between $\overline{t_{max}}$ and Δt_{max} as the composition changes from pure iron to pure protons for a two component approximation to the primary mass composition.

The models used employ the following actual region multiplicities and cross sections

(i) $E^{0.25}$, log s
(ii) $E^{0.25}$, $\log^2 s$
(iii) $E^{0.33}$, log s
(iv) $E^{0.33}$, $\log^2 s$

(after Chantler et al.(1983)).

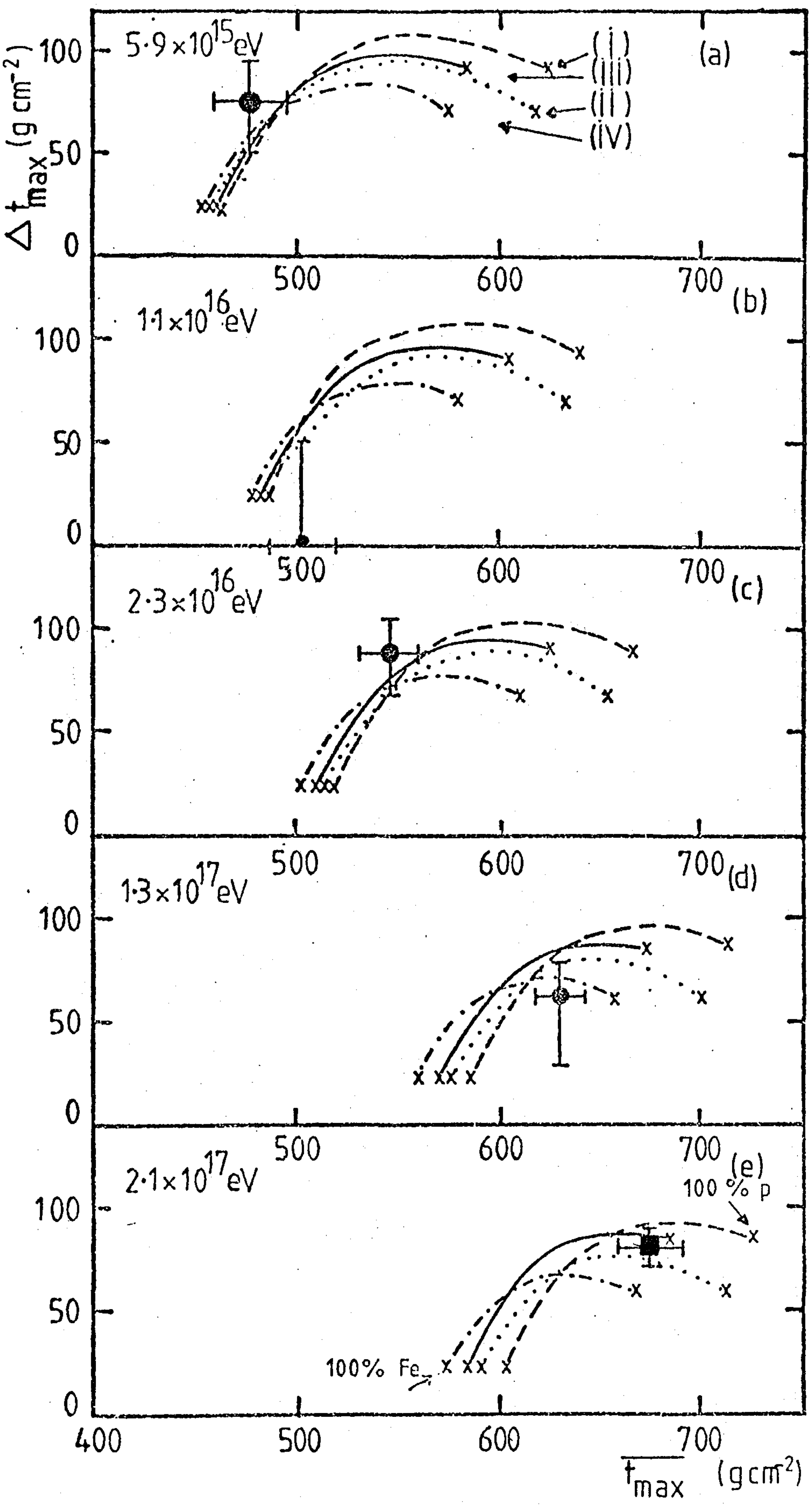
5·9×10^15 eV
(a)
(i)
(iii)
(ii)
(iV)
Δt_{max} (g cm^{-2})
100
50
0
500
600
700
(b)
1·1×10^16 eV
100
50
0
500
600
700
(c)
2·3×10^16 eV
100
50
0
500
600
700
(d)
1·3×10^17 eV
100
50
0
500
600
700
(e)
2·1×10^17 eV
100 % p
100% Fe
100
50
0
400
500
600
700
$\overline{t_{max}}$ (g cm^{2})

central region rising as $E^{0.33}$ with a cross-section increasing as $\ln^2 s$ at the one standard deviation confidence level. The lateral distribution measurement at 1.3 x 10^{17}eV suggests that the model using $E^{0.33}$ multiplicity and $\ln s$ rising cross section is also not appropriate since this model is just outside the joint 68% confidence level. This model has however, been retained for interpreting the $\overline{t_{max}}$, Δt_{max} results as a measurement of the proportion of heavy nuclei in the primary mass composition whereas the $E^{0.33}$, $\ln^2 s$ model has not.

Figure 6.5 shows the interpretation of the five measurements displayed in Figure 6.4 in terms of the percentage of iron nuclei which would be required in a binary primary mass composition (Fe and protons only) to produce the observations made at Dugway. The quoted uncertainty is due to the joint 68% confidence interval of the measured points taking into account differences in interpretation due to the different allowed interaction models. This clearly shows that the proportion of heavy primaries decreases with increasing energy over the energy range of the Dugway data and predicts that the flux around 10^{16}eV is predominantly iron-like. It should be noted that the relative insensitivity of a predominantly heavy primary mass composition to interaction model changes at lower energy leads to a more precise estimate of composition at these energies. However, large uncertainties remain around 10^{17}eV where a wealth of data exists because of the diversity of the results from different models. Despite this a significant

Figure 6.5 The interpretation of the simultaneous $\overline{t_{max}}$ and Δt_{max} measurements in terms of a two component (iron and proton) model of the primary mass composition. (after Chantler et al. (1983)).

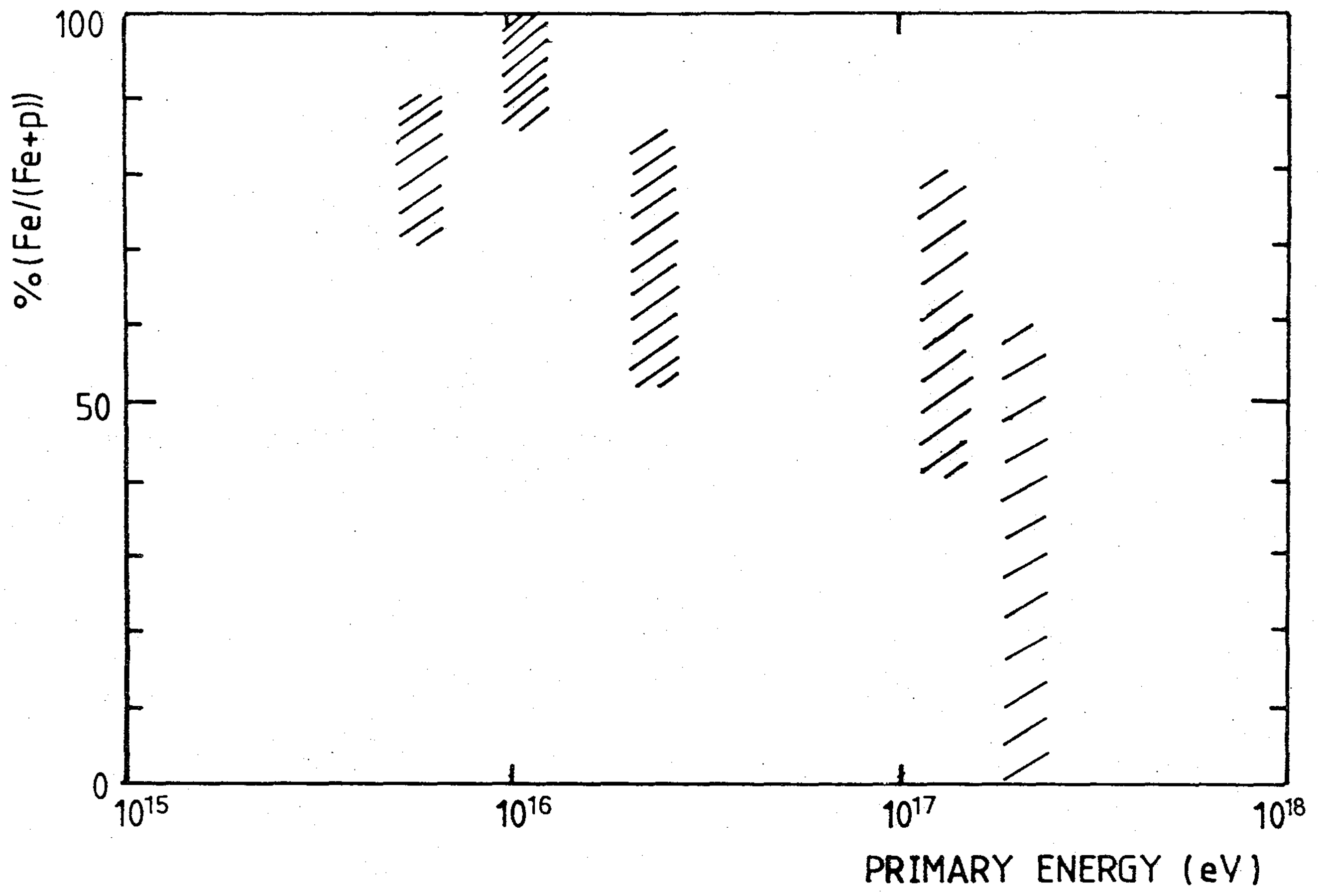
100
50
0
%(Fe/(Fe+p))
10^{15}
10^{16}
10^{17}
10^{18}
PRIMARY ENERGY (eV)

increase in the proportion of light nuclei is clearly indicated over a decade and a half of primary energy.

These results will be compared with other measurements in Chapter 7.

6.6 Conclusion

This chapter has drawn together all the results from the Dugway Cerenkov Light Detector Array. By interpreting measurements of lateral distribution and the time structure of the light signal it has been possible to make measurements of $\overline{t_{max}}$ and Δt_{max} over a decade and a half of primary energy from 6×10^{15} to 2×10^{17}eV. These measurements have been compared with the absolute values and energy dependence of t_{max} predicted by computer simulations using a number of scaling based models (reasonable extrapolations of accelerator measurements at $\sim 10^{12}$eV) and proton or iron primary particles. The dependence of $\overline{t_{max}}$ on energy has been shown to be inconsistent with a pure scaling model of interactions and also with enhanced multiplicity models using a constant interaction cross-section. The models which are consistent with the observed energy dependence of $\overline{t_{max}}$ indicate a predominantly iron-like composition at $\sim 10^{16}$eV with an increasing proportion of light nuclei at higher energy. The composite measurement of $\overline{t_{max}}$, Δt_{max} enhanced the quality of the measurements allowing a further interaction model to be rejected. Finally, a simple model of a two component composition (protons and iron-nuclei) was used to interpret the composite $\overline{t_{max}}$, Δt_{max} measurement in terms of the percentage of iron-like nuclei in the primary cosmic ray flux and to display the change in mass composition with increasing energy.

CHAPTER 7

COMPARISON WITH OTHER MEASUREMENTS OF DEPTH OF MAXIMUM AND CONCLUSIONS

7.1 Introduction

In drawing the present work to a conclusion it is necessary to compare the measurements of the Dugway Cerenkov Light Detector Array with those recently made at other sites in the world. The data presented in this work covers an energy range which stretches from the region around 10^{17}eV where numerous measurements have been made (this being the lower energy measured by the long established large air shower arrays) down to 10^{15} - 10^{16}eV where there are few current measurements. By including measurements from other arrays it is possible to reliably extend the range over which $\overline{t_{max}}$ has been measured from 10^{15} - 10^{19}eV, four decades of primary energy.

A distinction must be made when making comparisons of the Dugway results with other measurements between data from the Haverah Park site and from other arrays. This is so since the energy assignments from the Dugway Cerenkov Light Detector array and the Haverah Park deep water detector response have been intercalibrated using the optical sensors of the Haverah Park Cerenkov Light Detector Array (Hammond et al., (1978)). In other cases, in the absence of any such intercalibration, a consistent energy assignment cannot be guaranteed.

The Dugway project provides simultaneous measurements of two parameters, $\overline{t_{max}}$ and Δt_{max}. Other measurements in general either measure one or other but not both. Some attempt will be made to relate the many values of Δt_{max} to the simultaneous measurements of $\overline{t_{max}}$ and Δt_{max} presented in Chapter 6 and to interpret these in terms of the simple binary mass composition model discussed in Section 6.5.

Finally conclusions concerning the primary mass composition between 10^{15}eV and 10^{19}eV will be drawn from the compilation of results from Dugway and other projects.

7.2 Measurements of Mean Depth of Maximum at Haverah Park

Comparison between measurements made at Haverah Park which use the Haverah Park ground parameter ρ_{500} as primary energy estimator and those from the Dugway Cerenkov Light Detector Array can be made reliably because the two arrays have been accurately intercalibrated using the Haverah Park Cerenkov Light Detector Array (see Section 4.5). Three recent measurement techniques at Haverah Park have provided data which can be interpreted as determinations of absolute depth of maximum and which can therefore be related to the current work.

The most obvious additions to the Dugway results are the values of mean depth of maximum obtained from the data collected by the Haverah Park Cerenkov Light Detector Array (Protheroe and Turver (1979)). Two values of $\overline{t_{max}}$ separated by one decade of primary energy were obtained by averaging the results of the analyses of lateral distribution, pulse shape and direct imaging. The interpretation of these measurements is entirely consistent with the present work since Protheroe and Turver used the same simulation technique as McComb and Turver to infer t_{max} from measured ground parameters. The combination of Cerenkov light results from Dugway and Haverah Park immediately and reliably extends the range of primary energy over which a consistent technique has been used from 6 x 10^{15} to 2 x 10^{18}eV.

The other sources of $\overline{t_{max}}$ determinations from Haverah Park are both measurements of the particle component of the shower. A single value of $\overline{t_{max}}$ comes from the Durham group's measurements of muon spatial angles (Gibson et al. (1981)) and a further five from the interpretation by McComb and Turver of the measurements of the Nottingham group (Blake et al. (1979)) who investigated the ratio of muons to the deep water detector response. Both of these observations have been interpreted by McComb and Turver (1982b) using the same simulation technique as applied to the interpretation of Cerenkov light data and it is their interpretation which is quoted here.

The summary of Dugway and Haverah Park measurements is shown in Figure 7.1 together with the simulation-based predictions of $\overline{t_{max}}$ using scaling-based models incorporating $E^{0.25}$ and $E^{0.33}$ multiplicities with ln s and $\ln^2 s$ rising cross-sections. (These are the simulations used in Figure 6.3 omitting the pure scaling predictions and those using an enhanced model with a constant cross-section which were inconsistent with the Dugway measurements.)

Figure 7.1 The combination of measurements of depth of maximum, $\overline{t}_{max}$, from the Dugway and Haverah Park Arrays

○ Dugway) Cerenkov Light
● Protheroe and Turver (1979)) Measurements

■ muon core angle measurements (Gibson et al. (1981)).

☐ muon/deep water tank response measurement (Blake et al. (1979)) interpreted by McComb and Turver (1982b).

The simulation models use the following central region multiplicities and cross-sections.

(i) $E^{0.25}$, log s
(ii) $E^{0.25}$, $\log^2 s$
(iii) $E^{0.33}$, log s
(iv) $E^{0.33}$, $\log^2 s$

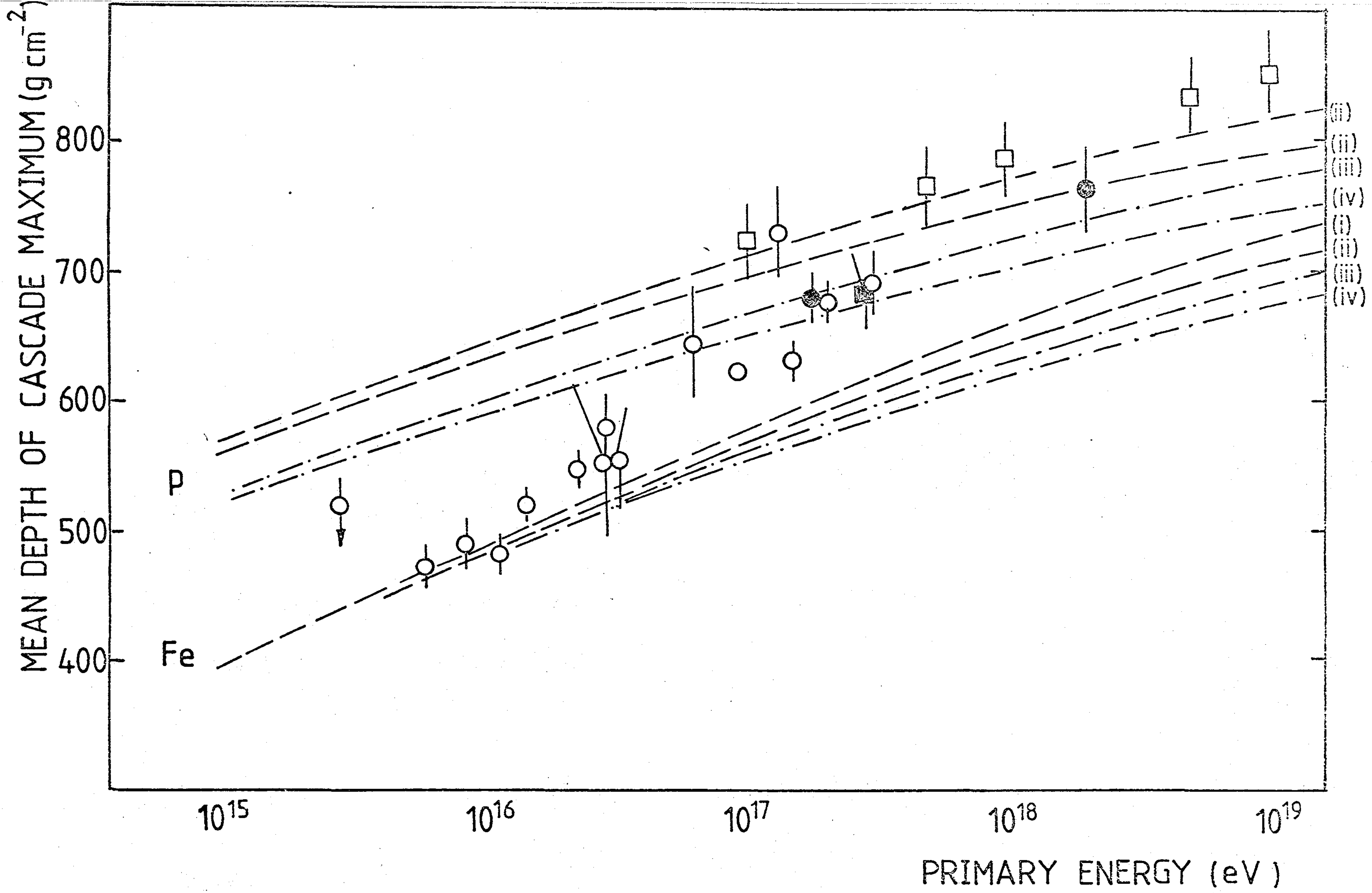
MEAN DEPTH OF CASCADE MAXIMUM (g cm^{-2})
800
700
600
500
400
P
Fe
(ii)
(ii)
(iii)
(iv)
(i)
(ii)
(iii)
(iv)
10^{15}
10^{16}
10^{17}
10^{18}
10^{19}
PRIMARY ENERGY (eV)

The other recent observations at Haverah Park - the measurement of the rise time of the deep detector response (Walker and Watson (1981)) and the lateral distribution of the deep detector response (Craig et al. (1979) with results reinterpreted by McComb and Turver (1982b)) - have measured the energy dependence of the depth of maximum, the elongation rate, but have not provided determinations of absolute depth of maximum at a prescribed primary energy. These measurements cannot therefore, be displayed in Figure 7.1 without being normalised to some other measurement and therefore it is inappropriate to include them.

In view of the fact that a popular view involves a change in primary mass between 10^{16} and 10^{17}eV the elongation rate obtained from the Dugway data will not be quoted here. Under the non-linear relationship shown in Figure 7.1, the elongation rate is heavily dependent on the precise range of primary energy over which the value is calculated. However, it should be pointed out that the measurements of the rise time and lateral distribution of deep detector response measured above 2×10^{17}eV show that the strong energy dependence of $\overline{t_{max}}$ observed between 10^{16} and 10^{17}eV is not continued in the highest energy region. In fact the elongation rate above 2×10^{17}eV is consistent with the composition remaining substantially unchanged with increasing energy.

7.3 Other Measurements of the Mean Depth of Maximum above 10^{15}eV

Before comparing the measurements from the Dugway and Haverah Park installations as presented above with results from other arrays it should be reiterated that some residual uncertainty remains about the assignment of primary energy given the different techniques of primary energy estimation employed. In addition the method of interpreting measured shower parameters as determinations of t_{max} is not consistent for different measurements. Wherever possible the values of $\overline{t_{max}}$ are those obtained by McComb and Turver (1982b), who have reinterpreted the measured shower parameters using the same computer simulations as were applied to the Dugway data. Greater confidence can therefore be placed in the interrelation of the measurements with those displayed in Figure 7.1.

Apart from the Dugway and Haverah Park Cerenkov Light Detector arrays four other experiments have provided measurements of the Cerenkov light component of extensive air showers. Three sets of results have been produced by analysis of the lateral distribution of Cerenkov light and these extend the Dugway measurements to both higher and lower energy. Measurements from the Yakutsk array (Dyakanov et al. (1982a)) measure the value of $\overline{t_{max}}$ above 10^{18}eV and earlier results (Glushkov et al. (1979)) overlap the upper energy of the current experiment at $\sim 10^{17}$eV. The work of Tornabene at Bowie, Maryland (Tornabene (1979)) is of considerable interest in the present context since at 10^{15}eV it supplies the lowest energy determination in this survey of $\overline{t_{max}}$ dependence on primary energy. The values of $\overline{t_{max}}$ quoted for this experiment are the result of interpretation by McComb and Turver.

Pulse shape measurements from other arrays span approximately the same energy range as the Dugway results. This reflects the fact that the technique of measuring pulse shape is appropriate to a more limited energy range than that of lateral distribution determination because of limited sensitivity at lower energies (< 10^{16}eV) and the problems of obtaining enough high quality measurements above 10^{18}eV. The measurements from the Yakutsk array (Kalmykov et al. (1981)) in fact extend to slightly higher energies than the Dugway array. The Cerenkov array results between 10^{16} and 10^{17}eV confirm the Dugway measurements displaying the strong energy dependence which is interpreted as a change in primary mass composition. The Adelaide group (Thornton and Clay (1980)) predict an even greater elongation rate from their results and the criticisms of their work by Orford and Turver (1980) should be noted. The result from the Samarkand array reported in 1981 is somewhat at variance with other measurements at that energy and must be regarded as preliminary. In these cases, the pulse shape measurements have not been reinterpreted by McComb and Turver because of difficulty in accounting accurately for the effect on the measured pulse of the measuring system itself and therefore the authors' own interpretation has been used.

Other measurements of absolute depth of maximum are based on the detection of the particle component. Data above 10^{17}eV are available from the Chacaltya array (Aguirre et al., (1979)) where electron development curves are observed at a vertical atmospheric depth of 530 g cm^{-2}. It should be noted however, that the interpretation of these results in terms of depth of shower maximum remains controversial. The measurements at ~10^{15}eV by Antonov (1981) also use electron development curves in this case obtained from balloon borne experiments.

The composite plot of all these $\overline{t_{max}}$ measurements is displayed in Figure 7.2 together with the simulation predictions, as shown previously. The low energy points of Antonov and Tornabene are the most significant additions to the results already presented in Figure 7.1. Regardless of which of the preferred models is considered this confirms that the primary mass composition around 10^{16}eV is largely iron-like nuclei. The increase in elongation rate between energies of 10^{16} and 10^{17}eV measured by the Dugway array is reinforced by other measurements in that energy region and this indicates a change in primary mass composition. Some uncertainty still remains at higher energies ($> 3 \times 10^{17}$eV) The measurements from Chacaltaya (Aguirre et al. (1979)) and the Nottingham group (Blake et al. (1979) reinterpreted by McComb and Turver (1982b)) represent the extremes of the data and seem to favour different interaction models. The Nottingham data is compatible only with an $E^{0.25}$ model

Figure 7.2

The combination of recent measurements of $\overline{t_{max}}$ from 10^{15}eV to 10^{19}eV.

D	Dugway	Cerenkov light measurements	this work
H	Haverah Park		Protheroe & Turver (1979
Y	Yakutsk		Dyakonov et al. (1981a)
G	Yakutsk		Glushkov et al. (1979)
B	Bowie		Tornabene (1979) interpreted by McComb & Turver (unpublished)
K	Yakutsk		Kalmykov et al. (1979) with errors quoted by Linsley & Watson (1981)
I	Akeno		Inoue et al. (1981)
T	Adelaide		Thornton & Clay (1980)
S	Samarkand		Aliev et al. (1981)
N	Haverah Park	muon deep detector response	Blake et al. (1979) interpreted by McComb & Turver (1982b)
M	Haverah Park	muon core angles	Gibson et al. (1981)
C	Chacaltya	electron cascade development curves	Aguirre et al. (1979)
A	Balloon-borne measurements	electron cascade development curves	Antonov et al. (1981)

The simulation predictions are as Figure 7.1.

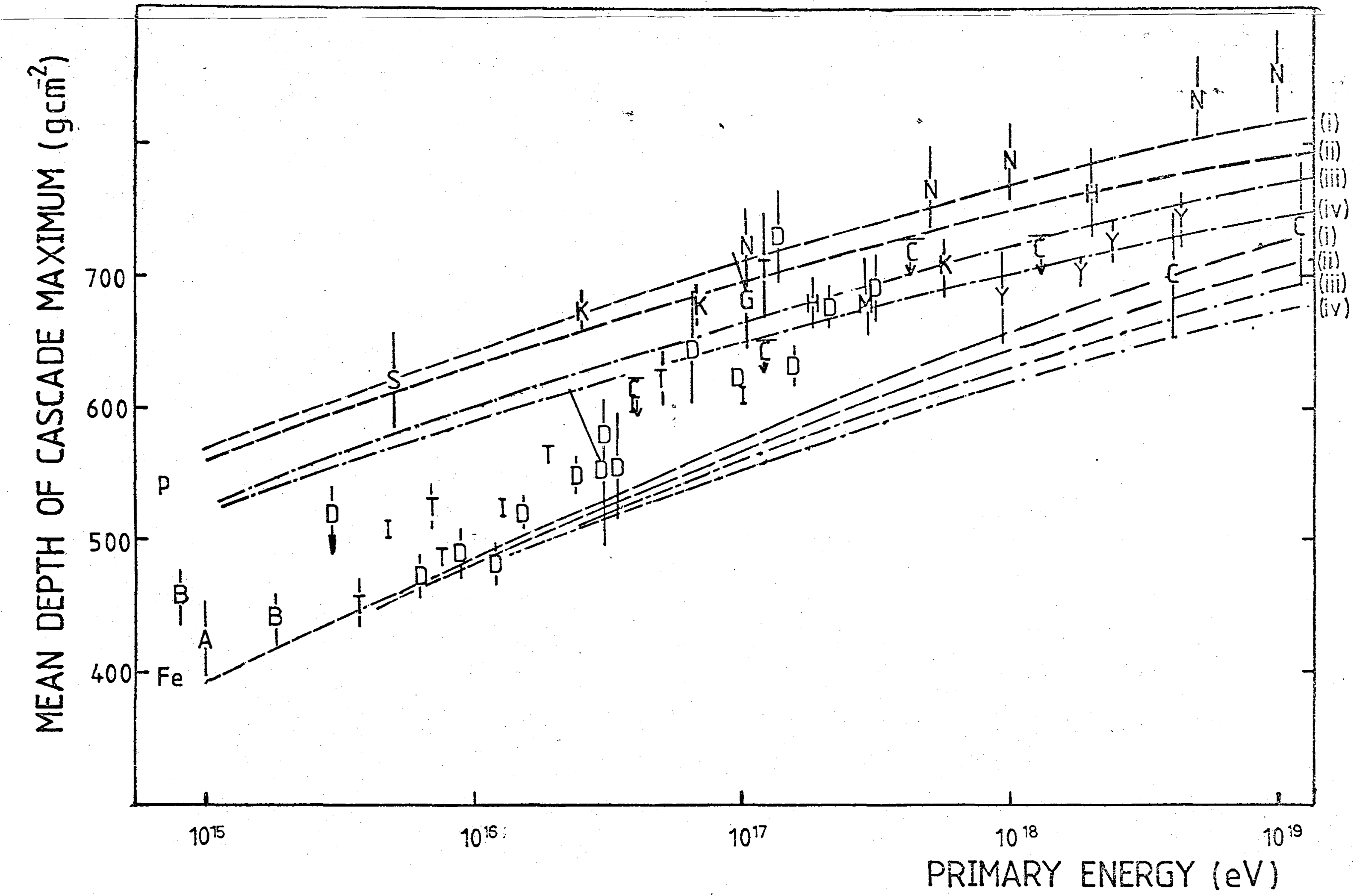
MEAN DEPTH OF CASCADE MAXIMUM (gcm^{-2})
400
500
600
700
PRIMARY ENERGY (eV)
10^{15}
10^{16}
10^{17}
10^{18}
10^{19}
P
Fe
(i)
(ii)
(iii)
(iv)
(i)
(ii)
(iii)
(iv)
A
B
S
K
N
G
T
D
C
I
H
M
Y

with a largely protonic composition whereas the Chacaltya data is consistent with either an $E^{0.33}$ multiplicity with mixed composition or an $E^{0.25}$ multiplicity with the composition returning to iron-like nuclei. The scatter in measurements of $\overline{t_{max}}$ around 10^{17}eV can probably be accounted for by uncertainty in the energy attribution between different arrays.

Despite the proviso made about the interrelation of data when energy assignment is made by different methods, the accumulation of results from all recent observation serves to reinforce the relationship between $\overline{t_{max}}$ and E_p detected in the composite plot of Dugway and Haverah Park measurements. This adds considerable weight to the argument in favour of a changing primary mass composition across the energy range under consideration. At energies below 10^{17}eV there is good agreement between measurements from different sources and since there is little difference in the dependence of $\overline{t_{max}}$ on E_p predicted by the use of different interaction models it is possible to map the change in primary mass composition from predominantly iron-like nuclei at 10^{15}eV to a mixed composition with a significant proportion of light nuclei at 10^{17}eV. Only at energies above 10^{17}eV would it be possible to resolve the appropriate interaction model using $\overline{t_{max}}$; the discrepancy between measurements above 3 x 10^{17}eV leaves considerable uncertainty over the interaction model and primary mass composition.

7.4 Other Fluctuation Measurements

There are fewer measurements of Δt_{max} than of $\overline{t}_{max}$ available from other locations in the world. Recent measurements, before the Dugway results become available, are summarised by Walker and Watson (1982) together with their own results from the Haverah Park array. The Dugway measurements of Δt_{max} overlap with these data only at 2×10^{17}eV with all other reported determinations of Δt_{max} being at higher energy. As before, the uncertainty in the intercalibration of energy between arrays must be borne in mind.

The main source of fluctuation measurements is from Walker and Watson themselves measuring the Haverah Park deep detector rise times over the energy range 2×10^{17} - 10^{19}eV. Also from the Haverah Park array is one measurement of fluctuations in the lateral distribution of deep detector response (Coy et al. (1981)). In addition Walker and Watson have interpreted the early work of Watson and Wilson (1974) on fluctuations from the analysis of pulse profiles at Haverah Park. Finally, the Yakutsk array provides two measurements of Δt_{max} (Dyakanov et al. (1981b) taken from measurements of the lateral distribution of Cerenkov light in showers at 7×10^{17} and 4×10^{18}eV.

Figure 7.3 shows a compilation of all these measurements with the three results from the Dugway array. The simulation lines added to this figure are the predicted fluctuation of proton and iron initiated showers with interaction cross-sections rising as lns and $\ln^2$s. The calculated

Figure 7.3 A compilation of measurements of Δt_{max} of primary energy from 10^{15}eV to 10^{19}eV.

Dugway

D	Dugway	lateral distribution
F	Dugway	FWHM

From Walker and Watson (1982)

R	Haverah Park	deep detector rise time Walker and Watson (1981)
C	Haverah Park	lateral distribution of deep detector response Coy et al. (1981b)
W	Haverah Park	pulse profiles from deep detector response Watson & Wilson (1974) reinterpreted by Walker & Watson
Y	Yakutsk	lateral distribution of Cerenkov light Dyakanov et al. (1981b)

The simulation lines represent log s and $\log^2$s cross-sections.

(After Chantler et al. (1983)).

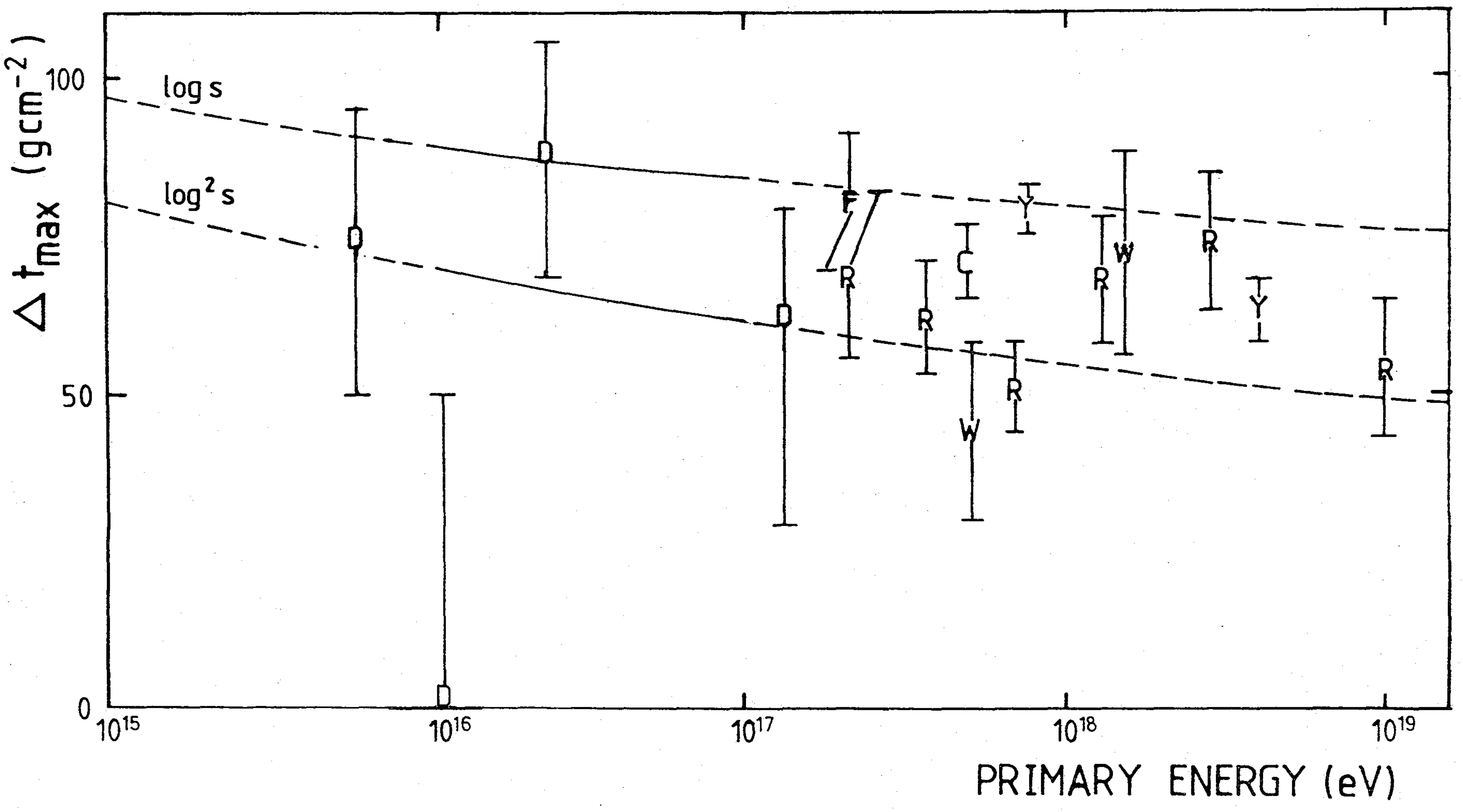
Δt_{max} (gcm^{-2})
100
50
0
log s
log^2 s
D
F
R
C
W
Y
10^{15}
10^{16}
10^{17}
10^{18}
10^{19}
PRIMARY ENERGY (eV)

value of Δt_{max} is virtually insensitive to the multiplicity of produced particles in the central region for the scaling based models used in this work for both proton and iron primary particles. In addition, for iron-initiated showers it shows negligible dependence on the rising cross-section (for reasonable models).

Figure 7.3 is however, inconclusive in its predictions about primary mass composition. It is more instructive to consider these results in terms of a mixed composition and following the method of Chantler (1982), the simple binary composition model used in Section 6.5 has been employed. These measurements represent only estimates of Δt_{max} and not simultaneous determinations of $\overline{t_{max}}$ and Δt_{max}. Table 7.1 is a summary of all the fluctuation measurements together with an estimate of $\overline{t_{max}}$ for each measurement. These were obtained from a weighted least squares fit to the values of $\overline{t_{max}}$ and E_p for all measurements greater than 2×10^{17}eV shown in Figure 7.2. The exception to this is the measurement of deep detector density lateral distribution (Coy et al. (1981)) since Δt_{max} is calculated on the assumption of a mean depth of maximum of 721 ± 12 g cm^{-2} and this value has therefore been used instead of the regression estimate for this case.

Figure 7.4 shows the result of using only Δt_{max} to estimate the percentage or iron nuclei in the simple binary composition for each of the three preferred interaction models (see Section 6.5). Each line represents the uncertainty at the one standard deviation level.

TABLE 7.1

Measurements of t_{max} from Walker and Watson (1982)

E_p -eV	Inferred $\overline{t_{max}}$ g cm^{-2}	Δt_{max} g cm^{-2}	Source of Measurements
2×10^{12}	664 ± 34	69 ± 14	Walker & Watson (1982)
3.6×10^{17}	680 ± 32	62 ± 9	
6.8×10^{17}	696 ± 31	51 ± 7	
1.3×10^{18}	714 ± 31	68 ± 10	
2.8×10^{18}	734 ± 32	74 ± 11	
10^{19}	768 ± 36	54 ± 11	
4.9×10^{17}	721 ± 12	71 ± 6	Coy et al. (1981a)
5×10^{17}	688 ± 31	44 ± 14	Watson & Wilson (1974)
7.5×10^{17}	699 ± 31	79 ± 4	Dyakonov et al. (1981)
1.5×10^{18}	717 ± 31	72 ± 16	Watson & Wilson (1974)
4×10^{18}	744 ± 32	63 ± 5	Dyakonov et al. (1981)

Figure 7.4 The measurements of Δt_{max} from Walker and Watson (1982) interpreted in terms of a binary model of primary mass composition (iron and protons). The simulation models use the following central multiplicities and cross-sections.

(i) $E^{0.25}$, log s

(ii) $E^{0.25}$, $\log^2 s$

(iii) $E^{0.33}$, log s

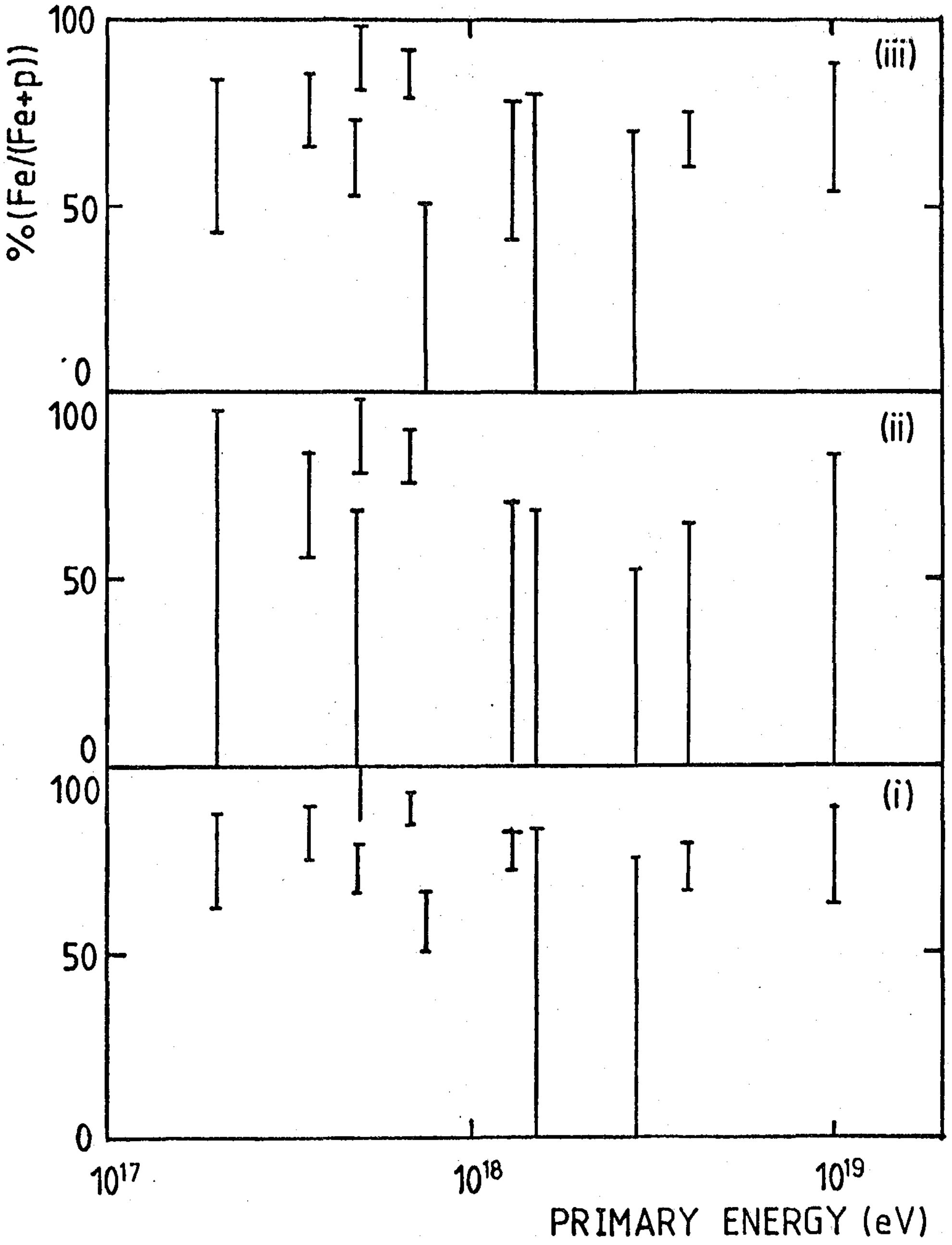
%(Fe/(Fe+p))
100
50
0
(iii)
100
50
0
(ii)
100
50
0
(i)
10^{17}
10^{18}
10^{19}
PRIMARY ENERGY (eV)

No attempt has been made to indicate the uncertainty in primary energy attribution. These figures show that any firm prediction of primary mass composition in this energy range demands a better understanding of the nature of hadronic interactions.

The estimates of Figure 7.4 have been modified by attributing the $\overline{t_{max}}$ measurement of Table 7.1 and treating the results as simultaneous determinations of $\overline{t_{max}}$ and Δt_{max} using the method displayed in Figure 6.4. The combined measurement using the three preferred models is shown in Figure 7.5. Two fluctuation measurements have been omitted from the plot since the inferred depth of maximum is not compatible with the measured value of Δt_{max} at the one standard deviation level for any of the models. Whilst the measurement at 6.8 x 10^{17}eV just fails at this level the reinterpreted early measurement by Watson and Wilson (1974) at 5 x 10^{17}eV is significantly different and this should be investigated.

In addition to the fluctuation measurements from other arrays, the two depth of maximum estimates from the Haverah Park Cerenkov Light Detector array have been interpreted using the same model and added to Figure 7.5.

The value of Figure 7.5 is that it demonstrates clearly that the composition obtaining at 10^{16}eV of almost entirely iron-like nuclei does not continue into higher energies where a significant proportion of the primary flux must be light nuclei.

Figure 7.5 Simultaneous measurement of $\overline{t_{max}}$ and Δt_{max} interpreted in terms of a binary model of primary mass composition (iron and protons) using simulation models (i) - (iii).

▨ Dugway

| t_{max} measurements taken from Walker and Watson (1982) using the best estimate of $\overline{t_{max}}$ from current depth of maximum measurements.

¦ $\overline{t_{max}}$ measurements from the Haverah Park Cerenkov Light Detector Array (Protheroe and Turver (1979)).

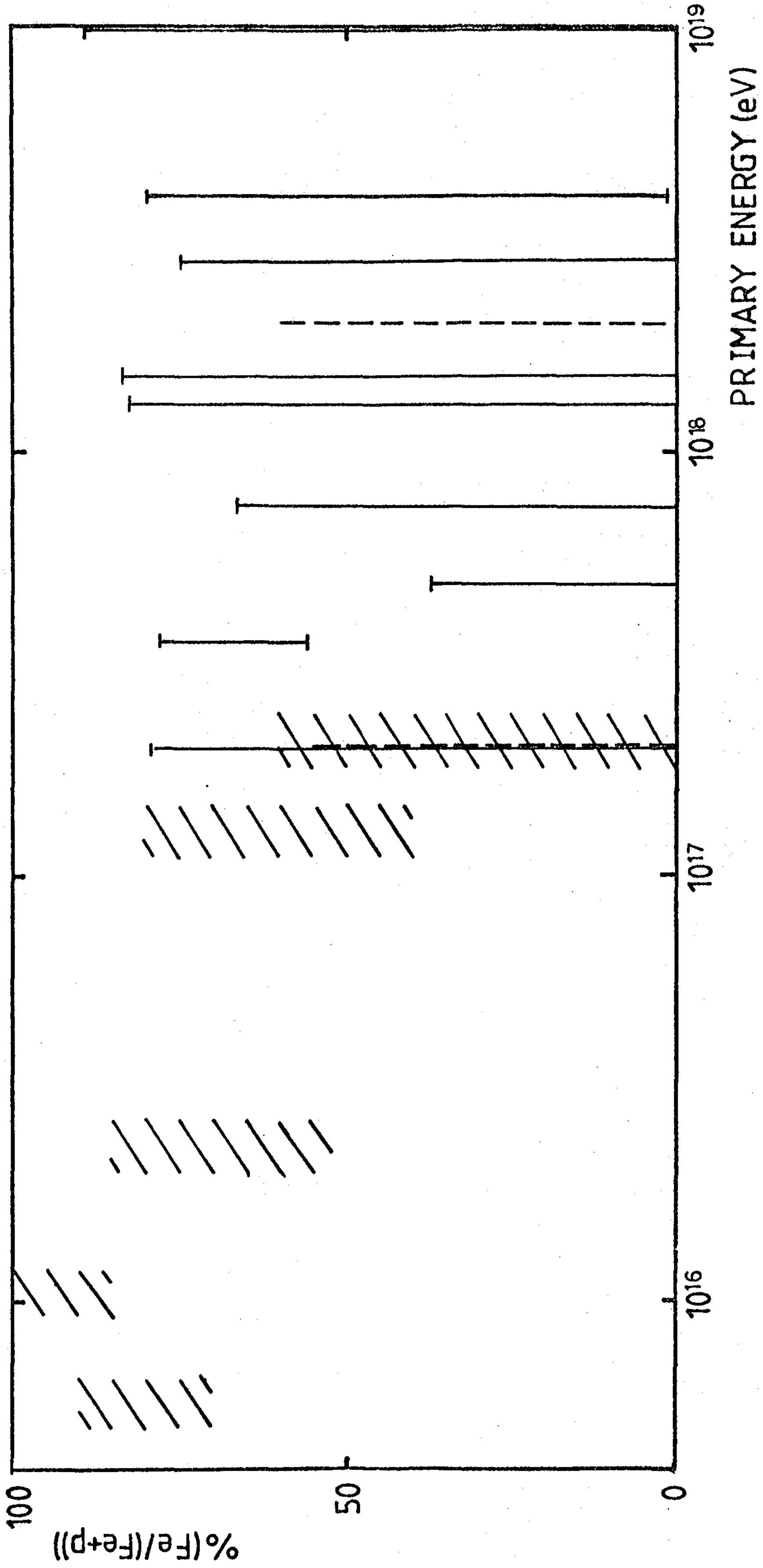

100
50
0
%(Fe/(Fe+p))
10^16
10^17
10^18
10^19
PRIMARY ENERGY (eV)

7.5 Conclusions

The Dugway Cerenkov Light Detector Array has recorded considerable success in measuring the longitudinal development of cosmic ray showers. The flexibility of the array allowed measurements to be made over nearly two decades of primary energy employing a single shower component using the independent techniques of lateral distribution and pulse time-structure analysis. The lateral distribution technique proved the more successful in measuring over the full range of primary energy accessible with the three array configuration used at Dugway.

This work has described the analysis procedures used to determine both the mean depth of maximum and fluctuations in depth of maximum from the lateral distribution of Cerenkov light in showers recorded by the largest array configuration ($\sim 10^{17}$eV). These procedures were subsequently applied to data collected by the other two array configurations to provide measurements of $\overline{t_{max}}$ and Δt_{max} down to 6×10^{15}eV. The interpretation of these results rests on the findings of simulation calculations that a transformation, virtually independent of interaction model, can be made between the lateral distribution shape parameter and the depth of cascade maximum. The behaviour of lateral distribution shape has been shown to be in good agreement with scaling-based simulations.

The values of $\overline{t_{max}}$ and Δt_{max} obtained from this analysis together with those from the analysis of pulse shape have provided valuable information about the energy dependence of the development of shower cascades. In particular the values of $\overline{t_{max}}$ are incompatible with a hadronic interaction model employing pure scaling but demand that an enhanced multiplicity in the central region is used. (Multiplicities rising as $E^{0.25}$ or $E^{0.33}$ would both be appropriate). Whichever of these models is used the measurements of $\overline{t_{max}}$ and Δt_{max} require a change of primary mass composition from almost entirely iron-like nuclei at $\sim 10^{16}$eV to a mixed composition with a significant proportion of light nuclei above 10^{17}eV. Interpretation of data from other arrays indicates that this protonic component remains significant from 2 x 10^{17}eV to 10^{19}eV.

At energies $\sim 10^{15}$eV independent evidence of the predominance of heavy nuclei is provided by the measurements of the arrival time distribution of hadrons in the shower core (Cowsik et al. (1981)). In addition the interpretation of shower density spectrum measurements at ~3 x 10^{15}eV by Hillas (1981) tends to further confirm this view.

The interpretation of data from the Dugway array relies heavily on computer simulations of shower development using reasonable extrapolations to higher energy of current accelerator data (at energies of 10^{11} - 10^{12}eV). In particular, the models used have assumed that scaling operates in the fragmentation region. It must therefore be pointed out that a change in the nature of the hadronic interactions at higher energy could account for the increase in elongation rate between 10^{16} and 10^{17}eV without demanding a change in primary mass composition. However, there is no need to invoke any such disruption of the underlying physics to explain the observed data.

Assuming that scaling based models of hadronic interactions are substantially correct, and therefore that the interpretation of the Dugway data as indicating a change in primary mass composition, is valid these results must be related to current theories of propagation of cosmic rays. Until the current data was presented astrophysical models have been constructed to account for the 'knee' in the cosmic ray energy spectrum at $\sim 3 \times 10^{15}$eV (e.g. Bell et al. (1974)). A diffusion model which would account for the energy spectrum would predict that containment of protons in the galaxy by the galactic magnetic fields begins to fail between 10^{14} and 10^{15}eV. Particles of increasing charge would escape at progressively higher energies and thus the composition at $\sim 10^{16}$eV would be predominantly heavy nuclei. An alternative model (Karakula et al. (1974)) suggesting galactic pulsars as a source of cosmic rays also predicts the iron-like composition at $\sim 10^{16}$eV. The protonic component observed in the current data at energies above 3×10^{16}eV would, under either of these models, be accounted for by an extragalactic source.

The Dugway Cerenkov Light Detector Array has therefore, contributed measurements over a particularly interesting energy region using a consistent measurement technique and method of interpretation. The simultaneous determination of $\overline{t_{max}}$ and Δt_{max} has proved a considerable enhancement of the value of each of the individual measurements. The present determination of the behaviour of extensive air showers between 6 x 10^{15} and 2 x 10^{17}eV calls for better measurements of the situation around 10^{15}eV and above 2 x 10^{17}eV to improve the understanding of primary mass composition and its astrophysical implications.

7.6 Future Work

The analysis of the data collected by the Dugway Cerenkov Light Detector Array is now completed and nothing further of value is expected from that source. The result of this analysis has provided considerable information in the energy range 6 x 10^{15}eV - 2 x 10^{17}eV and suggest that the greatest area of interest is now at energies above 5 x 10^{17}eV where considerable ambiguity exists about the depth of maximum measurements and where the greatest hope of resolving different hadronic interaction models lies. This will be aided by the results from the new $p\bar{p}$ collider experiments currently being conducted at CERN and at FNAL in the near future which investigate hadronic interactions up to 10^{15}eV. If inappropriate interaction models could be excluded from the interpretation of the current measurements it would be possible to make more exact inferences about the primary mass composition over the range of energy from 10^{15} to 10^{18}eV.

The greatest hope of worthwhile quantities of improved information at high energy comes from the Fly's Eye experiment (Bergeson et al. (1977)) which observes the scintillation light emitted isotropically from the shower cascade. This light can be detected and analysed to map the development of the shower and because the trajectory of the cascade is best observed from the side data can be collected over a wide area of the sky. This experiment should have a high data collection rate with a measurement technique which is readily interpreted in terms of cascade development. Results from this experiment are awaited.

More measurements are also required around 10^{15}eV in order to investigate the change from the "normal" composition observed by satellite and balloon borne experiments to the predominantly iron-like composition which the current work detects at ~ 10^{16}eV. The improved data on hadronic interactions available from the new generation of accelerator experiments measuring energies up to 10^{15}eV should allow unambiguous simulations to reliably interpret such measurements. A more detailed knowledge of the primary mass composition between 10^{15} and 10^{16}eV where the 'knee' of the energy spectrum occurs would allow the resolution of theoretical models.

REFERENCES

Aguirre, C., Anda, R., Trepp, A., Kaneko, T., Yoshii, H., Nishi, K., Yamada, Y., Tajima, N., Nakatani, H., Gotoh, E., Kakimoto, F., Mizumoto, Y., Suga, K., Izu, N., Kamouchi, Y., Inoue, N., Kawai, M., MacKeown, P.K., Toyoda, Y., and Murakami, K., (1979), Proc. 16th Int. Conf. on Cosmic Rays, Kyoto, 8, 107.

Aliev, N., Alimov, T.A., Kaharov, M., Makhmudov, B.M., Sevirenko, S., Kalmykov, N.N., Khristiansen, G.B., and Prosin, V.V., (1981), Proc. 17th Int. Conf. on Cosmic Rays, Paris, 11, 262.

Andam, A., (1982), Ph.D. thesis, University of Durham.

Anderson, C.D., (1932), Science, 76, 238.

Antonov, R.A., Kuzmin, V.A., and Fateeva, I.M., (1981), Proc. 17th Int. Conf. on Cosmic Rays, Paris, 6, 229.

Bell, M.C., Kota, J., and Wolfendale, A.W., (1974), J. Phys. A, 7, 420.

Bergeson, H.E., Cassiday, G.L., Chiu, T.W., Cooper, D.A., Elbert, J.W., Loh, E.C., Steck, D., West, W.J., Linsley, J., and Mason, G.W. (1977), Phys. Rev. Lett., 39, 847.

Blackett, P.M.S. (1948), Dep. Gassiot Comm. of the Roy. Soc., 34.

Blake, P.R., England, C.D., Lapikens, J., Nash, W.F., Norwood, H., O'Connel, B., Reid, R.J.O., Strutt, R.B., and Watson, A.A. (1979), Proc. 16th Int. Conf. on Cosmic Rays, Kyoto, 8, 67.

Boley, F.I., (1964), Rev. Mod. Phys., 36, 792.

Boley, F.I., Baum, J.H., Pasledge, J.A., and Pereve, J.H., (1961), Phys. Rev., 124, 1205.

Boone, J., Cady, R., Cassiday, G.L., Elbert, J.W., Loh, E.C., Sokolsky, P.V., Steck, D., and Wasserbaech, (1983), Proc. of the Cosmic Ray Workshop, University of Utah.

Cerenkov, P.A. (1934), Dokl. Akad. Nauk.SSSR., 2, 451.

Chantler, M.P., (1982), Ph.D. thesis, University of Durham.

Chantler, M.P., Orford, K.J., Shearer, J.A.L., Turver, K.E., and Walley, G.M. (1979), Proc. 16th Int. Conf. on Cosmic Rays, Kyoto, 9, 56.

Chantler, M.P., Craig, M.A.B., McComb, T.J.L., Orford, K.J., Turver, K.E., and Walley, G.M., (1983), J. Phys. G., 9, L27.

Chudakov, A., (1965), Proc. 9th Int. Conf. on Cosmic Rays, London, 2, 50.

Cowsik, R., Tonwar, S.C., Viswanath, P.R., Ellsworth, R.W., Goodman, J.A., Ito, A.S., Steitmatter, R.E., and Yodh, G.B. (1981), Proc. 17th Int. Conf. on Cosmic Rays, Paris, 2, 120.

Coy, R.N., Lloyd-Evans, J., Patel, M., Reid, R.J.O., and Watson, A.A., (1981a), Proc. 17th Int. Conf. on Cosmic Rays, Paris, 9, 183.

Coy, R.N., England, C.D., Pearce, D., Reid, R.J.O., and Watson, A.A., (1981b), ibid, 6, 43.

Craig, M.A.B., McComb, T.J.L., and Turver, K.E., (1979), Proc. 16th Int. Conf. on Cosmic Rays, Kyoto, 8, 180.

Diminstein, O.C., Kolosov, V.A., Krasilnikov, D.D., Kusmin, A.I., Kulakovskaya, V.P., Orlov, V.A., Sleptsov, I.Y., Yefimov, N.N., and Yegerov, P.A., paper presented to the European Symposium on Air Showers, September 1972. (Paris, 1972).

Dixon, H.E., and Turver, K.E., (1974), Proc. Roy. Soc. Lond. A, 339, 171.

Dyakanov, M.N., Egorov, T.A., Egorova, V.P., Ivanov, A.A., Knurenko, S.P., Kozlov, V.I., Kolosov, V.A., Krasilnikov, A.D., Krasilnikov, D.D., Lishchenuk, F.F., Pavlov, V.N., Sidorov, R.G., Sleptsov, I.Y., and Nikolsky, S.I., (1981a), Proc. 17th Int. Conf. on Cosmic Rays, Paris, 6, 106.

Dyakanov, M.N., Knurenko, S.P., Kozlov, V.I., Kosolov, V.A., Krasilnikov, D.D., Lishchenuk, F.F., Makarov, K.N., Pavlov, V.N., Sleptsov, I.Y, Shamsutdinova, F.K., and Nikolsky, S.I. (1981b), ibid, 6, 110.

Dzikowski, T., Gawin, J., Grochalska, B., Wasilewski, A., Wdowczyk, J., (1981), Proc. 17th Int. Conf. on Cosmic Rays, Paris, 1, 8.

Efimov, N.N., Krasilnikov, D.D., Khristiansen, G.B., Shikalov, F.V., and Kuzmin, A.I., (1973), Proc. 13th Int. Conf. on Cosmic Rays, Denver, 4, 2378.

Egorov, T.A., Kolosov, V.A., Krasilnikov, D.D., Orlov, V.A., and Sleptsov, H.E., (1971), Proc. 12th Int. Conf. on Cosmic Rays, Hobart, 6, 2164.

Elterman, L., (1968), Air Force Cambridge Research Labs., Ref. AFC RL-68-0153.

Feynman, R.P., (1969), Phys. Rev. Lett., 23, 1415.

Frank, I.M., and Tamm, I.G., (1937), Dolk. Akad. Nauk. SSSR, 14, 109.

Freier, P.S., and Waddington, C.J., (1975), Astrophys. Space Sci., 38, 419.

Gaisser, T.K., McComb, T.J.L., Protheroe, R.J., and Turver, K.E., (1978), Rev. Mod. Phys., 50, 859.

Gaisser, T.K., and Yodh, G.B., (1980), Ann. Rev. Nucl. Part. Sci., 30, 475.

Galbraith, W., and Jelley, J.V., (1953), Nature, 171, 349.

Galbraith, W., and Jelley, J., (1955), J. Atmos. Terr. Phys., 6, 250.

Gibson, A.I., Mc Comb, T.J.L., and Turver, K.E., (1981), Proc. 17th Int. Conf. on Cosmic Rays, Paris, 6, 16.

Giler, M., Wdowczyk, J., and Wolfendale, A.W., (1980), J. Phys. G., 6, 1561.

Ginzberg, V.L., (1940), Zh. Fiz. SSSR, 2, 441.

Glushkov, A.V., Grigorev, V.M., Efimov, N.N., Pravdin, M.I., Diminstein, O.S., and Sokurov, V.F., (1979), Proc. 16th Int. Conf. on Cosmic Rays, Kyoto, 8, 158.

Gol'danskii, V.I., and Zhdanov, G.B., (1954), Sov. Phys. JETP, 26, 405.

Goodman, J.A., Ellsworth, R.W., Ito, A.S., MacFall, J.R., Siohan, F., Streitmatter, R.E., Tonwar, S.C., Vishwanath, P.R., and Yodh, G.B. (1979), Phys. Rev. Lett., 42, 854.

Greisen, K., (1960), Ann. Rev. Nucl. Sci., 10, 63.

Greisen, K., (1966), Phys. Rev. Lett., 16, 748.

Hammond, R.T., Orford, K.J., Protheroe, R.J., Shearer, J.A.L., Turver, K.E., Waddoup, W.D., and Wellby, D.W., (1978), Il Nuovo Cim., 1C, 315.

Hess, V., (1912), Physik Zeitschr., 13, 1804.

Hillas, A.M., (1981), Proc. 17th Int. Conf. on Cosmic Rays, Paris, 13, 69.

Hillas, A.M., Marsden, D.J., Hollows, J.D., and Hunter, H.W., (1971), Proc. 12th Int. Conf. on Cosmic Rays, Hobart, 3, 1001-6, and Hillas, A.M., Hollows, J.D., Hunter, A.W., and Marsden, D.J., (1971), ibid., 3, 1007-12.

Hillas, A.M., and Ouldridge, M., (1975), Nature, 253, 609.

James, M., and Roos, M., (1975), Comp. Phys. Comm., 10, 413.

Jelley, J.V., (1958), "Cerenkov Radiation and its Applications", Pergamon Press, London.

Jelley, J.V., and Galbraith, W., (1953), Phil. Mag., 44, 619.

Kalmykov, N.N., Khristiansen, G.B., Nechin, Yu.A., Prosin, V.V., Grigorev, V.M., and Efimov, N.N., (1977), Proc. 15th Int. Conf. on Cosmic Rays, Plovdiv, 8, 244.

Kalmykov, N.N., Nechin, Yu.A., Prosin, V.V., Efimov, N.N., Fomin, Yu.A., Khristiansen, G.B., and Grigorev, V.M., (1981), Proc. 17th Int. Conf. on Cosmic Rays, Paris, 6, 114.

Karakula, S., Osborne, J.L., and Wdowczyk, J., (1974), J. Phys. A., 7, 437.

Kiraly, P., Kota, J., Osborne, J.L., Stapley, N.R., and Wolfendale, A.W., (1979), Riv. Nuovo Cim., 2, No. 7, 1.

Krasilnikov, D.D., (1979), Proc. 16th Int. Conf. on Cosmic Rays, Kyoto, 8, 26.

Kreiger, A.S., and Bradt, H.V., (1969), Phys. Rev., 185, 1629.

Kuhlmann, J.D., and Clay, R.W., (1981), Proc. 17th Int. Conf. on Cosmic Rays, Paris, 6, 96.

Landau, L.D., (1953), Izv. Akad. Nauk. SSSR, 17, 51, translated in "Collected Papers of L.D. Landau", 1965, edited by D. Ter Haar, Gordon and Breach, New York.

Linsley, J., (1977), Proc. 15th Int. Conf. on Cosmic Rays, 12, 89.

Lloyd-Evans, J., Pollock, A.M.T., and Watson, A.A., (1979), Proc. 16th Int. Conf. on Cosmic Rays, Kyoto, 13, 130.

Mallet, L., (1926), C.R. Acad. Sci. (Paris), 183, 274.

McComb, T.J.L., and Turver, K.E., (1981), Proc. 17th Int. Conf. on Cosmic Rays, Paris, 6, 130.

McComb, T.J.L., and Turver, K.E., (1982a), Nuovo Cim., C, 5, 131.

McComb, T.J.L., and Turver, K.E., (1982b), J. Phys. G., 8, 1119.

Nestorova, N.M., and Chudakov, A.E., (1955), Zh. Eksp. Teor. Fiz., 28, 384.

Orford, K.J., and Turver, K.E., (1976), Nature, 264, 727.

Orford, K.J., and Turver, K.E., (1980), Phys. Rev. Lett., 44, 959.

Orford, K.J., Turver, K.E., and Wellby, D.W., (1975), Proc. 14th Int. Conf. on Cosmic Rays, Munich, 8, 3019.

Peters, B., (1961), Il Nuovo Cim., 22, 800.

Protheroe, R.J., (1977), Ph.D. thesis, University of Durham.

Protheroe, R.J., and Turver, K.E., (1979), Il Nuovo Cim., 51A, 277.

Rossi, B., and Greisen, K., (1941), Rev. Mod. Phys., 13, 240.

Shearer, J.A.L., (1981), Ph.D. thesis, University of Durham.

Samorski, M., and Stamm, W., (1983), Astrophys. J. Lett., 268, 147.

Thornton, G.J., Kuhlmann, J.D., Leibing, D.F., Clay, R.W., Gregory, A.G., Patterson, J.R., and Prescott, J.R., (1979), Proc. 16th Int. Conf. on Cosmic Rays, Kyoto, 9, 103.

Thornton, G.J., and Clay, R.W., (1980), Phys. Rev. Lett., 45, 1463.

Tornabene, H., (1979), Proc. 16th Int. Conf. on Cosmic Rays, Kyoto, 9, 99.

Waddoup, W.D., and Stubbs, R.J., (1976), Nucl. Inst. and Meth., 137, 603.

Waddoup, W.D., and Stubbs, R.J., (1977), ibid., 146, 569.

Walker, R., and Watson, A.A., (1981), J. Phys. G., 7, 1297.

Walker, R., and Watson, A.A., (1982), ibid., 8, 1131.

Watson, A.A., and Wilson, J.G., (1974), J. Phys. G., 7, 1297.

Wellby, D.W., (1977), Ph.D. thesis, University of Durham.

White, J., Porter, N.A., and Long, C.D., (1961), J. Atmos. Terr. Phys., 20, 40.

Wilson, C.T.R., (1901),Proc. Roy. Soc., 68, 151.

Wolfendale, A.W., (1975), in "The Origin of Cosmic Radiation", p.1., ed. by J.L. Osborne and A.W. Wolfendale, Reidel, Dordrecht, Holland.

Zatsepin, G.T., and Kuzmin, V.A., (1966), Zh. Eksp. Teor. Fiz., 4, 78.